



HAL
open science

New Seismotectonic Zoning Model for Seismic Hazard Assessment of the Lesser Antilles

Océane Foix, Stéphane Mazzotti, Hervé Jomard, Céline Beauval, Didier Bertil, Marie-Paule Bouin, Éric Calais, Jean-Jacques Cornée, Nathalie Feuillet, Roser Hoste-Colomer, et al.

► **To cite this version:**

Océane Foix, Stéphane Mazzotti, Hervé Jomard, Céline Beauval, Didier Bertil, et al.. New Seismotectonic Zoning Model for Seismic Hazard Assessment of the Lesser Antilles. Géosciences Montpellier. 2023. hal-04249274

HAL Id: hal-04249274

<https://hal.science/hal-04249274>

Submitted on 19 Oct 2023

HAL is a multi-disciplinary open access archive for the deposit and dissemination of scientific research documents, whether they are published or not. The documents may come from teaching and research institutions in France or abroad, or from public or private research centers.

L'archive ouverte pluridisciplinaire **HAL**, est destinée au dépôt et à la diffusion de documents scientifiques de niveau recherche, publiés ou non, émanant des établissements d'enseignement et de recherche français ou étrangers, des laboratoires publics ou privés.



Distributed under a Creative Commons Attribution 4.0 International License

New Seismotectonic Zoning Model for Seismic Hazard Assessment of the Lesser Antilles

Océane **Foix**¹, Stéphane **Mazzotti**¹, Hervé **Jomard**², Céline **Beauval**³, Didier **Bertil**⁴, Marie-Paule **Bouin**⁵, Éric **Calais**⁶, Jean-Jacques **Cornée**¹, Nathalie **Feuillet**⁵, Roser **Hoste-Colomer**⁴, Mireille **Laigle**⁷, Serge **Lallemand**¹, Jean-Frédéric **Lebrun**¹, Anne **Lemoine**⁴, Boris **Marcaillou**⁷, Mélody **Philippon**¹, Agathe **Roullé**⁴, Claudio **Satriano**⁵, Jean-Marie **Saurel**⁵, Elenora **van Rijsingen**⁸

1. Géosciences Montpellier, Université de Montpellier, Université des Antilles, CNRS. 2. Institut de Radioprotection et Sûreté Nucléaire, Fontenay-aux-Roses. 3. ISTERre, Université de Grenoble Alpes, CNRS. 4. BRGM, Orléans. 5. Institut de Physique du Globe, Paris. 6. Laboratoire de Géologie, ENS Paris. 7. Géoazur, Université Côte d'Azur, CNRS, IRD, Observatoire de la Côte d'Azur. 8. Utrecht University, Department of Earth Sciences, the Netherlands.

Availability

The datasets used in this study and the GIS shapefiles defining the seismotectonic zoning can be found on the OSU OREME online database under a Licence Creative Commons Attribution 4.0 International (CC BY 4.0):

<https://data.oreme.org/doi/view/dd520135-7656-4e80-91fe-f0284accbc76>

Citation for this report and associated data

Foix, Océane; Mazzotti, Stéphane; Jomard, Hervé (2023). A New Seismic Source Zone Model for Lesser Antilles Seismic Hazard Assessment - Data. OSU OREME. (Dataset). DOI: <https://doi.org/10.15148/dd520135-7656-4e80-91fe-f0284accbc76>

Summary

Seismic hazard levels used as reference for the French Lesser Antilles are derived from probabilistic seismic hazard assessment studies performed in 2002. However, scientific knowledge has greatly increased over the past 20 years in this area, warranting an update of the seismic hazard models. As part of a project linking the French Ministry of Ecological Transition and Territory Cohesion, and the Seismicity Transverse Action of RESIF-EPOS (French seismological and geodetic network), we developed a new seismotectonic zoning model of the Lesser Antilles. The Lesser Antilles tectonic system results from the subduction of the North and South American plates beneath the Caribbean plate since the Eocene. The boundary extends along 850 km with a convergence of 18-20 mm/yr oriented ENE-WSW. Significant north-south variations in tectonics, seismic and volcanic activities highlight the lateral variability of the undergoing geodynamic processes. Oceanic fractures and ridges entering into the subduction zone impact the trench, the subduction interface, and upper plate tectonics, adding seismotectonic complexities. Several controversial questions remain, such as the origins of the 1839 ($M_w=7.5-8$) and 1843 ($M_w=8-8.5$) earthquakes or the state of interseismic coupling of the subduction interface (potentially very low compared to other subduction systems). In this study, we propose new seismotectonic models and associated seismotectonic zoning for seismic hazard. We treat all components of the Lesser Antilles system: subducted oceanic plate, subduction interface, mantle wedge, upper plate crust and associated volcanisms. Our work is based on a compilation of up-to-date seismicity and fault catalogs as well as research-based active tectonic hypotheses, completed by an analysis of focal mechanisms rupture styles and strain tensor derived from geodetic data. Compared to previously published models, our new seismotectonic zoning model provides better depth resolution, a fully revised zoning around Guadeloupe, new mantle wedge and volcanic zones, and a complete redefinition of the subduction interface and slab. Our results also highlight specific needs for better seismic hazard assessment in this region.

Table of Contents

SUMMARY	3
TABLE OF CONTENTS.....	4
INTRODUCTION	5
STUDY FRAMEWORK	5
DEFINITIONS AND CONCEPTS	6
1-SEISMIC AND TECTONIC SETTING OF THE LESSER ANTILLES.....	8
1A-GEODYNAMIC AND TECTONIC SETTINGS	8
1B-PAST AND PRESENT SEISMICITY	13
1C-ZOOM ON GUADELOUPE	16
1D-PREVIOUS SEISMOTECTONIC MODELS	18
2-SEISMOTECTONIC MODELS FOR THE SEISMIC HAZARD ASSESSMENT	19
2A-MATERIALS.....	19
2B-CRUSTAL SEISMOTECTONIC ZONING	21
2C-MANTLE SEISMOTECTONIC ZONING	28
2D-VOLCANIC SEISMOTECTONIC ZONING	31
2E-SUBDUCTION INTERFACE SEISMOTECTONIC ZONING	32
2F-SLAB SEISMOTECTONIC ZONING.....	36
3-BRIEF CONCLUSION ON THE NEW SEISMOTECTONIC ZONING MODEL	39
4-FUTURE NEEDS AND RECOMMENDATIONS.....	40
REFERENCES.....	42
ANNEXES	52

Introduction

Study framework

The work presented in this report follows a request from the *Direction Générale de la Prévention des Risques* (DGPR) of the French *Ministère de la Transition Écologique et de la Cohésion des Territoires* to the *Action Transverse Sismicité* (ATS) of the RESIF-EPOS consortium (French seismological and geodesic network – European Platform Observing System). This request, made in early 2019, aimed at identifying new scientific knowledge that could warrant an update of the seismic hazard calculations for the Lesser Antilles arc. Among the three priorities identified by the RESIF-EPOS ATS (20/08/2019 report), a project was established for the development of a new seismotectonic zoning integrating the most up-to-date geological and geophysical data. The model best characterizes current knowledge on the dynamics of the Lesser Antilles. Adaptations might be necessary in order to simplify it for the seismic hazard assessment calculations.

New and improved data and knowledge of Lesser Antilles system warrants an update of the proposed seismotectonic models (Bertil & Lemoine, 2017). In particular, new understanding has been brought to light regarding slab interface geometry and properties (Bie et al., 2020; Braszus et al., 2021; Laurencin et al., 2018; Paulatto et al., 2017), crustal faults geometries and activities (Boucard et al., 2021; Laurencin et al., 2017), seismicity characteristics and behavior (Bie et al., 2020; Corbeau et al., 2021; González et al., 2017; Massin et al., 2021; Oral & Satriano, 2021), or heat and fluid interactions (Ezenwaka et al., 2022; Harmon et al., 2021; Marcaillou et al., 2021).

The project was conducted through a two-year post-doctoral contract funded by the DGPR, executed by Océane Foix at the Geosciences Montpellier laboratory (Univ. Montpellier, CNRS) in collaboration with the Institute for Radiation Protection and Nuclear Safety (IRSN). During these two years, several researchers working on the Lesser Antilles have been contacted. Regular exchanges as well as work meetings were organized to define the current scientific knowledge and uncertainties concerning the Lesser Antilles geodynamics. The Lesser Antilles Working Group is composed of:

- **BRGM, Orléans:** Didier Bertil, Roser Hoste Colomer, Anne Lemoine & Agathe Roullé ;
- **ENS Paris:** Eric Calais & Elenora van Rijsingen ;
- **Géoazur Nice:** Mireille Laigle & Boris Marcaillou ;
- **Géosciences Montpellier, Guadeloupe:** Jean-Jacques Cornée, Jean-Frédéric Lebrun & Mélody Philippon ;
- **Géosciences Montpellier, Montpellier:** Océane Foix, Serge Lallemand & Stéphane Mazzotti ;
- **IPGP, Paris:** Marie-Paule Bouin, Nathalie Feuillet, Claudio Satriano, Jean-Marie Saurel ;
- **IRSN, Fontenay-aux-Roses:** Hervé Jomard ;
- **IsTerre, Grenoble:** Céline Beauval.

This report is divided in three main sections: (1) the description of the tectonic and seismic behavior of the Lesser Antilles, including historical and more recent knowledge, as well as corresponding interpretations and hypotheses from literature; (2) the description of the proposed seismotectonic zoning models according to literature knowledge and new data analyses, such as stress distribution and geodetic motion, with discussions on their limitations and questioning; (3) important points and recommendations in order to improve the seismotectonic models and to move towards seismic hazard assessment.

Definitions and concepts

Seismotectonic model – includes area whose limits have been determined through a variety of data (historical and instrumental seismicity, regional geology and tectonic styles of deformation, measured or inferred stress and strain, etc.), and fault sources, whose limits have been determined through field mapping, aerial photo and satellite imagery, seismicity studies and geophysical imageries (McGuire, 2004).

Seismotectonic zoning – study of relationship between earthquakes and active tectonics to determine seismotectonic sources:

- **Area sources** – “areas within which future seismicity is assumed to have distributions of source properties and locations of energy release that do not vary in time and space” (McGuire, 2004).
- **Fault sources** – “faults or zones for which the tectonic features causing earthquakes have been identified. They are usually individual faults, but they may be zones comprising multiple faults or region of faulting if surface evidence of these faults is lacking but the faults are suspected from seismicity patterns, tectonic interpretations of crustal strain, and other evidence” (McGuire, 2004).

Lesser Antilles (LA) – we define the LA as the entire tectonic system from the outer-rise region to the backarc area.

Magnitude (M) – depends on the energy released during an earthquake. Several laws were developed depending on the wave type to cover all focal depths. In this study, we will keep our interest in M_w , which is the scale used for hazard studies. M will be used when no information is provided about the used scale.

- **M_L (Richter magnitude)** – logarithm to base 10 of the maximum seismic wave amplitudes.
- **M_b (P-wave magnitude)** – based on maximum P-wave amplitude, generally used at large distances.
- **M_s (S-wave magnitude)** – based on maximum S-wave amplitude.
- **M_d (duration magnitude)** – based on the signal duration of the earthquake.
- **M_0 (seismic moment)** – quantity used to estimate the size of an earthquake from the shear modulus, the rupture area and the average slip.
- **M_w (moment magnitude)** – proportional to the M_0 .

M_{max} – determines the maximum magnitude associated with a fault or an area source.

- **$M_{max.cat}$** – from our seismic catalog.
- **$M_{max.obs}$** – from the literature and not observed in our seismic catalog.
- **$M_{max.struct}$** – estimated from the largest fault geometry of an area using Wells & Coppersmith (1994) scaling law (which is the most common law).
- **$M_{max.proxy}$** – observed worldwide at similar tectonic settings.

Magnitude Frequency Distribution (MFD) – empirical relations to define earthquake occurrence rate for each considered magnitude from a seismic statistical analysis (instrumental and historic), or from fault dimensions and recurrence models (globalquakemodel.org/gem).

Gutenberg Richter distribution (GR) – empirical power law MFD computed for all seismic sources. We divided the GR results into three groups: usable (seismicity in the zone allows computing a robust GR), unusable (seismicity in the zone is not sufficient to compute a robust GR), and “to improve” (catalog improvements could allow computing a robust GR).

Probabilistic Seismic Hazard Assessment (PSHA) – aims to quantify the probability of exceeding given ground-motion levels at specific sites given all possible earthquakes (opensha.org).

1-Seismic and tectonic setting of the Lesser Antilles

1a-Geodynamic and tectonic settings

The Lesser Antilles (LA) geodynamic is resulting from the subduction of the North and South American Plates beneath the Caribbean Plate along 850 km since the Eocene (**Figure 1**). The subducted plates are dated 83-110 Ma (Carpentier et al., 2008). The plate convergence follows the N254°E direction at a rate of 18-20 mm/yr (e.g., DeMets et al., 2010; Symithe et al., 2015). About 1 mm/yr of NS shortening is recorded at the trench between North and South American plates (Patriat et al., 2011a). The convex shape of the LA trench combined with the ENE-WSW convergence direction make the subduction almost arc-perpendicular along the southern and central sections, while it becomes more oblique toward the northern extremity. The obliquity ranges from about 0° in the south to 75° in the north. The subduction is bounded to the north by the Anegada Passage, characterized by an EW left-stepping *en échelon* strike-slip system (e.g. Laurencin et al., 2017) and to the south by the right-lateral El-Pilar strike-slip fault (e.g. Mann et al., 1991). To the west, the LA is bordered by the Grenada basin that separates the volcanic arc from the Aves ridge considered as remnant of the Cretaceous-Paleocene ‘Great Arc of the Caribbean’ (Burke, 1988). To the east, numerous fracture zones and aseismic ridges enter the subduction, deforming the trench and affecting sediment distribution in the accretionary wedge (e.g., Pichot et al., 2012 and references therein). The slab geometry and Wadati-Benioff zone thickness vary significantly (Bie et al., 2020). Their variations have been attributed to the subduction of the fractures (Bie et al., 2020; Schlaphorst et al., 2016) or the presence of a slab tear (Bie et al., 2020; Schlaphorst et al., 2017; van Benthem et al., 2013).

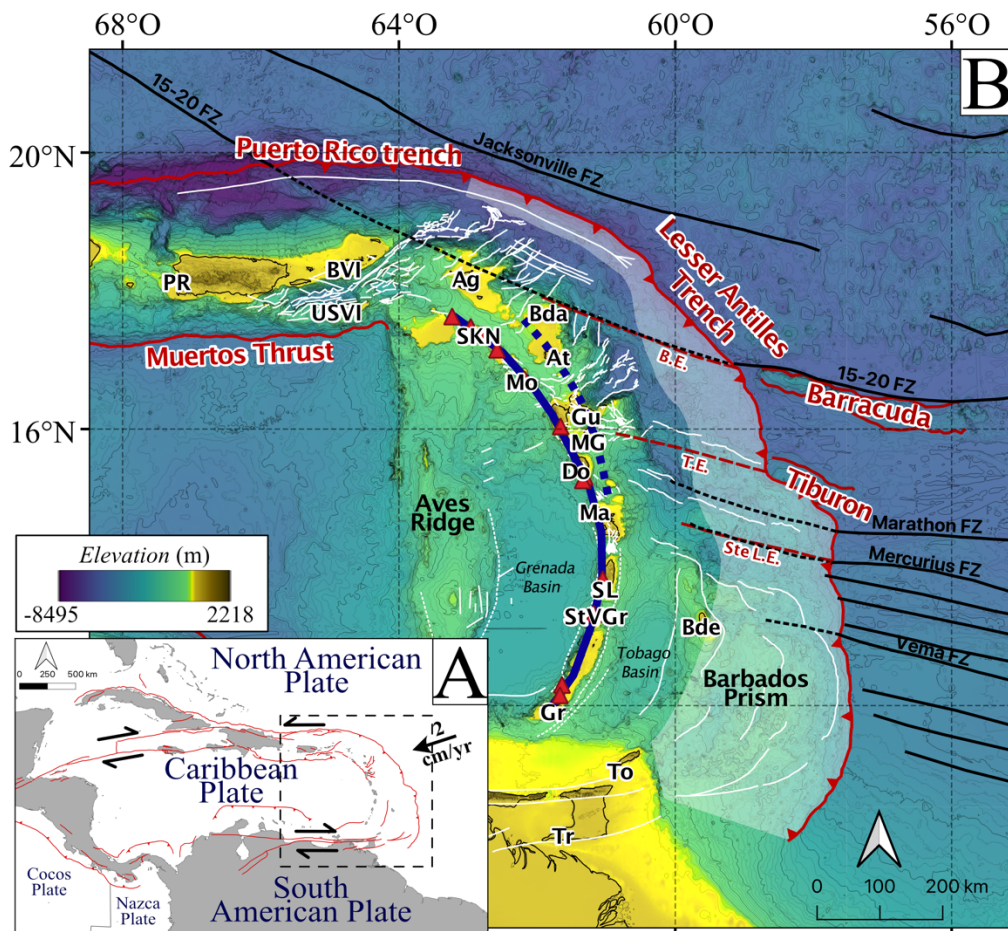


Figure 1: Overview of the Lesser Antilles geodynamic system. **A:** inset of the Caribbean region, arrows indicate global plate motions; dashed square reports to **B**; red lines: main fault structures from Global Earthquake Model (GEM). **B:** main structural features of the LA; white area: accretionary wedge; red triangles: active volcanoes; thick blue line: active volcanic arc; thick

blue dashed line: inactive volcanic arc; FZ: fracture zones; black lines: FZ; black dashed lines: subducted FZ; white lines: crustal faults; red lines: ridges; red dashed lines: subducted ridges; *StL.E.*: Saint-Lucia ridge Extension, *T.E.*: Tibubon ridge Extension, *B.E.*: Barracuda ridge Extension, *PR*: Puerto Rico, *BVI*: British Virgin Islands, *USVI*: United States Virgin Islands, *Ag*: Anguilla, *Bda*: Barbuda, *SKN*: Saint-Kitts-and-Nevis, *At*: Antigua, *Mo*: Montserrat, *Gu*: Guadeloupe, *MG*: Marie-Galante, *Do*: Dominique, *Ma*: Martinique, *SL*: Saint-Lucia, *StVG*: Saint-Vincent-and-Grenadines, *Bde*: Barbade, *Gr*: Grenade, *To*: Tobago, *Tr*: Trinidad. Faults are from Feuillet et al. (2001, 2002, 2004, 2011a and b), Leclerc et al. (2016), Laurencin et al. (2017, 2019), Boucard et al. (2021), Garroq et al. (2021). FZ were extracted from Global Seafloor Fabric (soest.hawaii.edu) and bathymetry from Global Multi-Resolution Topography (gmrt.org).

To a first order, the GPS velocities show very small relative motions of the arc with respect to the Caribbean Plate (Manaker et al., 2008; Symithe et al., 2015; van Rijsingen et al., 2021). To a second order, they indicate a small (< 1 mm/yr) component of arc-parallel motion that may be indicative of intra-arc extension (van Rijsingen et al., 2021) with the northern segment (Guadeloupe to Virgin Islands) moving northwest and the southern segment (Guadeloupe to Grenada) moving south (**Figure 2**). Note that these velocities with respect to the Caribbean Plate are often within their 95% error ellipse.

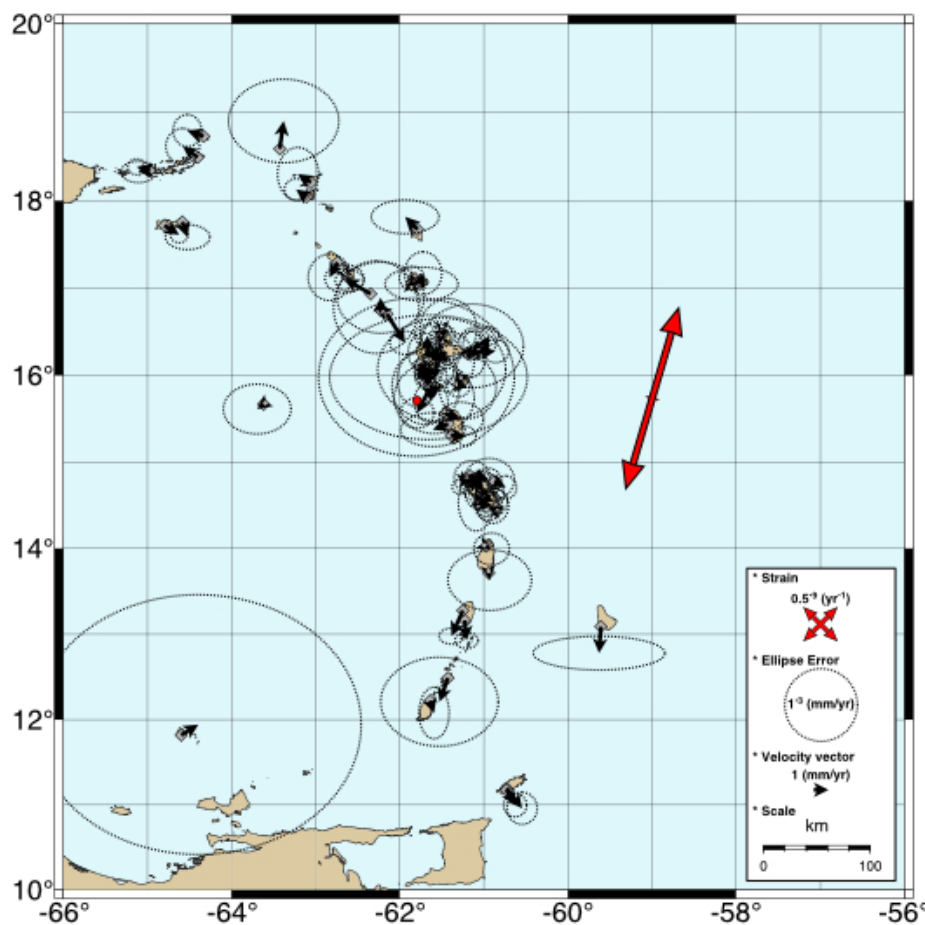


Figure 2: GPS vector velocities (black arrows) along the Lesser Antilles arc, in the Caribbean reference frame. Geodetic velocities were provided by van Rijsingen et al. (2021). Black circles are error ellipses with 95% confidence. Red arrows are the strain through the arc, and the red dot is the original location of the strain arrows. Strain values: $e1 = 2.1 \cdot 10^{-9} \pm 1.10^{-11} \text{ yr}^{-1}$; $e2 = -0.6 \cdot 10^{-9} \pm 1.10^{-11} \text{ yr}^{-1}$.

Three oceanic ridges are interacting with the subduction dynamic. Sainte-Lucia is a buried ridge identified by seismic reflection beneath the Barbados accretionary wedge (Westbrook et al., 1982). The Tiburon rise is 150 km long by 30 km wide, cutting the trench with ESE-WNW orientation, producing a positive free-air gravity anomaly of 70 mGal (Pichot et al., 2012). The Barracuda ridge is 450 km long by 40 km wide, cutting the trench with a 288° azimuth orientation (Peter & Westbrook, 1976), producing a positive free-air gravity anomaly of 80 mGal (Pichot et al., 2012). Roest & Collette (1986) interpreted the Barracuda ridge and trough as the continuation of the Fifteen-Twenty fracture zone. The Barracuda and Tiburon ridges were likely generated at the Mid Atlantic Ridge along transform faults (Westbrook et al., 1984).

Harmon et al. (2019) suggest an extension of Tiburon and Barracuda ridges beneath the accretionary wedge. The limit between the South and North American Plates has been proposed to be located between these two ridges, as diffuse plate boundary (Patriat et al., 2011b), which also separates the Proto-Caribbean (south) and Equatorial Atlantic (north) lithospheres (Braszus et al., 2021; Cooper et al., 2020). Fracture zones and ridges of the slow-spreading American Plates may affect the plate interface seismogenic behavior through fluid circulation and pore pressure (Bie et al., 2022; Ezenwaka et al., 2022; Harmon et al., 2019; Marcaillou et al., 2021).

The arc, forearc and accretionary wedge morphologies are characterized by a strong NS dissymmetry (**Figure 1**), also observed on seismic activity (**section 1b**):

- South of 15° of latitude, the volcanic arc is located at about 400 km from the trench, bordered to the east by the Tobago forearc basin and the 240 km wide, 15 km thick Barbados accretionary wedge (Speed & Larue, 1982). The slab dip beneath the forearc is about 10° (Bie et al., 2020). The accretionary wedge is marked by thrust faults, and the arc fault spatial distribution is not well known.
- North of 15° of latitude, the volcanic arc is separated in two alignments north of Martinique island (thick solid and dashed blue lines in **Figure 1**). The western line marks the continuity of the active volcanic arc located at about 250 km from the trench, whereas the eastern line marks the outer arc, composed of extinct volcanic edifices (Bouysse et al., 1990 and references therein). The accretionary wedge varies from 100- to 40-km-wide, with a trench fill thickness lower than 500 m (Laigle, Becel, et al., 2013). The thin sedimentary fill combined with the rough topography of the north American Plate favor a long-term margin erosion (Boucard et al., 2021). The slab dip beneath the forearc is about 15° (Bie et al., 2020). The forearc is affected by several deep V-shaped basins controlled by NE-SW normal faults perpendicular to the trench (Boucard et al., 2021; Feuillet et al., 2002). The arc is shaped by normal to strike-slip/normal faults parallel to the trench (Feuillet et al., 2011 and references therein).

The arc and inner forearc crustal thickness have been estimated to about 28±7 km along the arc (Bie et al., 2020; Kopp et al., 2011; Laigle, Hirn, et al., 2013), with value ranging from 20 to 24 km in the south (Christeson et al., 2008; Padron et al., 2021), and 28 km in the central area (Paulatto et al., 2017).

From east to west, the forearc region stress is influenced by the along-arc bending and oblique subduction, while the arc and back-arc regions stress is characterized by trench-perpendicular extension possibly reactivating structures formed during the back-arc opening (Allen et al., 2019; Lindner et al., 2023).

From north to south, the fault kinematics identified and the relationships between faults and crustal seismicity are not obvious, and are still debated. In the north area (**Figure 3b**), the Anegada Passage (AP) (**Figures 3a (5) and 4**) is interpreted as part of the Puerto Rico Virgin Islands microplate (Byrne et al., 1985; Mann et al., 1995). Relatively low motion was recorded by geodesy at its eastern limit (Symithe et al., 2015). Various interpretations were given on the AP fault system activity from extensional faulting to sinistral or dextral transtension (Feuillet et al., 2002; Jany et al., 1990b; Mann et al., 1991). Laurencin et al., (2017) investigated the region with new bathymetric imagery and concluded that the 450-km-long and N54° AP fault system presents a main EW trending left-stepping *en échelon* strike-slip motion.

At the eastern AP, the 87-km-long, 25-km-wide Sombrero Basin (**Figure 4**) is interpreted as a pull-apart basin bounded by normal and strike-slip transtensive faults (Laurencin et al., 2019).

To the northeast of the AP, the Bunce Fault (**Figure 4**) is described as a steep subvertical 535-km-long fault, reaching 5 km at depth, with a sinistral strike-slip component (Laurencin et al., 2019). The Bunce Fault is connected to the west to the strike-slip Bowin Fault (Grindlay et al., 2005) and marks the limit between the backstop and the thin accretionary wedge. Its existence may reveal a partitioning motion induced by the strong subduction obliquity (Laurencin et al., 2019). From seamount deformation, the authors estimate a maximum slip rate of about 1.6 ± 0.2 cm/year on the Bunce Fault. The fault is potentially able to generate moderate size earthquake because of its only 5 km depth roots and may rupture partially consolidated accretionary sediments (U. ten Brink & Lin, 2004).

From La Désirade (Guadeloupe) to Anguilla islands, the forearc is marked by V-shaped basins formed during the Paleogene and resulting from the collision of the Bahamas Bank against the northeastern Caribbean Plate (Boucard et al., 2021). At the northern end, the normal faults that flank the basins are sealed and are crosscut by the normal Tintamarre Faults (**Figures 3a (2) and 4**). The Tintamarre Faults mark the margin erosion and subsidence occurring since the mid-Miocene (Boucard et al., 2021). Seismic imagery indicates fault deep roots, possibly down to the subduction interplate contact (Boucard et al., 2021).

In the central area (**Figure 3b**), the arc and forearc are marked by series of trench perpendicular and parallel normal faults (Feuillet et al., 2001, 2002). The first set of faults bounds grabens and spurs oriented perpendicular to the trench, such as the Marie-Galante graben or the Bertrand-Falmouth spur system, indicating a NS to NNW-SSE extension (**Figure 6**). The second set shapes an *en-échelon* system of normal faults located roughly along the active volcanic arc. These faults are parallel to the trench, and may accommodate a sinistral motion north of Guadeloupe as the Montserrat fault, or a strict normal motion as the Roseau fault (Feuillet, Beauducel, & Tapponnier, 2011; Feuillet et al., 2001). Several historical and instrumental earthquakes have ruptured these systems with magnitude greater than 5.5 (**sections 1b and 1c**). Feuillet, Beauducel, & Tapponnier, (2011) and Feuillet et al. (2001) proposed that these series of faults are related to regional strain partitioning, with V-shaped basins, induced by the increase of plate motion along the curved trench and accompanied by a strike-slip system (trench-parallel *en-échelon* faults). However, this hypothesis remains debated as the V-shaped basins mostly opened when the subduction was supposed to be linear, during the Oligocene, and appear inactive nowadays (Boucard et al., 2021; Smithe et al., 2015). Seismic imagery also highlighted ridge-parallel intra-crustal reverse faults above Barracuda and Tiburon ridges extents, possibly rooting down to the subduction interplate contact resulting in localized outer forearc basement highs (Laigle, Becel, et al., 2013).

In the south area (**Figure 3b**), knowledge about fault systems south of Sainte-Lucie is sparse. The possible extension of the *en-échelon* trench-parallel faults is unknown (Feuillet pers. comm.). Christeson et al. (2008) and Aitken et al. (2011) interpreted large-offset normal faults along both flanks of the LA volcanic arc. They interpreted these faults as a consequence of uplift induced by magmatism intrusion through the thinned Paleogene basins of Grenada and Tobago. However, based on deep-penetrating multichannel seismic reflection data, no evidence of these large normal faults was found (Garrocq, 2021; Garrocq et al., 2021). The seismic profiles indicate possible normal faults along the west flank of the LA volcanic arc, between Saint-Vincent-and-the-Grenadines and Sainte-Lucie, and subvertical faults, possibly normal to strike-slip, similar to north of Martinique. This deformation may be more related to the present-day tectonic context. Further south, the Tobago terrane marks the edge of the Caribbean Plate and is bounded by the North Coast fault (Christeson et al., 2008). The major transition between

the northern and southern tectonic areas is marked by lateral ramps that follows the Barracuda and Tiburon ridges trend (e.g., Brown & Westbrook, 1987).

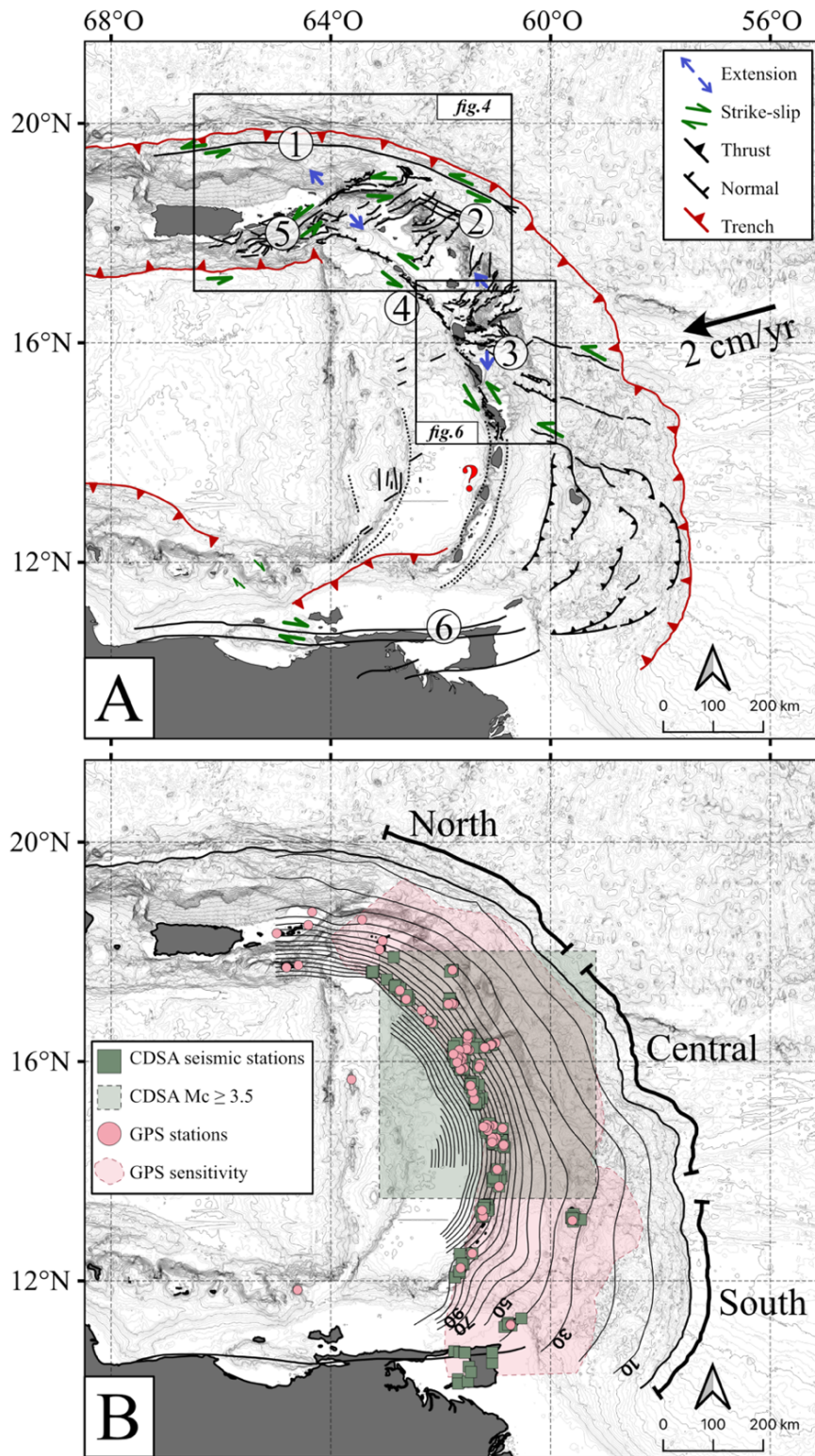


Figure 3: Crust faults, subduction interface geometry and instrument sensitivities. **A:** crustal faults and interpreted fault relative motions; faults and relative motions are extracted from Boucard et al. (2021); Feuillet, Beauducel, & Tapponnier (2011); Feuillet, Beauducel, Jacques, et al. (2011); Feuillet et al. (2001, 2002, 2004); Garrocq et al. (2021); Laurencin et al. (2017, 2019); Leclerc et al. (2016) and the dot black lines are normal faults proposed from (Aitken et al., 2011; Christeson et al., 2008); black squares highlight zooms available on **Figure 4**; (1) Bunce fault, (2) Tintamarre faults, (3) Marie-Galante

graben, (4) Montserrat-Bouillante fault, (5) Anegada passage fault system, (6) El Pilar fault system. **B**: slab geometry and GPS (Global Positioning System) and seismic stations locations and sensitivities; thin black lines are the unified slab top from Bie et al., (2020) and Laurencin et al., (2018) constructed for this study, with depth indicated every 20 km from 10 to 90 km depths; GPS stations sensitivity is from van Rijsingen et al. (2021) for $\log(\text{sensitivity}) \geq 0.5$; seismic stations used for the CDSA catalog indicate a magnitude of completion (M_c) of 3.5 (Massin et al., 2021).

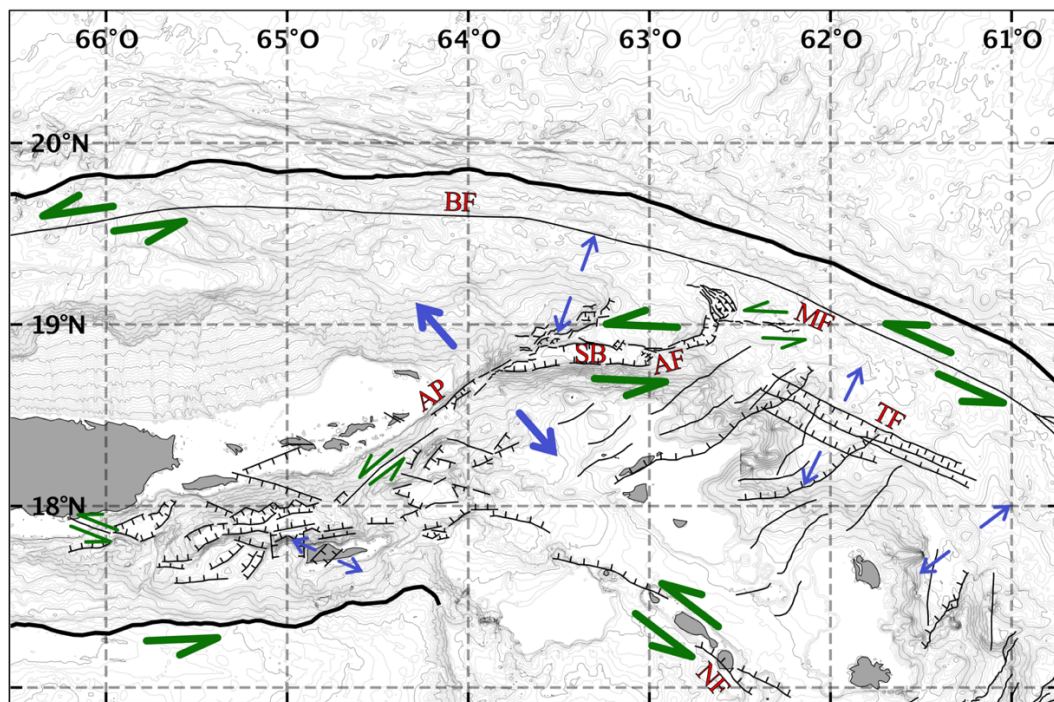


Figure 4: Crustal fault systems and relative motions summary of the northeastern Lesser Antilles extracted from Laurencin et al. (2019) and references therein. Blue arrows are relative to extension and green arrows to strike-slip motions. BF: Bunce Fault. AP: Anegada Passage fault system. SB: Sombrero Basin. MF: Malliwana Fault. AF: Anguilla Fault, located between the Sombrero basin to the west and the Malliwana basin to the east. TF: Tintamarre Faults. NF: Nevis Fault.

1b-Past and present seismicity

Instrumental and historical studies along the LA reveal significant seismic activity along the entire system, slightly higher in the central and north areas, above 15°N (Hayes et al., 2014; McCann et al., 1984). Only a few damaging earthquakes were reported until the 19th century, but several events had estimated magnitudes exceeding 7, such as the April 5, 1690 event in Nevis, the February 8, 1843 in Guadeloupe, or the November 18, 1867 in the Virgin Islands (**Figure 5**). Recently, the $M_w=7.4$ event on November 29, 2007 generated minor damage in Fort-de-France (Régnier et al., 2013). This event likely broke an oblique normal fault within the subducted slab at about 152 km depth (Bouin et al., 2010). Relocation with dense sea-bottom seismometers (OBS) revealed a dip-parallel extension mechanism interpreted as being associated with a potential slab tear (Laigle, Hirn, et al., 2013). In the last century, few events exceeded M_7 according to USGS (United State Geological Survey):

- 1914 Oct.3, near Guadeloupe, $M_w=7.0$
- 1953 Mar. 19, south of Martinique, $M_w=7.3$
- 1969 Dec. 25, near Barbados, $M_w=7.2$
- 1974 Oct. 8, between Barbuda and Antigua, $M_w=7.5$
- 2007 Nov. 29, below Guadeloupe at 128.8 km depth, $M_w=7.4$

Two major earthquakes were reported in the 19th century. The first occurred on January 11, 1839, which destroyed Fort-de-France, occurred offshore Martinique, with a magnitude estimation of about $M_w=7.5-8$. The second on February 8, 1843, which destroyed Pointe-à-Pitre, occurred close to Guadeloupe with a magnitude estimation of about $M_w=7.5-8.7$

(Bernard & Lambert, 1988; Feuillet et al., 2011; Ten Brink et al., 2011; Hough, 2013). The exact locations of these events are debated. Bernard & Lambert (1988) and McCann et al. (1984) interpreted them as megathrust earthquakes, despite the absence of large tsunami or significant vertical deformation of the coast. van Rijnsingen et al. (2021) proposed that the 1843 event had a smaller magnitude, or different mechanism or location within the subducted slab, and that the 1839 event could also be located in the subducted slab (similar to the $M=7.5$ in 1953 or the $M=7.4$ in 2007).

Recent geodetic data highlight a very low interseismic coupling of the seismogenic portion of the subduction interface (van Rijnsingen et al., 2021, 2022), which, depending on interpretations, may only allow for one earthquake $M_w=8$ every 2000 years (Symithe et al., 2015). van Rijnsingen et al. (2022) observed subsidence from geodetic vertical motions, in coherency with coral and atoll data (Philibosian et al., 2022). While Philibosian et al. (2022) proposed that the deep portion of the subducting interface is affected by strong interseismic coupling to explain the subsidence, van Rijnsingen et al. (2022) recent geodetic observation exclude an interface coupling. These interpretations and its implications are discussed in more details in the subduction interface zoning (**section 2e**).

Lindner et al., (2023) investigated 151 focal mechanisms solution (FMs) to invert for stress regime in the LA from an offshore deployment of 14 months in 2016-2017. They observed: 1) typical compression on the plate interface, 2) dominant slab perpendicular extension at 100-200 km depth, beneath the central part of the arc, and 3) strike-slip and extension in the upper-plate northern area (north of Guadeloupe) changing to near arc-perpendicular extension to the south (west of Guadeloupe and south). The megathrust seismic slip is highlighted by thrust-fault earthquakes at depths shallower than 50 km and events are becoming more frequent towards the trench (Lindner et al., 2023). North of Guadeloupe and east of Martinique, most events are located in the 1839 and 1843 estimated rupture areas (González et al., 2017; Lindner et al., 2023). This megathrust activity is lacking in the south where no shallow events are recorded near the trench, but also between $\sim 15^\circ\text{N}$ and $\sim 16.5^\circ\text{N}$ (Lindner et al., 2023). Dense offshore deployments over the forearc domain in 2007 revealed interplate seismicity clusters offshore northern Martinique island with thrust mechanisms down to 45 km depth, but almost no event at depths shallower than 20 km (Laigle, Hirn, et al., 2013; Ruiz et al., 2013).

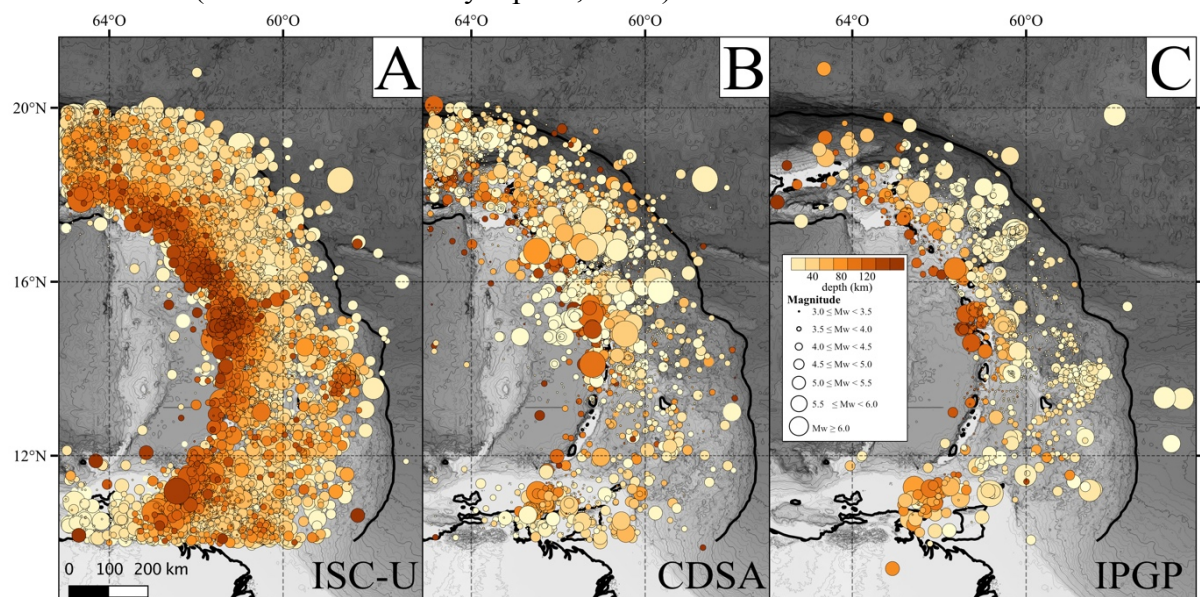
At depths greater than 100 km, most of the intraslab seismicity is generated by normal or strike-slip faults, related to processes within the subducted slab (González et al., 2017). Abundant seismicity is observed between the Martinique and Dominique islands, possibly associated with the Marathon or Marcurius fracture zone, and host the majority of strong deep earthquakes (Bie et al., 2020; Lindner et al., 2023). The 2007 $M_w=7.4$ event is the largest of this group and the LA strongest instrumentally measured. Below the central LA area, at depths around 170-200 km, Lindner et al. (2023) observed a seismic gap within the subducted American Plates lithosphere, where Braszus et al. (2021) observed a continuous slab, in accordance with Bie et al. (2020) tomography.

Seismic activity of the Caribbean upper-plate crust shows a strong variability along the arc, where normal faulting dominates (**Figures 3a and 5**). From FMs, Lindner et al. (2023) observed a transitional regime in the north and central areas, with normal to strike-slip faulting as attested by shallow seismicity along the arc-parallel and -perpendicular faults. North of Martinique ($14.5\text{-}15^\circ\text{N}$), the seismicity rate is higher than to the south, especially for events with magnitude greater than 5 (**Figure 5**). Some of these faults have produced disastrous event, such as the 1867 earthquake $M_s=7.5$, located at the Virgin Islands (McCann et al., 1982). In the central area,

high normal-faulting activity is observed between Guadeloupe and Dominique. This seismicity includes the shallow 2004 $M_w=6.3$ Les Saintes earthquake, which ruptured the Roseau fault, revealing arc-perpendicular extension (Feuillet, Beauducel, Jacques, et al., 2011). Towards the south, large-magnitude events are scarce and the deformation regime is characterized by arc-parallel extension, interpreted as the result of the tight arc curvature (Lindner et al. (2023)).

Pervasive seismicity is observed in the cold mantle wedge (Bie et al., 2020; Laigle et al., 2013; Ruiz et al., 2013). Laigle et al. (2013) interpreted this seismicity as “supraslab” earthquakes, as observed in Japan (Uchida et al., 2010), and is characterized by normal-faulting focal mechanisms. This type of seismicity is questioned as the upper plate mantle is supposed to be composed of serpentinized peridotite, which should favor aseismic fault behavior. Laigle, Hirn, et al. (2013) proposed that, because the Caribbean Oceanic Plateau upper plate was formed by a mantle plume, the corresponding mantle could have been modified and may include pyroxenitic material within peridotites. Modelled temperature at this location also suggests that supraslab seismicity could also be related to dehydration embrittlement due to deserpentinization reaction in the serpentinized mantle wedge, as invoked beneath northeast New Zealand (e.g. Davey & Ristau, 2011). Recent seismic imageries highlight a cold and stagnant mantle wedge, where fluids expelled from slab favor for abundant seismicity in the LA mantle wedge (Hicks et al., 2023). Only few other subduction zones present mantle wedge seismicity as Japan, New-Zealand or Greece. Authors interpreted them as the deformation of subducted seamount (Uchida et al., 2010) or fracturing due to fluid paths and pressure.

In association with upper plate deformation induced by the subduction active system, the LA is subject to numerous volcanic eruptions (**Table 2**). Sixteen seismo-volcanic crises have been reported between 1530 and 1960 (Robson, 1964). Five led to eruptions: the Soufriere of St. Vincent (1812, 1902), the Mt. Pelée (1902, 1929) and the Soufriere of Guadeloupe (1956) (Robson & Tomblin, 1951). The 1950-51 Nevis crisis was responsible for building damages, with the largest earthquake of $M_w=4.3$ (ISC catalog) and intensity VIII (Willmore, 1952). Montserrat was also struck in 1897-98 and 1933-37 (Shepherd et al., 1971). The 1966–67 Montserrat volcano-seismic crisis was marked by 32 felt earthquakes. Unfortunately, no seismographs were installed at that time in or near the island (Shepherd et al., 1971). Since 1960, several eruptions have struck the LA active volcanic arc, leading sometimes to significant seismic event such as the $M=4.6$ earthquake of the 1976-77 La Soufrière Guadeloupe seismo-volcanic crisis (Smithsonian monthly reports, IPGP).



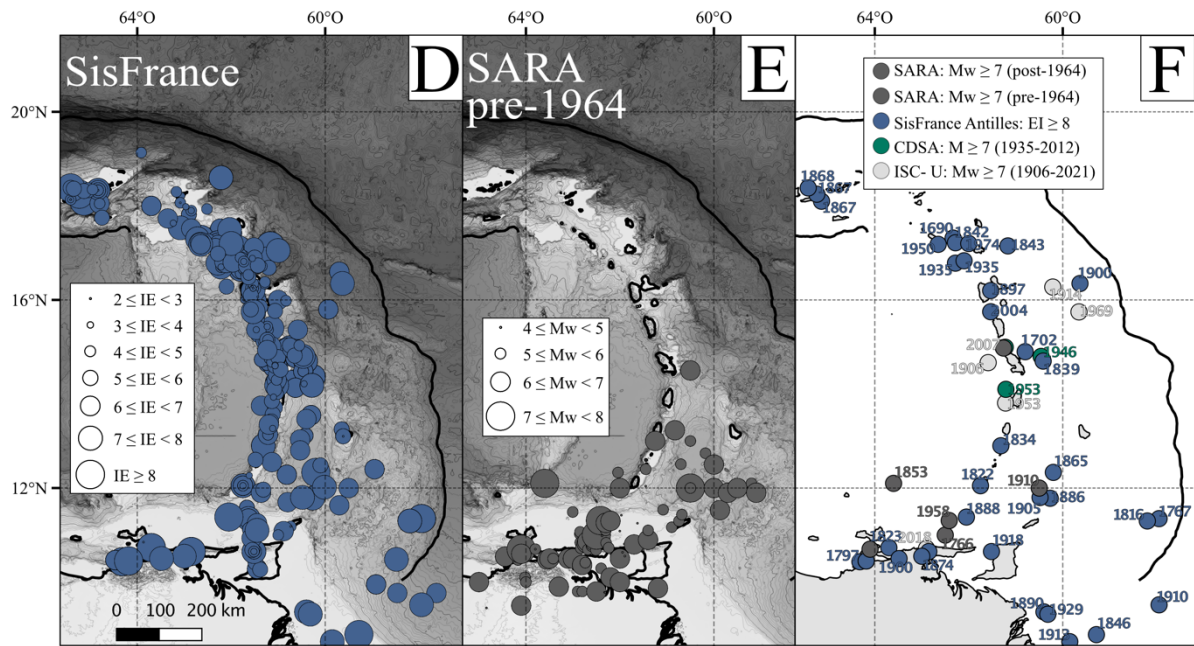


Figure 5: Historic and instrumental seismicity of the Lesser Antilles. Thick black lines mark the Lesser-Antilles, Puerto-Rico and Muertos trenches. **A:** ISC-U catalog instrumental seismicity introduced in section 2a. **B:** CDSA catalog instrumental seismicity (Massin et al., 2021). **C:** IGP catalog instrumental seismicity (Saurel et al., 2022). **D:** SisFrance Antilles historic seismicity (Lemoine pers. comm.). **E:** SARA pre-1964 historic seismicity (Gómez-Capera et al., 2017). **F:** significant instrumental and historic earthquakes.

1c-Zoom on Guadeloupe

The central LA area has been intensively investigated inducing a higher amount of knowledge compare to remaining arc. Here, we proposed a specific focus on Guadeloupe. We currently lack the same level of information to be able to deliver the same approach on Martinique.

The Guadeloupe area is affected by several set of active faults described by Feuillet, Beauducel, & Tapponnier (2011); Feuillet, Beauducel, Jacques, et al. (2011); Feuillet et al. (2001, 2002, 2004); Leclerc et al. (2016). A zoomed view is presented in **Figure 6**. A first set of faults is oriented $N40\pm 20^\circ E$ and is defined as the Bertrand-Falmouth graben. The Grande-Vigie fault is part of this system and exhibits a 40-m-high cumulative scarp. The second set cuts the south of Grande-Terre and Marie-Galante, and marks the Marie-Galante Graben (MGG). South of Grande-Terre, the EW-striking faults show a southward dip. The Gosier Fault is part of this system and is marked by a 40 to 60-m-high cumulative scarp. The 1897 earthquake (EI=VIII) was inferred to be linked to the Gosier fault with $M_w=5.5$ or Montserrat fault with $M_w=6.5$ (Bernard & Lambert 1988; Feuillet et al. 2011). To the south, the MGG faults are characterized by an opposite vergence, northward dip, and cut Marie-Galante Island. The main structure is named the Morne Piton fault (MPF), with 130-m-high cumulative scarp and a total length of about 80 km for minimum depth of 15-km and could be responsible for the 1851 earthquake (EI=VII) (Feuillet et al. 2011). The MPF presents five segments of 5 to 15 km-long with 75° dip with an estimated slip rate of 0.2 ± 0.05 mm/year (Philippon et al., under review). Feuillet et al. (2004) highlights that these characteristics are compatible with potential $M=6.5$ earthquakes every 1400 to 3300 years, or with a $M=5.5$ every 400 to 1000 years (e.g., the events of May 16, 1851 and August 5, 1992). The MGG supposedly generated three historical earthquakes in the last 150 years, with intensity from VII to VIII, including the destructive April 29, 1897 earthquake, with $M=5.5-6$, located closed to Pointe-à-Pitre (Bernard & Lambert, 1988). To the east, the MGG extends to the Karukera spur and cuts the associated arc-parallel

normal faults. To the west, the MGG cuts the Basse-Terre volcanic complex to merge, at sea, with the arc-parallel faults.

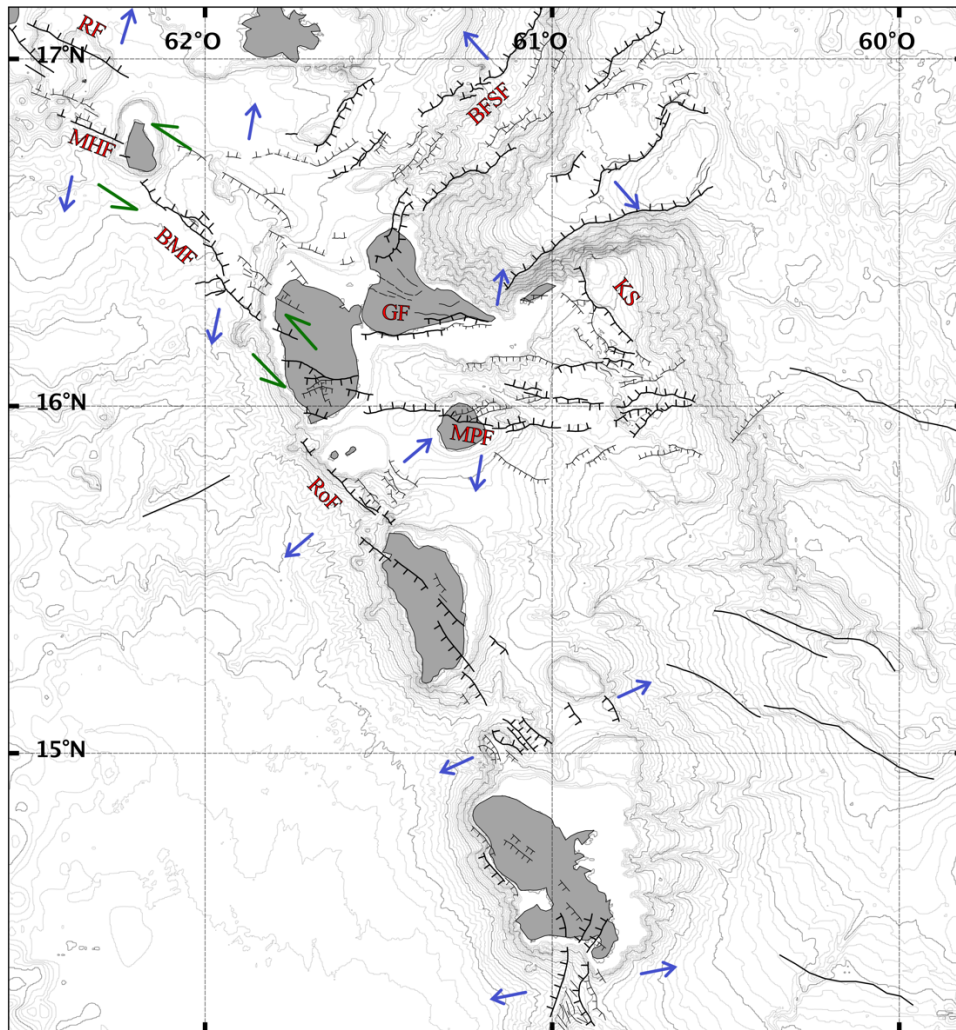


Figure 6: Guadeloupe to Martinique fault systems and relative motions summary extracted from Feuillet, Beauducel, & Tapponnier (2011) and Leclerc (2014). Blue arrows are relative to extension and green arrows to strike-slip motions. RF: Redonda Fault. MHF: Montserrat-Harvers Fault. BMF: Bouillante-Montserrat Fault. RoF: Roseau Fault. GF: Gosier Fault. MPF: Morne-Piton Fault. KS: Karukera Spur. BFSF: Bertrand-Falmouth Fault System.

The arc-parallel *en-échelon* faults system was responsible for large earthquakes such as the Nevis March 16, 1985, $M_s=6.3$ (Girardin et al., 1991) and Les Saintes November 21, 2004, $M_w=6.3$ (Feuillet, Beauducel, Jacques, et al., 2011) earthquakes. West of Marie-Galante, the Roseau Fault borders the Les Saintes graben and was responsible for the 2004 Les Saintes event. The fault is about 35-km-long and is marked with a 120-m-high cumulative scarp, except in its center where the fault is divided in three smaller segments with respectively 40, 10 and 40 m cumulative scarps (Leclerc et al., 2016). The Roseau fault is oriented $N135^\circ E \pm 15^\circ$, with an average dip of 50° northeastward. The 2004 earthquake reveals that the fault accommodates a normal motion. Its associated antithetic faults are 2 to 10-km-long (Feuillet, Beauducel, Jacques, et al., 2011). A rupture of the entire Roseau fault system could induce a $M_w=7$ event (Leclerc et al., 2016). Based on morphotectonic and geological analyzes of Les Saintes volcanic system, Leclerc et al. (2016) proposed a minimum slip rate of 0.15 mm/year and a maximum of 0.4 mm/year. No recurrence time is available, however, following scarp observations on the

seafloor, 2 to 3 ruptures prior to the 2004 Saintes earthquake were identified. Work is in progress to analyze associated turbidites (Feuillet pers. comm.).

North of the Roseau fault, the arc-parallel *en-échelon* faults system is marked by the Bouillante-Montserrat System (BMS). The BMS is composed of several *en-échelon* oblique faults that accommodate a sinistral motion component. Faults are 10 to 20-km-long, oriented $N130^{\circ}E \pm 20^{\circ}$, with a northeast dip, up to Basse-Terre, Guadeloupe (Feuillet et al., 2001). The 1985 $m_b=6.3$ and 1986 earthquakes were located close to the BMS. From the Kahouane volcano, located in the Bouillante-Montserrat basin, Carey et al. (2019) determined a subsidence rate of 0.2 mm/year. The authors proposed that 0.16 mm/yr correspond to tectonic subsidence and 0.03 mm/yr to regional subsidence. This 0.16 mm/year tectonic subsidence occurring on the graben corresponds to ~ 0.1 mm/year of horizontal extension and ~ 0.2 mm/year of slip rate for the BMS (assuming a standard 60° fault dip).

1d-Previous seismotectonic models

Continental scale seismotectonic models and probabilistic seismic hazard assessment (PSHA) have been proposed for the Caribbean region (e.g Zimmerman et al., 2022 and references therein; Pagani et al., 2020). These large-scale analyses of the Caribbean region may miss essential details for a LA and French islands. The last study dedicated to the LA, on behalf of the French government, was conducted by Geoter (2002). Geoter (2002) proposed a seismotectonic crustal deformation model divided into 21 area sources (down to a uniform 30 km depth) and a seismotectonic subducting plate model divided into 20 or 14 area sources (down 210 km depth). Two fault sources, the Marie-Galante and Gosier fault systems, were included. Shepherd & Lynch (2003) updated seismic hazard maps of the LA to be consistent with the requirement of the International Building Code. The following update was proposed by Bozzoni et al. (2011) who developed PSHA maps for the eastern Caribbean islands based on Cornell-McGuire seismogenic sources and the zone-free (or zoneless) methods. In this study, 15 seismogenic sources are divided into six upper-crustal and crustal sources, five interface sources, two intraplate sources, and two transition sources. The upper sources characterize the volcanic arc, the shallow crustal and interface activity down to 50 km depth. The deepest sources characterize the intra-plate activity of the subducting plate, from 50 to 200 km depth. The resulting seismic hazard estimations are systematically higher than previous studies of Shepherd & Lynch (2003) and Lynch (2005). In the light of new and improved data and knowledge of LA we propose new seismotectonic models exposed in the next sections.

2-Seismotectonic models for the seismic hazard assessment

In this section, we present our proposed seismotectonic models, based on published research (**sections 1a to 1c**) and combined with geodetic and focal mechanism information as well as unpublished data (**section 2a**).

The seismotectonic model is used to defined seismotectonic zoning composed of area sources and/or fault sources. Their geographical limits are meant to indicate significant spatial variations in tectonic and seismicity characteristics. The overall approach chosen in this work is based on three principles that consider existing information and associated uncertainties:

- We prefer one large zone over several small ones unless small zone distinctions are clearly warranted by local complexities.
- When appropriate, we divide and adjust zone limits to avoid dilution of seismicity in very large zones.
- We prioritize data in the following order: (1) seismicity, (2) faults and local tectonics, (3) geodesy, (4) structure and local geology.

For each source, we determine the earthquake magnitude-frequency distributions and seismic moment rates. We used the maximum likelihood estimation method of Weichert (1980) for different completeness periods and maximum magnitudes for the ISC-cat data. The earthquake magnitude-frequency distributions are discussed on Foix et al. (in prep.) and results are added in annexes of this report. An overview of the proposed area sources and corresponding characteristics is also provided in annexes (**Annex tables 1 to 6**).

In order to avoid biases in regional earthquake completeness, we put higher emphasis on *CDSA-cat* and *ISCU-cat* of magnitudes $M \geq 4$ (**section 2a**). Most of the characteristics were already exposed in **sections 1a** and **1b**, and additional references are given when needed.

2a-Materials

To define and characterize seismotectonic area sources, we treated and analyzed published and unpublished data up to 2022. In this section, we describe the materials used to develop the proposed models and we briefly expose the methods used to treat a part of the data. Instrumental and historic seismicity catalogs are mostly used for earthquake locations and depth information when available, not so much for magnitudes.

Instrumental seismicity

- The Antilles Seismological Data Center (CDSA) catalog aims to produce a unified catalog of known earthquakes from 1972 to 2012 (Bengoubou-Valerius et al., 2008; Massin et al., 2021). Hypocenters were evaluated and preferred location results were selected, building a 46,703 earthquakes catalog named *CDSA-cat* in this report. Volcanic earthquakes are not contained in the catalog. Magnitudes are estimated in M_L . According to seismometer and island locations, the magnitude of completeness for the seismically active crust is $M_c=3.2$, $M_c=2.7$ for Guadeloupe and Martinique and $M_c=3.5$ for the slab (Massin et al., (2021) for details on the catalog completeness). Geographical distribution is reported on **Figure 5b**.
- The IPGP catalog aims to complete the CDSA project up to present day, using data from the Guadeloupe and Martinique French observatories (Saurel et al., 2022). Magnitudes are estimated in M_d and M_L . The catalog is still under progress, and from now, it is composed of 13,220 events from 2014 to 2019. The catalog is named *IPGP-cat* in this report. Geographical distribution is reported on **Figure 5c**.

- The International Seismological Center (ISC) catalog was extracted and unified in Mw magnitude by Didier Bertil (BRGM). This unpublished catalog contains events from 1906 to 2021, incomplete before 1964, with magnitudes $M_w \geq 3$. It is named *ISC-cat* in the report. The Mw homogenization was done using reference magnitudes given by GCMT (Global Centroid Moment Tensor Project) and NEIC (National Earthquake Information Center). Geographical distribution is reported on **Figure 5a**.

Historical seismicity

- The historical seismicity was extracted from SisFrance Antilles (Vermeersch et al., 2002). The earthquake locations and intensities are considered in this study, but the very limited level of reliability of the observations and epicenters does not provide strong constraints. Work on this catalog is in progress by the BRGM team to better determined event locations, depths and magnitudes. Geographical distribution is reported on **Figure 5d**.
- For comparison, the SARA pre-1964 catalog is consulted (<http://sara.openquake.org>). The project produced a homogeneous earthquake catalogue for South America. Mw were estimated for each event. Geographical distribution is reported on **Figure 5e**.

Focal mechanisms

- We build a database of focal mechanisms (FMs), labeled as *FMAnt-2021*, composed of 572 events from Puerto-Rico to Venezuela for seismotectonic analyses, using GCMT, ISC, and IGP catalogues as well as recent published works of Corbeau et al. (2019, 2021), González et al. (2017) and Ruiz et al. (2013). We used Mazzotti et al. (2021) method to compute average near-horizontal P and T axis orientations and faulting types on a regular grid: for each grid point, parameter statistics are computed, using a minimum **N_{min}** of FMs, according to the distance **d** to the grid point and a Gaussian half-width smoothing distance **w**. P and T axis orientations are computed using only data whose plunge does not exceeded a near-horizontal angle **a**. Faulting style is determined by associating each FMs to a scalar value based on its rake. The same weight is applied for each earthquake and multiple-event FMs are weighted based on their compatibility with each other. In this study, we use **N_{min}**=3, **d**=50 km, **w**=40 km, and **a**=25°.

Slab geometry

- Slab surface geometries of Bie et al. (2020) and Laurencin et al. (2018) were used and combined in one unique surface named as *Bie-Lau-Slab* in this report (**Figure 3b**). Slab and Moho geometries of Paulatto et al. (2017) were not used in order to keep a consistency along the arc. However, we checked their consistency for local studies near Martinique and Guadeloupe.

Crustal faults

- A first-order Caribbean crustal fault distribution was obtained from the Global Earthquake Model (GEM – Styron et al., 2020). It was completed with the local work of Boucard et al. (2021); Feuillet, Beauducel, & Tapponnier (2011); Feuillet, Beauducel, Jacques, et al. (2011); Feuillet et al. (2001, 2002, 2004); Garroq et al., (2021); Laurencin et al. (2017, 2019); Leclerc et al. (2016). Currently, no unified database of crustal fault exists and knowledge is heterogeneous for the entire LA arc (mostly depending on oceanographic campaigns). Around Guadeloupe, we used the unpublished fault catalog developed by Philippon et al. (pers. comm.) to better define area sources limits. Their work is still under progress to provide a complete and sorted faults catalog.

Geodetic data

- Geodetic velocities at Global Navigation Satellite System (GNSS) sites along the LA arc was provided by van Rijsingen et al. (2021). We used these data to calculate a first-order strain rate tensor in a few specific areas.
- We used GNSS and micro-atolls geodetic data from Philibosian et al. (2022) and van Rijsingen et al. (2021) to model the possible interseismic coupling of the megathrust interface along a 2D cross section at the latitude of Guadeloupe. We tested three range of potential coupling depths, 0 to 40 km, 40 to 70 km and 40 to 90 km, with 10 or 100% of coupling. Results are discussed in **section 2e**.

2b-Crustal seismotectonic zoning

The Caribbean plate crust is first divided from east to west according to the limits of the accretionary wedge and the fore-arc basin due to their differences in structure, lithology and tectonics (**section 1**). A first division is located at the backstop, interpreted from existing data on accretionary wedge and arc tectonics and structure (Laurencin et al., 2019; Torrini & Speed, 1989). At the north, this limit is defined 10 km south of the Bunce fault which marks the backstop. A second division is defined between the arc and the forearc basins, where known tectonic and seismicity diversities justify it. We then proposed a third lateral limit, between the arc and the back-arc, to consider the low seismicity levels of the Grenada basin and Aves ridge. Finally, we divided from south to north, according to structures, fault types and seismic activity. Upper plate depth limit is defined by the Moho at 28 km (Paulatto et al., 2017), and by the downgoing plate surface depth (minus 5 km, in order to avoid interface seismicity) when its depth is located above the Moho depth. Downgoing plate depth limit, for the outer-rise region, is about 20 km. The resulting seismotectonic model is presented on **Figure 7**.

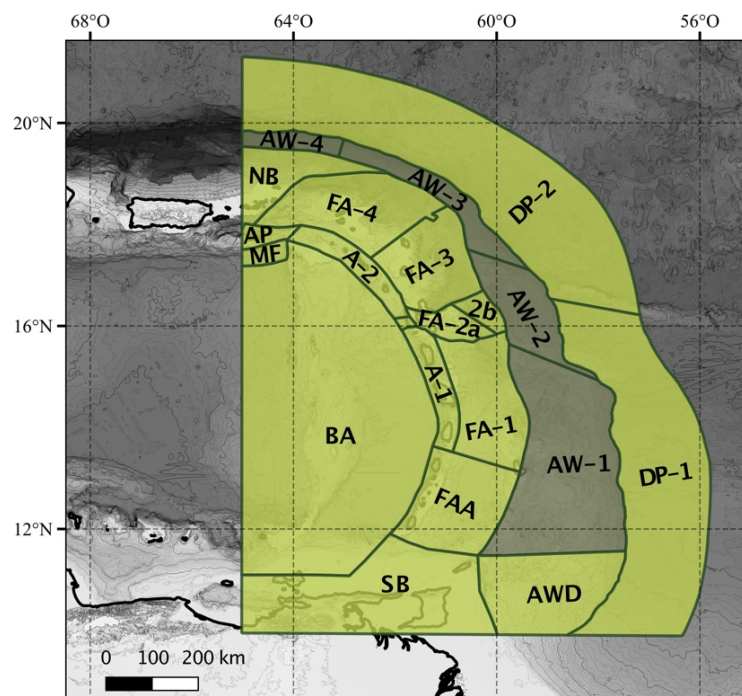


Figure 7: Upper-plate crust seismotectonic model. Black lines highlight the main tectonic features as fractures, ridges and subduction trenches from **Figure 1**. SB: South Boundary. AW: Accretionary Wedge. AWD: AW Death. FA: ForeArc. A: Arc. FAA: FA and A. BA: BackArc. MF: Muertos Fault. NB: North Boundary. AP: Anegada Passage. UL: Undefined Limit. DP: Downgoing Plate. AW-1 to AW-4 could eventually not be considered as explain in **section 2b**.

** Accretionary wedge and outer-rise seismogenic sources **

In the accretionary wedge seismogenic sources, the seismogenic potential of faults is considered. We do not integrate the possibility of rupture propagation or fault activation induced by an earthquake nucleated at the subduction interface. This case is implicitly integrated into the "subduction interface" model. Studies on the accretionary wedge seismicity mainly indicate very low frequency earthquake or tremors on stable reverse faults (Ito & Obara, 2006; Obana & Kodaira, 2009). No clear evidence of a potential to generate strong earthquakes is existing as the prism is considered as unconsolidated sediments and full of fluids (low seismogenic potential). The 2007 OBS Sismantilles experiment (Laigle et al., 2007) did not record earthquakes in this area during 4 to 6 months (Laigle pers. comm.). On the basis of the instrumental catalogs, earthquakes are located in the accretionary wedge (**Figure 5**). Consequently, we propose a zoning, but we should eventually consider the possibility that the majority of these earthquakes are on the interface or in the oceanic slab. This would change the density and frequency of earthquakes on these seismogenic sources.

AWD (Accretionary Wedge Death): the zone corresponds to the progressive disappearance of the accretionary wedge towards the south (**Figure 8c**), where the South American Plate oceanic crust gradually becomes continental and subduction ends (Padron et al., 2021). AWD is bounded to the east by the trench, to the west by the eastern termination of the El Pilar strike-slip fault system, to the south by the southern termination of surface fault distribution related to the accretionary wedge, and to the north by the appearance of the accretionary prism (AW-1 limit, poorly defined).

AW-1 (Accretionary Wedge 1): the zone corresponds to the Barbados accretionary wedge (**Figure 1**). As presented in **section 1**, it is characterized by a thick sediment layer from the Orinoco River, deformed through a sequence of thrust faults. Convergence direction is almost perpendicular to the trench and the subducted plate is highly fractured, referring to the Proto-Caribbean lithosphere. AW-1 is bounded to the east by the trench, to the west by the backstop, to the south by the progressive disappearance of the wedge (AWD limit, poorly defined) and to the north by the Tiburon ridge that limits the sediment supply coming from the Orinoco river.

AW-2: the zone corresponds to the north/south transition limit of the Tiburon and Barracuda ridges (**Figure 1**). The limits are poorly defined. The accretionary wedge, whose sediment transport is stopped by the ridges, decreases in thickness. The few known faults correspond to lateral ramps (Brown & Westbrook, 1987). AW-2 is bounded to the east by the trench, to the west by the backstop, to the south by the Barbados accretionary wedge filled by sediment (AW-1) and to the north by the narrow wedge with margin erosion dynamic (AW-3).

AW-3: the zone corresponds to the narrow accretionary wedge in erosion, with strike-slip deformation marked by the Bunce fault (**Figures 1 and 4**). The trench is curved and the convergence is oblique. The subducted North American Plate is less fractured compared to the South American Plate (**Figure 1**) and corresponds to the Equatorial Atlantic lithosphere. AW-3 is bounded to the north and east by the trench, to the west by the backstop, to the south by transition zone (AW-2) and to the north by the Puerto-Rico subduction system (AW-4).

AW-4: the zone corresponds to the narrow accretionary wedge of the Puerto-Rico subduction system (**Figure 1**). The convergence direction is about 75° . AW-4 is bounded artificially to the west by a distance of 200 km from the last French islands (Saint-Barth and Saint-Martin), where we consider seismic wave effects to be negligible for the PSHA calculation. To the east by the western end of the LA subduction system (AW-3), to the north by the trench and to the south

by a distance of 10 km south of the Bunce fault. The fault is described by Laurencin et al. (2019) as the limit between the accretionary wedge and the fore-arc.

DP-1 and DP-2 (DP - Downgoing Plate): We considered a band about 150-200 km width, seaward of the trench to include outer-rise seismicity of the American Plates. The eastern limit of this zone is uncertain but has no impact, given the distance, on the calculation of the seismic hazard. This area source can be divided in two distinct zone (DP-1 and DP-2), north of Barracuda ridge, where the diffuse limit between Central and Equatorial Atlantic lithosphere is located and is separated plates that differ in nature and fracturing amount.

**** Characteristics of associated seismicity ****

We defined, when it was possible, the Gutenberg-Richter (GR) magnitude-frequency distribution (MFD) for each area source (report to **Definitions and concepts**). Results are discussed in more details in Foix et al. (in prep.). Distributions are added in annexes of this report (**Annexes 1 to 7**), while this section exposes a short discussion on the seismic potential of the accretionary wedge. Based on the *ISCU-cat* earthquake catalog (**Annexes 1 and 2**), only AW-4 MFD distribution is usable. AW-3 is unusable because of the very small number of usable earthquakes (12 events). AW-1 and AW-2 are good examples of an uncomplete catalog below $M_w=4$ and should be later improved (**section 4**). AW-1 MFD does not follow a linear distribution for $M_w \geq 5$ and raises questions on earthquake location errors.

Due to its poorly consolidated sediments nature and high fluid content, the accretionary wedge may be unlikely to trigger large earthquakes. Due to the distance to the local seismic stations, earthquake locations and depths are poorly resolved, limiting the attribution to these zones (versus the subduction interface or slab). Current data does not allow us to determine structural M_{max} . The M_{max} catalog of AW-1, AW-2, AW-3 and AW-4 from the *ISCU-cat* are 6.5, 7.2, 4.6 and 4.6 respectively. The 1910 $M_{6.5}$ and 1969 $M_{7.2}$ earthquakes have controversial locations, and we decide to exclude them as M_{max} :

- **1910/01/23 – $M=6.5$:** *ISCU-cat* depth location is fixed at 10 km whereas USGS fixes it at 100 km. Not enough data are available to determine FMs that may help on the location interpretation.
- **1969/12/25 – $M=7.2$:** *ISCU-cat* depth location is fixed at 2.1 km, whereas USGS fixes it at 9.7 km and NOAA at 7 km. FMs indicate normal faulting, excluding an interface source (GCMT). According to the magnitude, an intra-slab source is more likely.

A few earthquakes could be used as reference for these zones, although their locations are questionable:

- **1922/05/11 – $M=6.07$:** $z=15$ km (ISC-GEM) - located by Russo et al. (1992) at 5 km in the accretionary wedge.
- **2014** ($M_w=6.4$) and **2015** ($M_w=5.7$) seismic clusters have not been deeply investigate. They are respectively located at 13.9 and 10.9 km depth according to the *ISCU-cat*.
- The **1767** historic earthquake, with intensity 8.5 is reported in this region (AWD), but its location and depth cannot be clarified. The presence of a tsunami suggests a shallow event (Le Roy et al., 2017).

The limited records of outer-rise earthquakes may be related to the instrumental recording time or the distance from the stations. The outer-rise region was struck by a $M=6.7$ and $M=5.6$ in 2003 and 2016 respectively along the transform faults that cut the American crust (USGS), while outer-rise earthquakes may reach magnitude 8.0 to 8.6 around the world (Craig et al., 2014, and references therein). In Sumatra, outer-rise strike-slip earthquakes from $M_w=8.2$ to

Mw=8.6 have been observed (Meng et al., 2012), as well as in Japan, with Mw=8.2 (Kanamori, 1971). At the LA, the work of Mathilde Cannat and Javier Escartin underlines the presence of large seismogenic structures where roots could reach 10-15 km in depth (Escartin pers. comm.).

**** Arc and fore-arc basins seismogenic sources/areas ****

FAA (Fore Arc and Arc): the area source corresponds to the southern arc and fore-arc basins (**Figure 1**). It is characterized by a significant decrease in instrumental seismicity in comparison with the arc zones to the north (**Figures 8a** and **b**). About 25 historic earthquakes are listed in FAA and about 60% have epicentral intensities greater than 6 (**Figure 5d**). Work is in progress to determine if these historical events are shallow or deep (A. Lemoine, R. Hoste-Colomer and D. Bertil, BRGM). South of Saint-Lucie, lack of multi-beam bathymetric data precludes the identification of particular fault structures. No difference in seismic activity between the arc and the fore-arc basins is observed (**Figures 8a** and **b**), given no justification to distinguish between arc and forearc area sources.

FAA is bounded to the south by the increase of seismicity related to the El Pilar strike-slip fault system (**SB - South Boundary** seismogenic source), to the north by an increase in seismic activity and by a GNSS velocity decrease between Sainte-Lucie and Saint-Vincent-and-the-Grenadines islands (GNSS data, **Figure 2**). The velocity gradient is about 0.15 and 0.56 mm/yr for the eastern and northern components. However, this is not accompanied by an increase in instrumental seismicity and no FMs exhibits extension (**Figures 8a, b** and **d**). To the east, the limit of the area is defined by the presence of the accretionary wedge, and to the west by the end of the volcanic arc.

FA-1 (Fore Arc 1), A-1 (Arc 1): the area sources correspond to the central arc and the fore-arc basin (**Figure 1**). They are both characterized by an increase in seismic activity, compared to FAA (**Figures 8a** and **b**). A-1 is characterized by the presence of normal faults parallel to the subduction trench (**Figure 8c**). FA-1 instrumental seismicity shows alignments in the continuity with *en-échelon* faults with NW-SE orientation (without clear association with specific fault structures, **Figures 8a, b** and **c**). FA-1 is considered as a zone of diffuse seismicity, as current knowledge does not allow us to divide it in more specific seismogenic sources. Data currently being acquired/processed should enable us to better characterize this transition between the arc and forearc.

FA-1 and A-1 are bounded to the south by a decrease of seismic activity (FAA), to the north by the fault system of the MGG (FA-2). FA-1 is bounded to the east by the presence of the accretionary wedge. A-1 is limited to the west by the end of the volcanic arc.

FA-3, A-2, and UL (Undefined Limit): the area sources correspond to the northern arc and fore-arc basin (**Figure 1**). A-2 differs from FA-3 by the presence of normal faults parallel to the subduction trench (**Figure 8c**). FA-3 presents a series of normal faults perpendicular to the trench and is marked by a sustained seismic activity throughout the area (**Figures 8a, b** and **c**). The seismic activity decreases to the north, marking the limit with FA-4. A-2 differs from A-1 by a senestral component of the arc-parallel normal faults. These two zones are separated by a diffuse, poorly defined limit UL. Moreover, given the proximity with Guadeloupe, this limit may have a strong impact on hazard estimations and should be treated as an uncertainty in future seismic hazard models.

FA-3 and A-2 are bounded to the south by the Marie-Galante fault system (FA-2) and the diffuse boundary with A-1 (UL). FA-3 is bounded to the north by the decrease in seismic

activity (FA-4) and to the east by the presence of the accretionary wedge. A-2 is bounded to the west by the end of the volcanic arc.

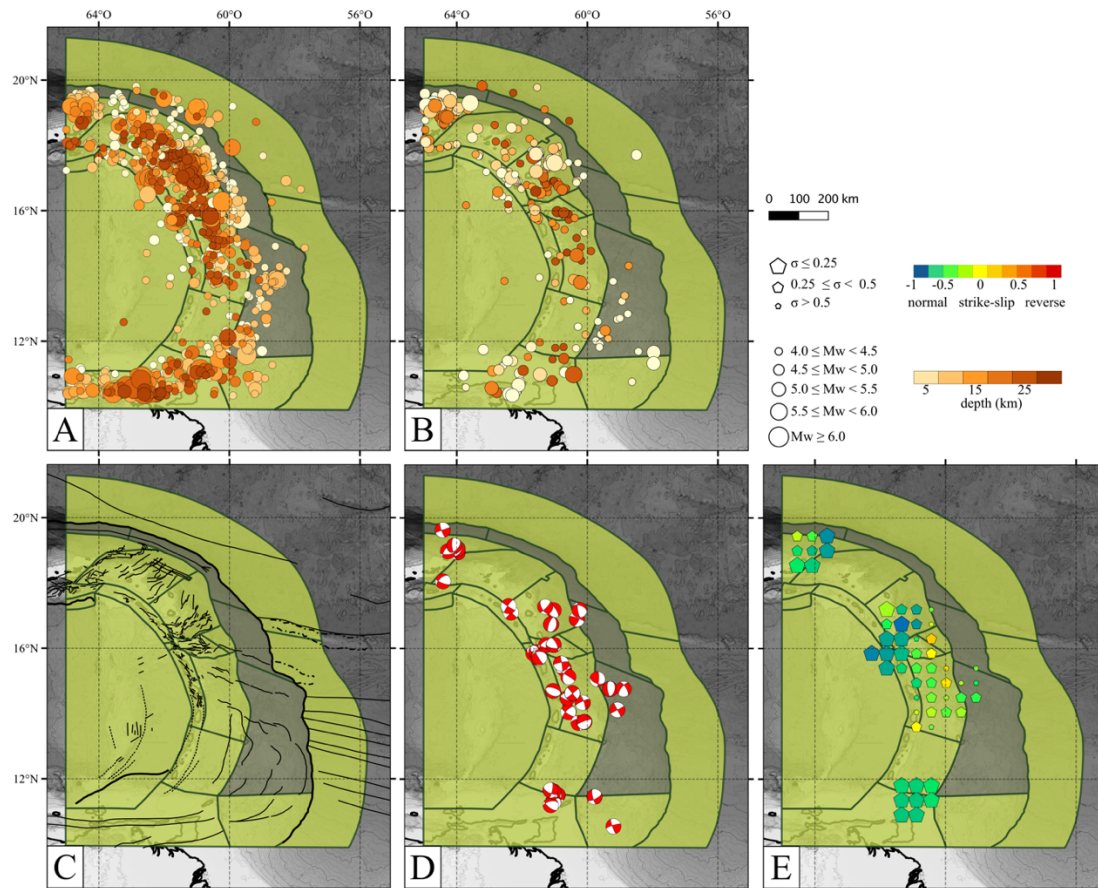


Figure 8: Crustal seismotectonic model and overlapped seismotectonic data overview. **A:** ISCU-cat for magnitude greater than or equal to 4 (circles). **B:** CDSA-cat for magnitude greater than or equal to 4 (circles). **C:** crustal fault distribution (thin black lines). **D:** focal mechanisms spatial distribution (FMAnt-2021). **E:** grid-average faulting style with symbol sizes inversely proportional to the standard deviation (pentagon).

FA-2a and FA-2b: the area sources correspond the Marie-Galante fault and associated fore-arc region (**Figure 1**). Guadeloupe is defined as a key transition point between the north and south of the LA in term of GNSS velocities, seismicity rate, faults orientations and tectonic style. The arc-parallel faults (Roseau, Bouillante-Montserrat) and arc-perpendicular faults (Marie-Galante graben - MGG) intersect near La Soufrière volcano (**Figure 6**). The northern part of Guadeloupe is marked by GNSS velocity trends to the north, whereas the southern part is characterized by velocity trends to the south (**Figure 9**). The main fault of the MGG system is the Morne-Piton fault (MPF), also named Barre-de-L'île fault (**Figure 6**). The MPF eastern end is located in the Marie-Galante canyon, east of Marie-Galante Island, and its western end is between the coast of Basse-Terre, near Capesterre-Belle-eau village, and Banc-Colombia. The MGG extends to the Karukera spur. To the east, the seismicity rate decreases drastically, marking the limit with the FA-2b seismogenic source (**Figures 8a and b**). The FA-2 division in two distinct areas allows the non-dilution of the seismicity for hazard calculations.

FA-2a and b seismogenic sources are bounded to the south by the end of the MGG, south of MPF, and to the north, by the change in GNSS velocity directions and the northern end of the MGG, north of the Gosier and Roche-de-May faults. To the west, FA-2a is bounded by the Bouillante-Montserrat fault system, part of the A-2 area source, and by the UL diffuse

boundary. To the east, FA-2b is bounded by the Karukera spur. Historically, the MGG was responsible for the 1851 event ($M \sim 5.5$) and possibly the 1897 event ($M \sim 5.5$) near Pointe-à-Pitre (Bernard & Lambert, 1988).

FA-4: the area source corresponds to the fore-arc and LA northern limit (**Figure 1**). FA-4 is characterized by a strong decrease in the seismic activity compared to FA-3 (**Figures 7a and b**). The Tintamarre faults, which intersect the V-shaped basins, have a normal component, and accommodate the margin erosion with roots estimated at 10-15 km depth. FA-4 encompasses the Sombrero basin to the north, an inactive transtensif system. To the west, it includes the northern section of the Anegada passage, an extension system with limited seismic activity.

FA-4 is bounded to the north by the southern zone of the Anegada passage (AP area) and by normal active faults parallel to the trench (A-2), to the east by the accretionary wedge, to the south by FA-3 and its high seismic activity, and to the west by the Puerto Rico subduction.

AP (Anegada Passage): the area source marks the southern zone of the Anegada Passage, a transtensif system with very few instrumental earthquakes of $M_w \geq 4$ (**Figures 8a and b**). Lower magnitude seismicity is observed with the *CDSA-cat* and only one historical earthquake was observed (**Figure 10**), the 1867 tsunamigenic Virgin Islands earthquake, $M_w = 7.2$ (Reid & Taber, 1920; Ten Brink et al., 2011). The British Virgin Islands (North Boundary – NB – area) and the US Virgin Islands (AP area) are characterized by opposite GNSS velocity directions (**Figure 2**). The velocity difference is estimated at about 0.64 and -0.46 mm/yr for the east and north components respectively. This raises the question of the compatibility of GNSS velocity data with the faults activity and seismicity rate.

AP is bounded to the south by the Muertos Fault (MF), to the north by Puerto Rico active subduction (NB) and to the east by the active arc (A-2).

NB (North Boundary) and SB (South Boundary): these area sources delimit the northern and southern limits of our study area. NB, in the north, corresponds to the seismicity associated with the Puerto-Rico subduction system. Its western limit is located at 200 km from the last French islands (Saint-Barth and Saint-Martin) and do not include the Puerto Rico fault system. SB, in the south, corresponds to the seismicity associated with the El-Pilar fault system. It is bounded by the dataset used and is not specifically addressed in this study.

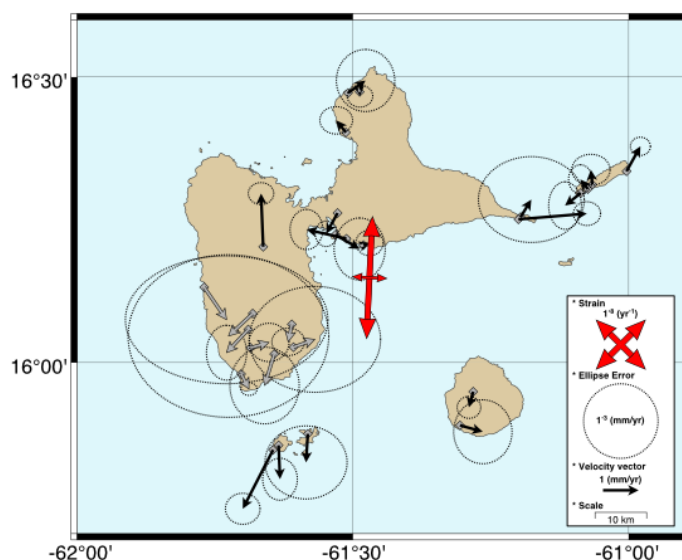


Figure 9: GNSS vector velocities (red arrows) through Guadeloupe, in the Caribbean reference frame with the estimated mean strain (black arrows) without GPS values from La Soufrière volcano (grey arrows). Strain values: $e1 = 1.7 \cdot 10^{-8} \pm 1.10^{-10} \text{ yr}^{-1}$; $e2 = 5 \cdot 10^{-9} \pm 1.10^{-10} \text{ yr}^{-1}$.

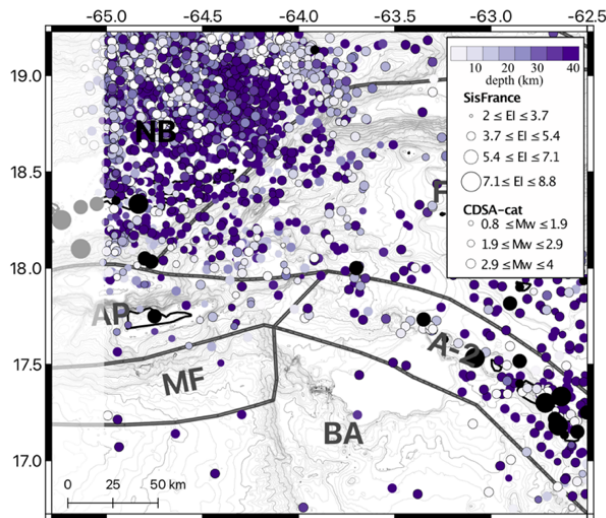


Figure 10: Background seismicity (≤ 4) and historic events of the northern end of the Lesser Antilles subduction. Thick black lines delineate seismogenic source areas of the Anegada Passage (AP), the Muertos Fault (MF), the BackArc region (BA) and the northern end of the Arc (A-2). The white transparent square marks the limit of our instrumental seismic catalogs.

BA (Back Arc): the area source reflects weak diffuse seismicity of the Aves ridge and Grenada basin. Seismicity and geological structure do not offer justifications to cut this area source into two distinct blocs.

**** Characteristics of associated seismicity ****

We defined, when it was possible, the magnitude-frequency distribution for each area source as previously exposed (**Annexes 1 to 4**, Foix et al., in prep). Regarding GR distribution, A-1, BA and NB are directly usable (**Annexes 1 to 3**). For future hazard modeling, we recommend to adapt the BA geometry to be more compatible with seismicity distribution. FA-1, FA-2a, FA-3, FAA, SB and FA-4 are characterized by uncomplete catalogs for $M_w=3$ to $M_w=3.5-3.8$ and could be later improved (**section 4**). A-1, A-2, FA-1, FA-2a, FA-3, FA-4, FAA and SB are all affected by an apparent step in the distribution around $M_w=3.8$, possibly related to conversions used for magnitude homogenization. A-2 presents a second slope variation between $M_w=4$ and $M_w=5$. Overall, all zones show a reasonable GR linear distribution and could be usable for future hazard analysis after cleaning and verifications on the magnitude completeness, magnitude estimations, M_w conversions and earthquake locations. AP, AW-3, DP-1 and MF magnitude-frequency distributions are unusable because of the very low number of earthquakes instrumentally recorded in these source areas.

Most of the seismicity is distributed in seismic clusters in the arc and forearc basins, with higher activity north of Sainte-Lucie. The arc and forearc area sources may generate magnitude of about $M_w=7.0-7.5$ according to active fault lengths. From instrumental and historical records, the arc was struck by $M_w=7.2$ and $M_w=6.3$, respectively located at the Virgin Islands and at Les Saintes in 1867 and 2004. About the forearc region, we may use the 1967, $M_w=6.4$ earthquake for M_{max} , as the 1910 and 1974 earthquakes locations and magnitude estimations are not constrained. Other large damaging events struck the arc and forearc areas in the last 400 years, but their locations are questionable (crust, interface or slab) and could not be used as references: April 5, 1690 near Barbuda ($M_s \sim 8.0$), January 11, 1839 offshore Martinique ($M_s \sim 7.8$), February 8, 1843 near Guadeloupe ($M_s > 8.0$), and November 18, 1867 near the Virgin Islands ($M_s \sim 7.2$).

**** Fault seismogenic sources ****

In order to characterize the fault seismogenic sources, their geometry, slip rate and associated earthquakes are needed. Only a few faults in the LA system fulfil these criterions. In this section, we briefly expose in the **Table 1** the characteristics of these faults, already introduced

on **section 1**. No seismicity analysis has been conducted. Most of the information is from published literature. The maximum magnitude is estimated using magnitude–rupture dimension scaling relationships (Wells & Coppersmith, 1994) or magnitudes of large historical earthquakes.

On the Guadeloupe and Martinique islands, some trenches have been dug across some faults. So far, they have not revealed any evidence of a paleo-earthquake (May Fault, Guadeloupe, Sedan & Terrier, (2001)), or indicated Quaternary activity without it being possible to make a chronological distinction (North Lamentin and Schoelcher faults, Martinique, Terrier (1996)). More explorations are needed to characterize fault sources.

Faults	Length (km)	Seismogenic Depth (km)	Slip Rate (mm/yr)	Mmax.struct.	Mmax.obs	References
Roseau	35	15	0.15 to 0.4	7.0	Mw=6.3 (2004)	(Feuillet, Beauducel, Jacques, et al., 2011; Leclerc et al., 2016)
Morne Piton	50	20	0.20 ± 0.05	7.5	Ms=5.5 (1851)	Philippon et al. (under review)
Redonda	~30	15?	~0.2	7.0	Ms=6.2 (1985, z=9±2km)	Carey et al., (2019): 0.3 mm/yr of regional subsidence with 0.16 mm/yr, 60° of fault dip is assuming. Feuillet et al., (2010) figure 2.
Bouillante-Montserrat	10 to 20 km segments (~60)	15?	~0.3 0.15-0.20	7.3	?	Beck et al., (2012): 10 m in 3500 year; Philippon et al. (under review) and references therein.
Anegada	220	?	1.0 * 1.25±0.15 **	6.8-8.0	Ms=7.5 (1867)	(Symithe et al., 2015; Zimmerman et al., 2022)
Muertos Trough	641	-	1.7 (East segment) *	7.6 (East segment)	Ms=6.7 (1984)	(Heuret et al., 2011; Symithe et al., 2015; Zimmerman et al., 2022)

Table 1: Fault seismogenic source characteristics. * modeled slip rate from Zimmerman et al. (2022). ** GPS block motion modelling from Symithe et al. (2015) where Anegada passage is considered as block boundary.

2c-Mantle seismotectonic zoning

The Lesser Antilles are marked by mantle wedge seismicity located at about 50 km east of the island arc coasts and at 25–60 km depths (Bie et al., 2022; Laigle, Hirn, et al., 2013; Ruiz et al., 2013). During the SISMANLILLES oceanographic campaign, the deployment of ocean bottom seismometers over a month allowed the recording of two magnitude 3.1 earthquakes located to the east of Martinique, and one magnitude 3.6 earthquake at the northeast of the island (M. Laigle, personal communication). We sorted seismicity in *ISCU-cat* based on the subduction geometry (island arc Moho = 28 km and slab interface = *Bie-Lau-Slab*). We identified more than 3,000 earthquakes, called as *wedge-cat* in this report, that can be linked to the mantle wedge domain. The earthquake distribution indicates an activity up to 70 km depth (**Figure 11**). Due to the geometry of the seismological network, part of this seismicity may be poorly localized and could be attributed to the crusts of the upper and lower plates, or to the subduction interface. Further study to know exact locations, and especially depths, is necessary. For a local study, Moho and top slab geometries of Paulatto et al. (2017) should be used in the future.

**** Mantle wedge seismogenic sources/areas ****

Considering the *wedge-cat* as representative of Lesser Antilles mantle wedge seismicity, the **MS** (Mantle Source) seismogenic source is here extending from Sainte Lucia to Barbuda, and is characterized by high seismic activity (**Figures 12** and **13a**). The **SMS** (South Mantle Source), including Barbuda and Anegada passage, and the **NMS** (North Mantle Source), from Sainte Lucia to Grenada, are characterized by quieter seismic activity. The northern end is related to the Puerto-Rico subduction system, named as **PRM** (Puerto Rico Mantle).

**** Characteristics of associated seismicity ****

We defined, when it was possible, the magnitude-frequency distribution for each area source as previously exposed (**Annex 7**, Foix et al., in prep). Regarding GR distribution, PRM is unusable because of the very low number of useable earthquakes. MS, NMS and SMS have to be improved in order to be usable for seismic hazard modeling. The three zones are characterized by uncomplete events beneath $M_w=3.5$. MS and SMS present a step around $M_w=4$ that could be induced by issues in magnitude completeness or conversions. All of the mantle area sources are characterized by a double distribution with two different slopes, before and after $M_w=4$. This could be the result of earthquake location errors where a part of the seismicity may not be in the mantle sources but in the oceanic slab or the upper crust.

FMs highlighted by Ruiz et al. (2013) include magnitudes between 2.7 and 3.9, and were observed thanks to Ocean Bottom Seismometers (OBS) during less than one year. They are located between Guadeloupe and Martinique and present large uncertainties on their solutions. FMs orientations are heterogenous and no systematic fault type is observed (**Figure 13c**).

Considering the *wedge-cat*, about 9% of the earthquake have magnitudes greater than 4, and the catalog present a maximum magnitude of 6.3. The rest of the catalog is composed of magnitude between 3 and 4.

From historical seismicity, McCann et al. (1982) associated the October 8, 1974 earthquake north of Antigua, in the mantle wedge, at ~ 35 km depth, along a NNE to NE striking and southeast-dipping normal fault. The magnitude was estimated at about M_s 7.1-7.6. Based on the same data, Feuillet et al. (2002) associated this earthquake to the upper-plate crust, rupturing an arc-perpendicular ENE striking normal fault system northeast of Guadeloupe.

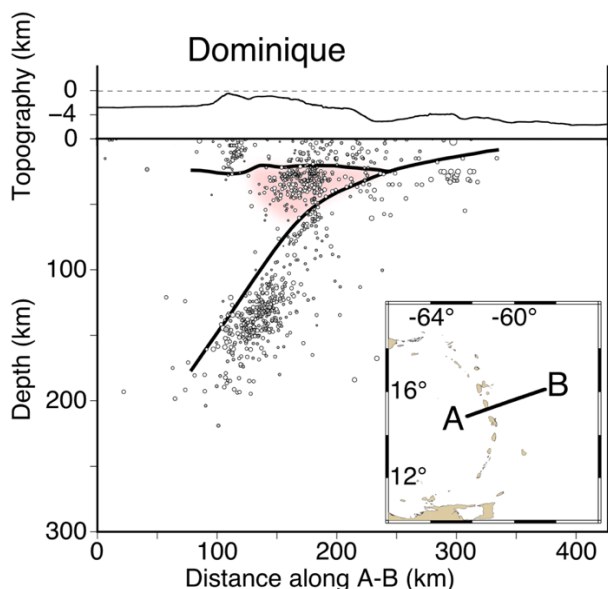


Figure 11: Seismic cross-section south of Dominique Island. **Insert:** Lesser Antilles subduction arc with AB cross-section surface trace. **Cross-section:** at the top is the topography linked to the AB cross-section. At the bottom is the seismicity from the ISCU-cat (white dots) and CDSA-cat (grey dots) along AB. Thick black lines are slab and Moho from Paulatto et al. (2017). The reddish triangle highlights mantle wedge seismicity.

The seismic catalog has to be better explored. The absence of attenuation law for the mantle wedge further complicates the integration in a PSHA calculation. However, tests can be conducted to assess its potential impact. Further studies are needed. Unknown exist on the maximum magnitude possibly generated as locations are poorly resolved. In New-Zealand, Davey & Ristau (2011) measured a M4.5 in the mantle wedge and point that it may cause some damage.

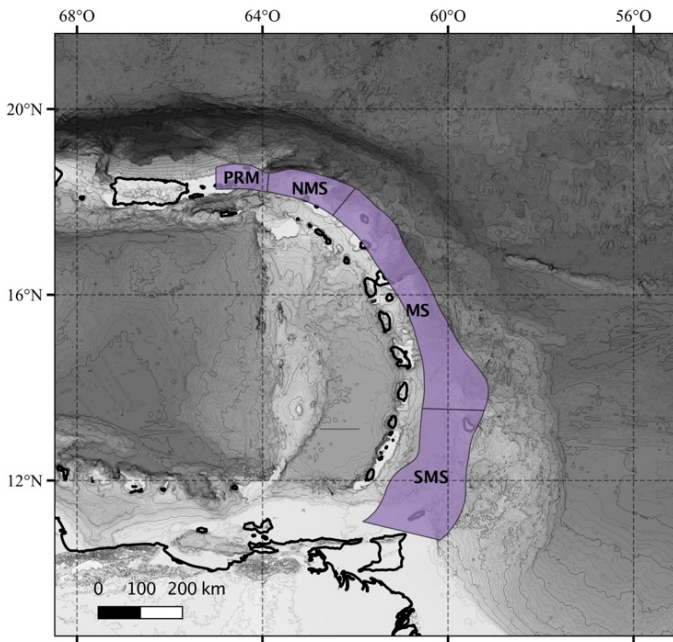


Figure 12: Mantle seismotectonic. MS: Mantle Source. SMS: South Mantle Source. NMS: North Mantle Source. PRM: Puerto Rico Mantle.

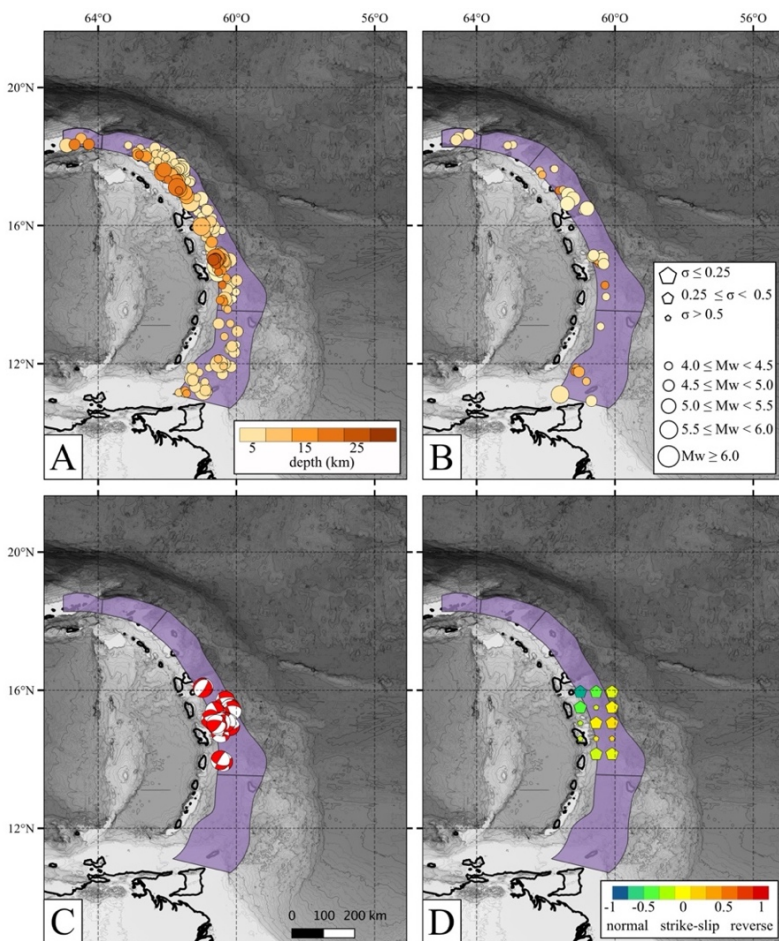


Figure 13: Mantle seismotectonic model and overlapped seismotectonic data overview. Black thick lines highlight the main tectonic features as fractures, ridges and subduction trenches from **Figure 1**. **A:** ISCU-cat for magnitude greater than or equal to 4 (circles). **B:** grid-average faulting style with symbol sizes inversely proportional to the standard deviation (pentagon).

2d-Volcanic seismotectonic zoning

Working on PSHA in a volcanic region is challenging because they are characterized by low magnitude earthquakes and high seismic wave attenuation. Most existing ground motion prediction equations can consequently not be used (Peruzza et al., 2017). Moreover, the characteristics and effects of volcanic earthquakes can be mixed with regional tectonic ones. Although uncommon, major volcano-related events of $M=6-7$ have caused severe damages worldwide (Japan, Indonesia, Hawaii, Azores islands, Abe (1979); Yokoyama (2009)). Volcanic earthquakes may reach in extreme cases $M=7.5-8$ (e.g., 1990, Mount Pinatubo, Philippines) but are generally limited to $M=5-6$ (McNutt & Roman, 2015). Few studies address these challenges to propose seismic hazard assessment for volcanic systems (Peruzza et al., (2017) for Mt. Etna).

In our study, we give general information to be considered for assessment of Lesser Antilles volcano-related seismic hazard. The first step aims to define specific zones associated with the volcanic edifices and their seismic activity. We propose a simple definition consisting of a 10 km radius circle around each edifice and the crust thickness as depth limit, in order to include all potential seismicity related to volcanic activity (**Figure 14**). However, a deep analysis of the VT earthquake distributions will be essential to ensure any exclusion of events outside of the 10 km radius.

Volcanic seismicity can be found in the *IPGP-cat* for the two French volcanoes, La Soufrière and Mont-Pelée. The *CDSA-cat* is cleaned from volcanic activity. The *ISCU-cat* may contain event with magnitude greater than 3 during the last hundred year, as the 1950 $M_w=4.3$ earthquake from the St. Kitts-Nevis seismo-volcanic crisis. Unfortunately, this is not enough to calculate magnitude-frequency distributions. In **Table 2**, we summarize volcano last activities, as well as associated M_{max} .

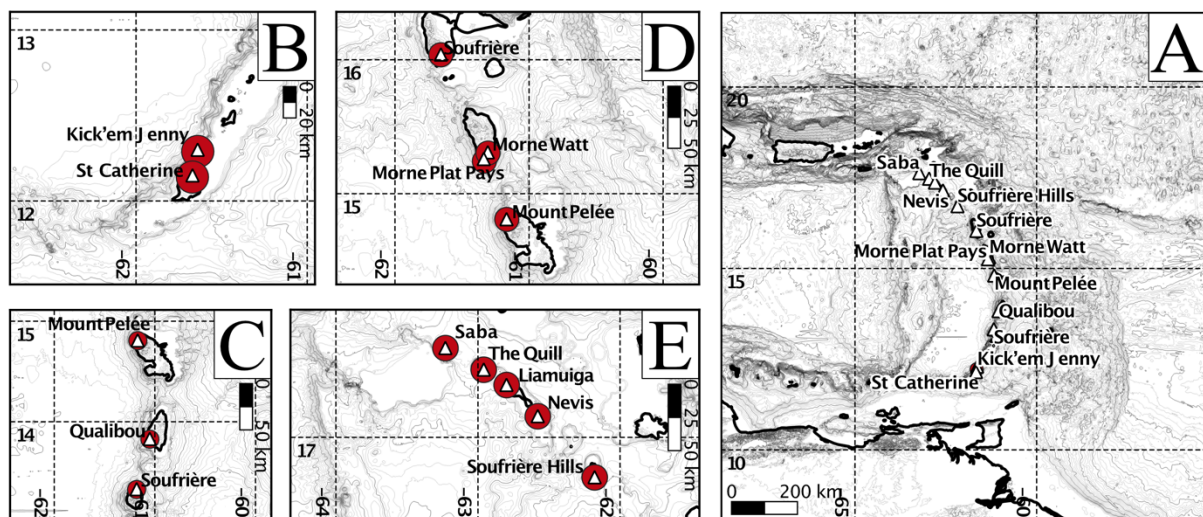


Figure 14: Volcanic seismotectonic models along the Lesser Antilles volcanic arc. **A:** active volcanoes. **B, C, D and E:** zoom on the active volcanoes to observe the area sources (red circle).

Volcano	Island	Latitude	Longitude	Last eruption	M_{max} - Instrumental records	Known Eruptions Dates
Saba	Saba	17.63	-63.23	1640	-	1640, 1636
The Quill	St Eustatius	17.478	-62.96	250AD	-	-
Liamuiga	St Kitts	17.37	-62.8	160	-	160AD±200, 60AD±100

Nevis	Nevis	17.15	-62.58	unknown	-	-
Soufrière Hills	Montserrat	16.72	-62.18	2013	$M_L=3.9$ (with eruption) $M_L=6.2$ (from seismic crisis, Shepherd, 1989)	Seismic activity on 1897, 1898, 1933-37, and 1966-67 without recorded eruption before 1995.
Soufrière	Guadeloupe	16.04	-61.66	1977	$M=4.5$	1976-77, 1956
Morne Watt	Dominica	15.31	-61.1	1997	?	1997, 1880
Morne Plat Pays	Dominica	15.26	-61.34	1270	-	1270 \pm 50, 390 AD \pm 40, 430 BC?, 4740 BC?
Mount Pelée	Martinique	14.81	-61.17	1932	?	1929-32, 1902-05, 1851-52, 1792, 1635
Qualibou	Ste Lucia	13.83	-61.05	1766	-	-
Soufrière	St Vincent	13.33	-61.18	2021	$M=3.3$	2021, 1979, 1971-72, 1902-03, 1880, 1814, 1812, 1784, 1718, 1640 \pm 50, 1550 \pm 50, 1480 \pm 150, 1395 \pm 75, 1325 \pm 75, 905 AD \pm 75, 530 BC \pm 75, 750 BC \pm 100, 1600 BC \pm 75, 2020 BC \pm 75, 2135 BC \pm 50, 2200 BC \pm 150, 2310 BC \pm 100, 2380 BC \pm 100
Kick'em Jenny	submarine	12.30	-61.64	2017	$M=4.0$	2017, 2001, 1990, 1988, 1977, 1972, 1966, 1965, 1953, 1943, 1939
St Catherine	Grenada	12.15	-61.67	unknown	-	

Tableau 2: Lesser Antilles volcanoes: locations and past activities. Information are mainly extracted from <https://volcano.si.edu> and <http://volcanolive.com/caribbean.html>

2e-Subduction interface seismotectonic zoning

Based on GNSS data, seismic imagery, heat flow and new knowledge of plate interface earthquake characteristics, we define two alternative models for the LA subduction interface seismogenic behavior to consider in future hazard calculations.

** Average worldwide characteristics of the seismogenic interface **

Based on worldwide interface earthquake distributions, Heuret et al. (2011) determined updip and downdip average limits of the seismogenic zone at about 11 ± 4 km and 51 ± 9 km depth, respectively.

Lay et al. (2012), Lay (2015) and Ye et al. (2016) characterized the nature of the subduction interface in 4 domains, based on the characteristics of high-frequency radiations of interface earthquakes:

- Domain A (0-15 km depth) = located close to the trench and characterized by stable slip, anelastic deformation, and low high-frequency radiation.
- Domain B (15-35 km depth) = domain of mega-earthquakes, such as the $M=9$ Tohoku 2011 event, and characterized by moderate high-frequency radiation.
- Domain C (35-55 km depth) = deep domain corresponding to moderate-slip earthquake ($M=7-8$) and characterized by strong high-frequency radiation.
- Domain D (below or at the lower end of domain C) = transition zone with slow slip events, very-low-frequency earthquakes, and seismic tremors.

** Extent of the Lesser Antilles seismogenic interface **

At the LA subduction zone, distributions of interface earthquake and thrust FM indicate an extension of the seismogenic interface to ca. 65 km depth (**Figure 15a** and **c**). Seismicity indicates along-strike variations of the seismogenic zone extension between 10 to 65 km depth in the north and 35 to 65 km depth in the south (Bie et al., 2020). In contrast, a 5-year OBS study located offshore Guadeloupe and Martinique islands did not record interface earthquakes below 35 km depth (Laigle, Becel et al., 2013), suggesting a possible specific seismogenic

behavior compare to the North or a peculiar temporal pattern. Overall, the quality of the seismicity data in the LA precludes any detailed conclusions regarding the long-term spatial distribution and potential variabilities of the subduction interface earthquakes.

Heat-flow data and thermal models agree with hypocenter locations. The modeled 350°C isotherm, which marks the transition between seismic and aseismic sliding, corresponds to 60-65 km depth at Martinique and Saint-Martin islands (Ezenwaka et al., 2022). Along strike variations in the margin thermal structure suggests variations in the limits of the seismogenic zone, consistent with the interplate seismicity distribution (Gutscher et al., 2013).

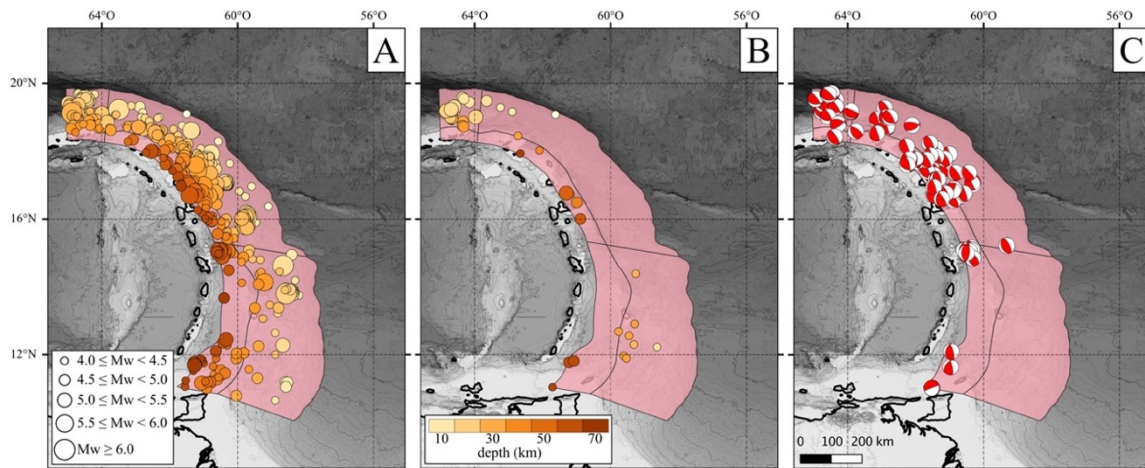


Figure 15: Interface seismotectonic model presented in **Figure 18** and overlapped seismotectonic data overview. Black thick lines highlight the main tectonic features as fractures, ridges and subduction trenches from **Figure 1**. **A:** ISCU-cat for magnitude greater than or equal to 4 (circles). **B:** Bie-Lau-Slab surface with depth. **C:** interface focal mechanism from the FMAnt-2021 catalog.

** Interface interseismic coupling **

Recent horizontal geodetic data indicate a very low interseismic coupling of the entire subduction seismogenic zone (van Rijsingen et al., 2021, 2022). Vertical motions from geodetic data and from coral and micro-atoll data both indicate subsidence (Philibosian et al., 2022; van Rijsingen et al., 2022). However, Weil-Accardo et al. (2016) and Philibosian et al. (2022) proposed that the deep portion (about 40 to 80 km depth) of the subducting interface is affected by a strong interseismic coupling based on coral and atoll data modelling, which disagrees with geodetic data modelling (van Rijsingen et al., 2021, 2022).

In order to compare GNSS and micro-atolls velocity data from Philibosian et al. (2022) and van Rijsingen et al. (2021), we ran a first-order computation to model the possible interseismic coupling of the megathrust interface along a 2D cross section at the latitude of Guadeloupe (**section 2a**). Our model does not consider for the 3D slab geometry, which may influence the results. These simple tests indicate that, if a strong interseismic coupling exists, it can only be on the deep part of the seismogenic interface (40-90 km depth, **Figure 16**). The very fast micro-atolls vertical velocities (5-8 mm/year subsidence) proposed by Philibosian et al. (2022) could be the result of other mechanisms than interseismic coupling, such as normal crustal faulting, local environmental changes as hurricane, site conditions, or to the sampled specimen being anomalous (Philibosian et al., 2022). As indicated in previous studies, a strong present-day coupling of the entire interface does not fit with geodetic horizontal velocities or coral data and must be excluded.

Worldwide, Aegean, Calabria, South Sandwich, and Mariana subduction zones are examples of low interseismic coupling and low seismicity (Carafa et al., 2018; Ruff & Kanamori, 1983; Vanneste & Larter, 2002; Vernant et al., 2014). In particular, the Hellenic subduction is characterized by very low interseismic coupling observed by geodetic data (Vernant et al., 2014) with only few records of large interface earthquakes ($M > 8$) (Polonia et al., 2013; Stiros, 2001), similar to the LA subduction.

An additional complexity may reside in temporal variations of interseismic coupling during the seismic cycle. Costa Rica and Mexico geodetic data illustrate potential changes in coupling over years to decades (Feng et al., 2010; Villafuerte et al., 2021). Coral studies show interseismic coupling variations over decades to centuries in Sumatra linked to major earthquakes (Philibosian et al., 2022; Tsang et al., 2015). Geodetic and coral data in the La subduction zone are not precise enough to address that question of temporal variations.

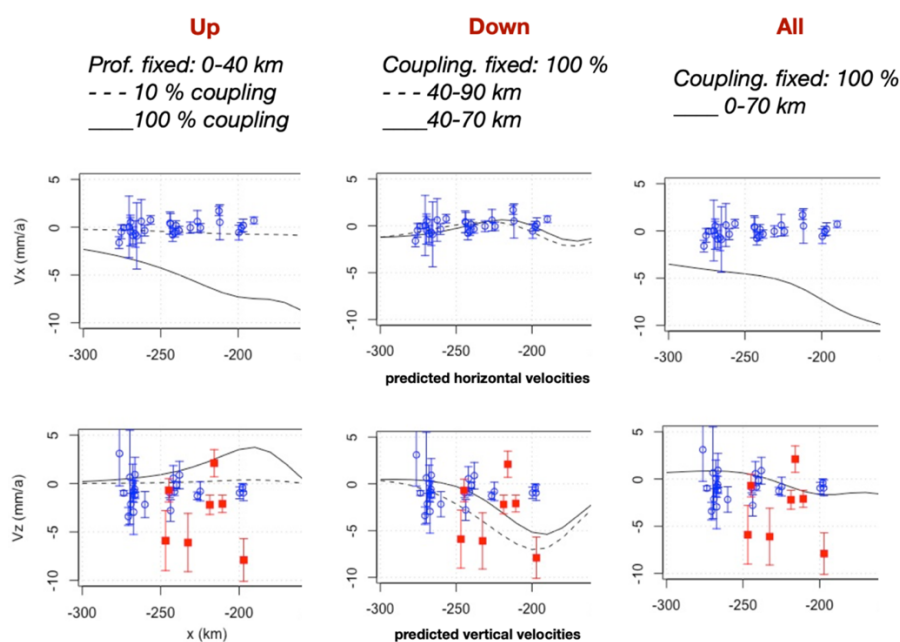


Figure 16 : Predicted vertical (V_z) and horizontal East component (V_x , profile direction) surface motions from GPS (blue square) and micro-atolls (red square) measurements. Three cases are considering: a coupling of the upper part of the interface (Up), a coupling of the downing part (Down), and a coupling of the entire interface (All).

** Proposed seismotectonic zoning of the Lesser Antilles subduction interface **

We consider a seismogenic zone between 0 and 65 km depth, according to earthquake and thrust FM distributions as well as thermal models discussed above. We define the updip limit at 0 km depth instead of 10 km to consider the possibility of rupture propagation up to the surface during a large earthquake (keeping in mind that this upper limit has no impact on seismic hazard in the island arc). We adapt the Lay et al. (2012) model to define A, B, C, and D domains that correspond to the LA subduction system (**Figure 17**). As there is no earthquake frequency content study along the LA subducting interface, we assume the average depth of 35 km of Lay et al. (2012) as B - C limit (**Figure 17**). We have no robust justification to propose along strike variations of these domains, and thus we consider them as consistent along the subduction.

Our proposed model is composed of (**Figure 18**):

- **UI-1** and **UI-2** area sources (Upper Interface – 0 to 35 km depth), which correspond to the domain B, able to generate earthquakes up to $M=9$, but characterized by a low interseismic coupling.

- **DI-1** and **DI-2** area sources (Deep Interface – 35 to 65 km depth), which correspond to the domain C that can generate earthquakes up to $M=7-8$. DI-1 and DI-2 can be associated with a low interseismic coupling (**Model 1**) according to geodetic modelling, or a strong interseismic coupling (**Model 2**) according to micro-atolls models. Because of the high variability and large error bars on the micro-atoll data, we propose a lower weight on Model 2. More data and further studies are required to address this major source of epistemic uncertainty.
- **UI-3** and **DI-3** correspond to the eastern end of the Puerto Rico subduction at the northern limit of our study area.

The lateral separations between zones 1, 2 and 3 are based on the *ISCU-cat* $M \geq 4$ earthquake distribution, structural variations of the subducting plate, and changes in the convergence direction along the trench (**Figure 15**). To the North, the limit between UI-3, DI-3 and UI-2, DI-2 is necessary in order to distinguish the LA subduction from the more sustained seismic activity of the Puerto Rico subduction. In the central region, active structures between the Barracuda and Tiburon ridges define a diffuse boundary between the North and South American Plates (Patriat et al., 2011b). They correspond to the limit between the Central and Equatorial Atlantic crusts associated with a different level of fracturing (**Figure 1a**). This deformation limit UI-2, DI-2 from UI-1, DI-1 is accompanied by a change in thrust events activity, more active in the north than in the south (**Figure 15**) and a change in convergence direction. The issue of lateral earthquake propagation across these lateral limits is unresolved.

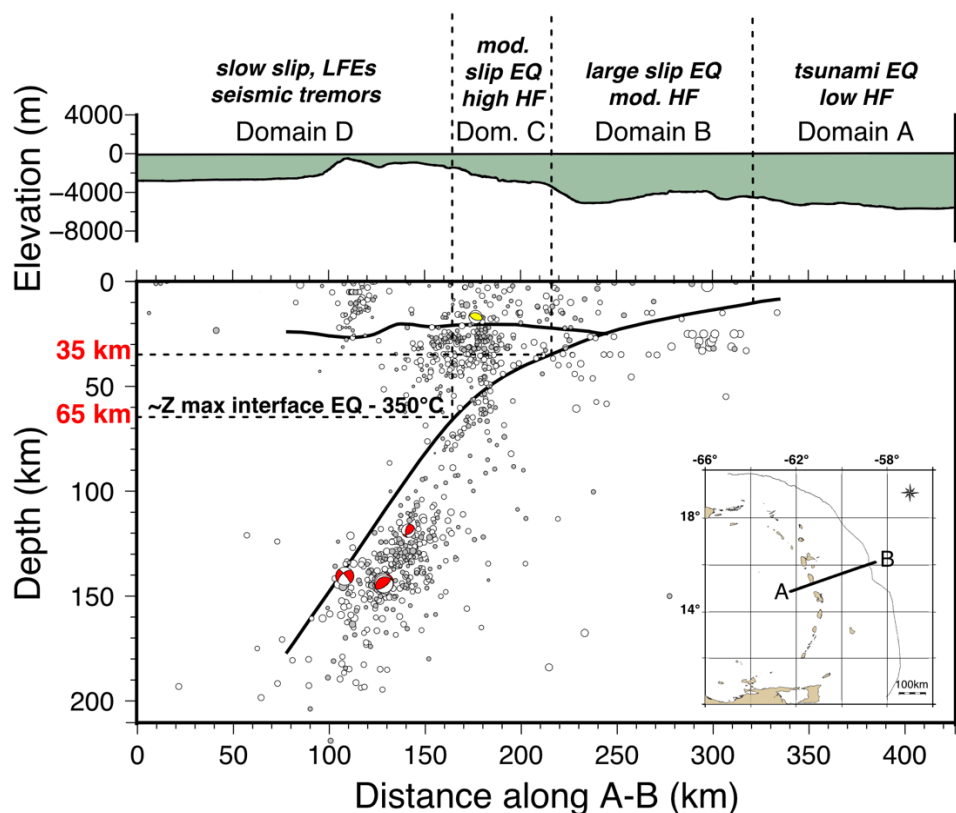


Figure 17: Proposed seismogenic behavior for the Lesser Antilles subduction based on Ye et al., (2016) work. **Top:** bathymetry along the AB cross-section reported in the inset with corresponding domain (dom.: domain; mod.: moderate; HF: High Frequency; LFEs: Low Frequency Events; EQ: Earthquakes). Green surface indicates the water level. **Bottom:** cross-section of the seismicity from the *ISCU-cat* (white dots) and *CDSA-cat* (grey dots) along AB. Thick black lines are slab and Moho from Paulatto et al., (2017). Focal mechanisms are from the *FMAnt-2021* catalog. Thin black lines and temperature are from Ezenwaka et al., (2022) and marked the upper and downdip limits of the seismogenic interface.

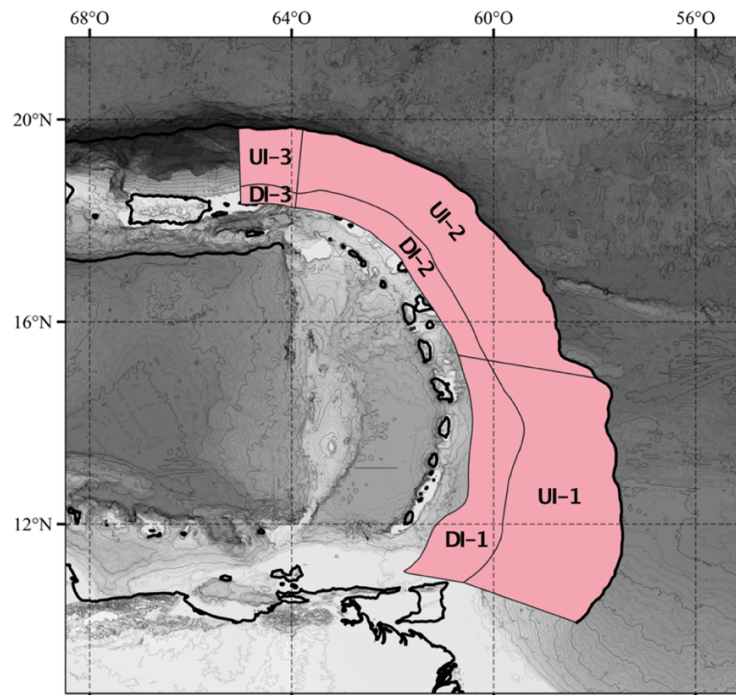


Figure 18: Interface seismotectonic model. Black thick lines highlight the main tectonic features as fractures, ridges and subduction trenches from Figure 1.

**** Characteristics of associated seismicity ****

We defined, when possible, the magnitude-frequency distribution for each area source as previously exposed (Annex 4, Foix et al., in prep). DI-3 is unusable because of the very low number of useable earthquakes. DI-1 and DI-2 are usable and are characterized by a small GR slope variation after $M_w=4$. This could be due to magnitude conversion or earthquake locations, with events that actually do not belong to the interface. UI-1 and UI-2 present a robust GR distribution but need to be improved or filtered for $M_w \leq 4$. UI-3 is usable for hazard modelling. These differences between UI-* MFD could be induced by the distances from the seismic network, explaining the limits in $M_w \leq 4$ recording.

Beside the GR distributions, the seismogenic characteristics of the subduction interface remain poorly understood. Since the instrumental period, over the last 100 years, no earthquake with $M \geq 6.5$ has nucleated on the interface. We have no constraint on a M_{max} and on the frequency of large earthquakes. The earthquakes of 1839 (intensity of 8 to 9) and 1843 (destruction of the city of Pointe-à-Pitre, ~1500 deaths) are sometimes interpreted as located at the interface (Feuillet et al., 2001), but this cannot be asserted and the question remains open. From the marine sedimentary deposits of the Guadeloupe area basins, the 1843 event was not detected (Feuillet pers. comm.) and only a moderate tsunami was reported (Le Roy et al., 2017). This could be explained by a destruction of the first sedimentary records during the coring (Seibert pers. comm.). Several works are in progress, in particular on the analysis of sedimentary cores around Guadeloupe (Seibert et al., 2022). Preliminary results could indicate an earthquake at about 2500 years ago (Feuillet pers. comm.). The possibility of a $M=9$ event with a very long recurrence time may be used in the PSHA calculation, but it remains a major source of epistemic uncertainty.

2f-Slab seismotectonic zoning

In the case slab seismic observation, FMs are only used to observe spatial variations deformation style, without considering the slab dip. The seismogenic model is presented in **Figure 19**.

** Slab seismogenic sources/areas **

SS-1, SS-2, SS-3 and SS-4 (SS - near Surface Slab): from 0 to 30 km depths, with constant slab dip of 10 to 15°. Seismicity is distributed in clusters, heterogeneously along the arc (**Figure 19a**) and includes the 2015 (south of the L-2 boundary) and 1969 (north of Tiburon ridge) seismic clusters. The near surface slab seismogenic areas are limited by the **L-2, L-3** and **L-4** limits:

- **L-2** (north of Saint-Lucie and Barbados): limit the seismic resurgence of SS-2, compared to the quiet seismic activity of SS-1 (**Figure 20a**).
- **L-3** (north of Barbuda): boundary between SS-2 and SS-3 with a change in deformation styles from FMs (**Figure 20b**), possibly due to subduction obliquity.
- **L-4** (west of the British Virgin Islands): major increase of seismicity rate and change in in deformation style according to the subduction of Puerto Rico of SS-4 (**Figures 20a and b**).

SB-1, SB-2, SB-3, SB-4 and SB-5 (SB – Slab Bending): from 30 to 80 km depths, with a progressive increase of the slab dipping. The seismogenic areas are divided by L-1 to L-4 limits. A change in deformation style is observed in front of Martinique (**Figure 20b**), however, it is based on only five FMs of very different orientations. We therefore do not distinguish any additional sub-zones here.

- **L-1** (north of Grenada and Tobago): resurgence of seismicity in the south, probably due to the interaction of the subduction end with the South American strike-slip fault system El Pilar (**Figure 20a**).
- L-2, L-3 and L-4, cf above.

SI-1, SI-2, SI-3, SI-4 and SI-5 (SB – Slab Intermediate depth): from 80 to 155-190 km depths, with a constant dip of about 55° in the north and 40° in the south (Bie et al., 2020). The slab intermediate depth seismogenic areas are divided by L-1 to L-4 limits. L-3 and L-4 limits extend S-3 down to 190 km depth, where the seismic activity is more intense and deeper (**Figure 18a**). The slab geometry could induce a stress concentration in this area, and therefore, an increase in the seismic rate.

SD (Slab Detachment): from 155 to 190 km depths. Zone of slab presence uncertainty, based on Braszus et al. (2021) passive tomography study.

** Characteristics of associated seismicity **

We defined, when it was possible, the magnitude-frequency distribution for each area source as previously exposed (**Annexes 5 to 7**, Foix et al., in prep). Only SD is unusable because of the low numbers of useable earthquakes. SB-1, SB-5 and SS-4 are usable. SI-5 could also be used but the catalog covers part of the Puerto Rico system and is incomplete. Most of the zones have to be filtered or improved for $M_w \leq 3.5$ to 4 (SB-2, SB-3, SB-4, SI-1, SI-2, SI-3, SI-4, SS-1, SS-2 and SS-3). A common slope step is observed around $M_w = 3.8-4$, which could be due to magnitude conversions (SB-2, SB-4, SI-1, SI-2, SI-3, SI-4, SS-1, SS-2, SS-3 and SS-4). Finally, a small change in the slope is observed around $M_w = 4.5$, which could be due to magnitude conversion or completeness (SB-2, SB-3, SB-5, SI-1, SI-3, SS-2 and SS-4).

From instrumental records, the SS-* area sources were struck by a Max=6.5 in 2014, the SI-* area sources by a Mmax=7.4 in 2007 whereas the SB-* area sources do not seem to experience events with $M \geq 6$ yet. The December 25 1969, $M_s=7.2$, could be related to SB-3, but location and depth are highly debated and a tsunami was recorded from Antigua to Barbados (Lander et al., 2002).

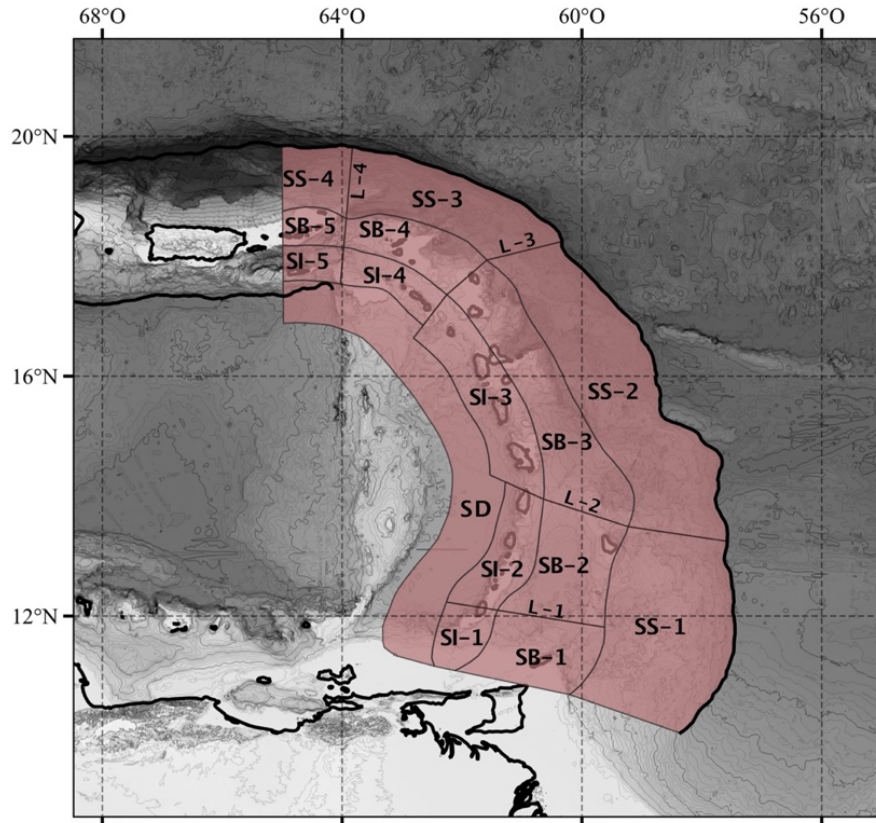


Figure 19: Slab seismotectonic model. Black thick lines highlight the main tectonic features as fractures, ridges and subduction trenches from **Figure 1**.

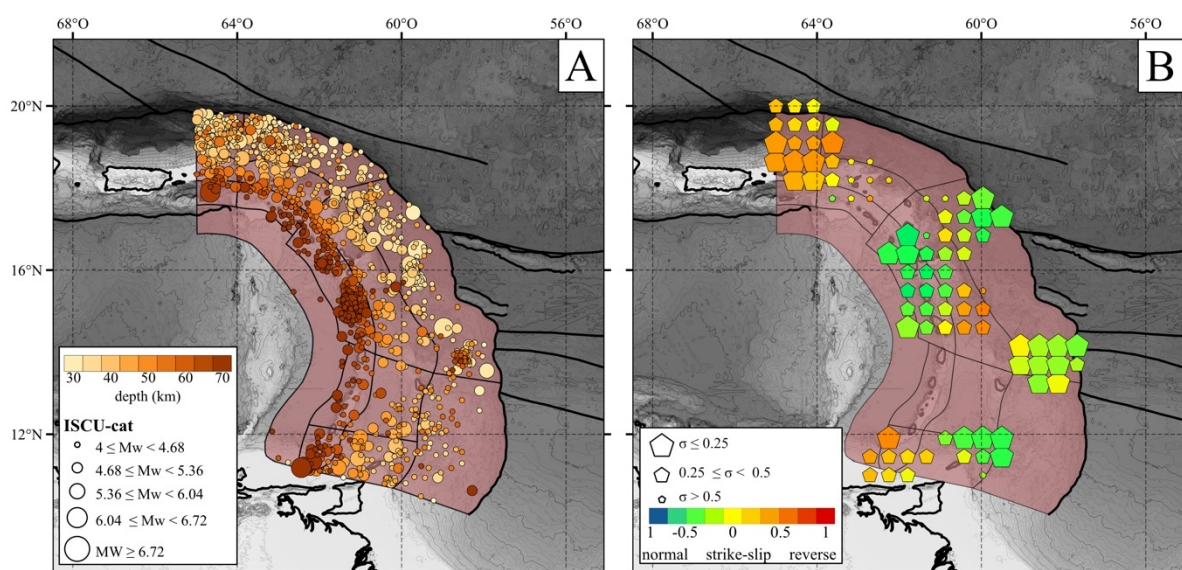


Figure 20: Slab seismotectonic model and overlapped seismotectonic data overview. Black thick lines highlight the main tectonic features as fractures, ridges and subduction trenches from **Figure 1**. **A:** ISCUCat for magnitude greater than or equal to 4 (circles). **B:** grid-average faulting style with symbol sizes inversely proportional to the standard deviation (pentagon).

3-Brief conclusion on the new seismotectonic zoning model

We propose a new seismotectonic zoning model for the Lesser Antilles system based on the major increase of scientific knowledge over the past 20 years. This model reflects the current knowledge and consensual analyses of the community within the RESIF-EPOS Seismicity Transverse Action framework. The model is composed of 20 area sources for the upper plate crust, 6 area sources for the subduction plate interface, 15 area sources for the subducting plate, and 4 area sources for the upper plate mantle. The model could directly be used for seismic hazard assessment and should be updated in the light of future scientific results. It best characterizes current knowledge on the dynamics of the Lesser Antilles. Adaptations might be necessary in order to simplify the model for the PSHA calculation, to be consistent with seismic catalogs limits.

Compared to previous studies, our model presents:

- a better depth resolution, owing to updated slab and upper crust Moho geometries;
- a better definition of accretionary wedge area source, resulting from the update of the upper plate backstop limits;
- a full update to the Marie-Galante and nearby area sources, owing to new constraints on local tectonics from geology, geomorphology, seismology and geodesy data;
- new propositions for mantle wedge and volcanic zoning;
- a full update of the subduction interface based on the integration of geodetic and coral-based data in a combined seismotectonic model;
- new oceanic slab sources based on improved seismicity catalogs.

4-Future needs and recommendations

The seismotectonic models proposed in this report can be used for seismic hazard modeling and should be updated in the light of new knowledge. A certain amount of work is in progress and will help in the future to better understand the global and local deformation of the LA. Unfortunately, some area remains poorly resolved and need for further explorations.

The southern segment of the LA and specific regions, as south of Sainte-Lucie island, need **multibeam bathymetric sonar exploration** to help in the understanding of the rapid increase observed in GNSS velocities between Sainte-Lucie and Saint-Vincent-and-the-Grenadines. This would also highlight potential extension on arc-perpendicular normal faults in this region. The oceanographic campaign GARANTI (Lebrun & Lallemand, 2017) is still under exploitation. Indeed, some seismic lines in the northern part of the Grenada Basin have been the subject of master works but have not been published yet. A GARANTI 2 campaign project (same PIs), classified as priority 1 for the last 3 years by the National Fleet Committee, and waiting to be scheduled, plans to map the northern backarc domain that is insufficiently surveyed.

To better constrain the seismic hazard assessment, **the construction of an active fault catalog**, with corresponding geometries and slip rates, should be a priority, at minima for the Guadeloupe and Martinique islands. GNSS data could potentially be used to estimate an extension rate on a regional scale and possibly across some specific faults. Unfortunately, the low expected slip rates make this possibility rather low. The **Table 1** should be generalized for each active fault of the arc, and available online for the scientific community. Several bathymetric data, and cores, remain unexploited right now and might give information on slip rate and last activity, as well as recurrence time (Leclerc pers. comm.).

We proposed a simple volcanic source model. An **adequate integration of the seismic hazard linked to volcanic activity** and in particular the influence of eruptive phases on the triggering of volcano tectonic earthquakes needs to be carried out. Some of these data can be obtained from the IPGP. Moderate and shallow volcanic earthquakes might represent an important contribution to the hazard.

At a larger scale, a better understanding of vertical motions and velocities is important for addressing the issue of subduction interface coupling. As an example, **on-land denudation rates and geomorphology analyses** on coastal terraces may provide useful constraints.

The seismic hazard induced by the mantle wedge seismicity, currently ignored in the hazard calculation chain, should be addressed. A dedicated project will aim to answer the following two questions:

- Impact for the seismic hazard estimation of the Lesser Antilles to drown out this seismicity in upper crust and intraslab zones
- Can this seismicity be specifically considered in ground motion estimations and seismic hazard calculation?

In the future, the ATLAS (AnTiLes Aléa Sismique) project aims to develop a community PSHA model, built by the RESIF-EPOS ATS group, for the Lesser Antilles, by 2026. Three main work packages are proposed:

- WP-1: homogenizing of seismic catalog (M_w) integrating instrumental data (ISC, CDSA, IPGP, neighboring networks) and historical data (macroseismic SisFrance-

Antilles), leading by the BRGM (Anne Lemoine, Roser Hoste Colomer, Didier Bertil, Agathe Roulle) and IPGP (Claudio Satriano, Jean-Marie Saurel)

- WP-2: finalization of the seismotectonic zoning model and PSHA tests (activity by zone, integration of geodetic data, targeted tests on Guadeloupe), leading by Geosciences Montpellier and IRSN (Océane Foix, Hervé Jomard, Stéphane Mazzotti)
- WP-3: PSHA models (construction of the earthquake recurrence model and associated uncertainties, selection of ground motion prediction models, PSHA calculations), leading by ISTerre (Céline Beauval, Emeline Maufroy).

References

- Abe, K. (1979). Size of great earthquakes of 1837–1974 inferred from tsunami data. *Journal of Geophysical Research*, 84(B4), 1561. <https://doi.org/10.1029/JB084iB04p01561>
- Aitken, T., Mann, P., Escalona, A., & Christeson, G. L. (2011). Evolution of the Grenada and Tobago basins and implications for arc migration. *Marine and Petroleum Geology*, 28(1), 235–258. <https://doi.org/10.1016/j.marpetgeo.2009.10.003>
- Allen, R., Collier, J., Henstock, T., Stewart, A., & Goes, S. (2019). A new tectonic model for the Lesser Antilles: Evidence for a buried arc in the eastern Caribbean. *Geophysical Research Abstracts*, 1–1.
- Beck, C., Reyss, J.-L., Leclerc, F., Moreno, E., Feuillet, N., Barrier, L., Beauducel, F., Boudon, G., Clément, V., Deplus, C., Gallou, N., Lebrun, J.-F., le Friant, A., Nercessian, A., Paterne, M., Pichot, T., & Vidal, C. (2012). Identification of deep subaqueous coseismic scarps through specific coeval sedimentation in Lesser Antilles: implication for seismic hazard. *Natural Hazards and Earth System Sciences*, 12(5), 1755–1767. <https://doi.org/10.5194/nhess-12-1755-2012>
- Bengoubou-Valerius, M., Bazin, S., Bertil, D., Beauducel, F., & Bosson, A. (2008). CDSA: a new seismological data center for the French Lesser Antilles. *Seismological Research Letters*, 79(1). http://web2013copy.ipgp.fr/~beaudu/download/2008_Bengoubou_SRL.pdf
- Bernard, P., & Lambert, J. (1988). Subduction and seismic hazard in the northern Lesser Antilles: Revision of the historical seismicity. *Bulletin of the Seismological Society of America*, 78(6), 1965–1983. <https://doi.org/10.1785/BSSA0780061965>
- Bertil, D., & Lemoine, A. (2017). Analyse des axes prioritaires de travail visant une révision des calculs d'aléa sismique aux Antilles à partir des données des Antilles françaises Rapport final. *BRGM/TP-67372-FR*.
- Bie, L., Hicks, S., Rietbrock, A., Goes, S., Collier, J., Rychert, C., Harmon, N., & Maunder, B. (2022). Imaging slab-transported fluids and their deep dehydration from seismic velocity tomography in the Lesser Antilles subduction zone. *Earth and Planetary Science Letters*, 586. <https://doi.org/10.1016/j.epsl.2022.117535>
- Bie, L., Rietbrock, A., Hicks, S., Allen, R., Blundy, J., Clouard, V., Collier, J., Davidson, J., Garth, T., Goes, S., Harmon, N., Henstock, T., Van Hunen, J., Kendall, M., Krüger, F., Lynch, L., Macpherson, C., Robertson, R., Rychert, K., ... Wilson, M. (2020). Along-arc heterogeneity in local seismicity across the Lesser Antilles subduction zone from a dense ocean-bottom seismometer network. *Seismological Research Letters*, 91(1), 237–247. <https://doi.org/10.1785/0220190147>
- Boucard, M., Marcaillou, B., Lebrun, J. F., Laurencin, M., Klingelhoefer, F., Laigle, M., Lallemand, S., Schenini, L., Graindorge, D., Cornée, J. J., Münch, P., Philippon, M., & the, A. (2021). Paleogene V-Shaped Basins and Neogene Subsidence of the Northern Lesser Antilles Forearc. *Tectonics*, 40(3). <https://doi.org/10.1029/2020TC006524>
- Bouin, M.-P., Bouchon, M., Olivier, C. O., Bazin, S., & Latchman, J. (2010). Source parameters of the Mw 7.4 Martinique intermediate-depth earthquake (Leeward islands) of November 29, 2007: A slab-pull event with horizontal fault plane. *EGUGA*, 12(4), 5555. <https://ui.adsabs.harvard.edu/abs/2010EGUGA..12.5555M/abstract>
- Bouysse, P., Westercamp, D., & Andreieff, P. (1990). The Lesser Antilles Island Arc. *Proceedings of the Ocean Drilling Program, Scientific Results*, 110.
- Bozzoni, F., Corigliano, M., Lai, C. G., Salazar, W., Scandella, L., Zuccolo, E., Latchman, J., Lynch, L., & Robertson, R. (2011). Probabilistic seismic hazard assessment at the eastern Caribbean Islands. *Bulletin of the Seismological Society of America*, 101(5), 2499–2521. <https://doi.org/10.1785/0120100208>

- Braszus, B., Goes, S., Allen, R., Rietbrock, A., Collier, J., Harmon, N., Henstock, T., Hicks, S., Rychert, C. A., Maunder, B., van Hunen, J., Bie, L., Blundy, J., Cooper, G., Davy, R., Kendall, J. M., Macpherson, C., Wilkinson, J., & Wilson, M. (2021). Subduction history of the Caribbean from upper-mantle seismic imaging and plate reconstruction. *Nature Communications*, *12*(1). <https://doi.org/10.1038/s41467-021-24413-0>
- Brown, K. M., & Westbrook, G. K. (1987). The tectonic fabric of the Barbados Ridge accretionary complex. *Marine and Petroleum Geology*, *4*(1), 71–81. [https://doi.org/10.1016/0264-8172\(87\)90022-5](https://doi.org/10.1016/0264-8172(87)90022-5)
- Burke, K. (1988). Tectonic Evolution of the Caribbean. *Ann. Rev. Earth Planet. Sci.*, *16*, 201–230. <https://doi.org/10.1146/ANNUREV.EA.16.050188.001221>
- Byrne, D. B., Suarez, G., & Mccann, W. R. (1985). Muertos Trough subduction—microplate tectonics in the northern Caribbean? *Nature* *1985 317:6036*, *317*(6036), 420–421. <https://doi.org/10.1038/317420a0>
- Carafa, M. M. C., Kastelic, V., Bird, P., Maesano, F. E., & Valensise, G. (2018). A “Geodetic Gap” in the Calabrian Arc: Evidence for a Locked Subduction Megathrust? *Geophysical Research Letters*, *45*(4), 1794–1804. <https://doi.org/10.1002/2017GL076554>
- Carey, S. ;, Sparks, R. S. J. ;, Tucker, M. E. ;, Robinson, L. ;, Watt, S. ;, Gee, M. ;, Hastie, A. ;, Barfod, D. N. ;, Stinton, A. ;, Leng, A. ;, Raineault, N. ;, & Ballard, R. D. (2019). The polygenetic Kahouanne Seamounts in the northern Lesser Antilles island arc. *Marine Geology*, *419*. <https://doi.org/10.1016/j.margeo.2019.106046>
- Carpentier, M., Chauvel, C., & Mattielli, N. (2008). Pb–Nd isotopic constraints on sedimentary input into the Lesser Antilles arc system. *Earth and Planetary Science Letters*, *272*(1–2), 199–211. <https://doi.org/10.1016/J.EPSL.2008.04.036>
- Christeson, G. L., Mann, P., Escalona, A., & Aitken, T. J. (2008). Crustal structure of the Caribbean - Northeastern South America arc-continent collision zone. *Journal of Geophysical Research: Solid Earth*, *113*(8). <https://doi.org/10.1029/2007JB005373>
- Cooper, G. F., Macpherson, C. G., Blundy, J. D., Maunder, B., Allen, R. W., Goes, S., Collier, J. S., Bie, L., Harmon, N., Hicks, S. P., Iveson, A. A., Prytulak, J., Rietbrock, A., Rychert, C. A., Davidson, J. P., Cooper, G. F., Macpherson, C. G., Blundy, J. D., Maunder, B., ... Wilson, M. (2020). Variable water input controls evolution of the Lesser Antilles volcanic arc. *Nature*, *582*(7813), 525–529. <https://doi.org/10.1038/s41586-020-2407-5>
- Corbeau, J., Gonzalez, O., Feuillet, N., Lejeune, A. M., Fontaine, F. R., Clouard, V., & Saurel, J. M. (2021). A Significant Increase in Interplate Seismicity near Major Historical Earthquakes Offshore Martinique (FWI). *Bulletin of the Seismological Society of America*, *111*(6), 3118–3135. <https://doi.org/10.1785/0120200377>
- Corbeau, J., Gonzalez, O. L., Clouard, V., Rolandone, F., Leroy, S., Keir, D., Stuart, G., Momplaisir, R., Boisson, D., & Prépetit, C. (2019). Is the local seismicity in western Hispaniola (Haiti) capable of imaging northern Caribbean subduction? *Geosphere*, *15*(6), 1738–1750. <https://doi.org/10.1130/GES02083.1>
- Craig, T. J., Copley, A., & Jackson, J. (2014). A reassessment of outer-rise seismicity and its implications for the mechanics of oceanic lithosphere. *Geophysical Journal International*, *197*(1), 63–89. <https://doi.org/10.1093/gji/ggu013>
- Davey, F. J., & Ristau, J. (2011). Fore-arc mantle wedge seismicity under northeast New Zealand. *Tectonophysics*, *509*(3–4), 272–279. <https://doi.org/10.1016/J.TECTO.2011.06.017>
- DeMets, C., Gordon, R. G., & Argus, D. F. (2010). Geologically current plate motions. *Geophysical Journal International*, *181*(1), 1–80. <https://doi.org/10.1111/J.1365-246X.2009.04491.X>

- Ezenwaka, K., Marcaillou, B., Laigle, M., Klingelhoefer, F., Lebrun, J. F., Paulatto, M., Biari, Y., Rolandone, F., Lucazeau, F., Heuret, A., Pichot, T., & Bouquerel, H. (2022). Thermally-constrained fluid circulation and seismicity in the Lesser Antilles subduction zone. *Earth and Planetary Science Letters*, 597, 117823. <https://doi.org/10.1016/J.EPSL.2022.117823>
- Feng, L., Newman, A. v., Protti, M., Gonzalez, V. M., Dixon, T. H., Luo, Y., & Jiang, Y. (2010). Interseismic Megathrust Coupling near Nicoya, Costa Rica Between 1994 and 2010. *AGU Fall Meeting, 2010*, T44B-05. <https://ui.adsabs.harvard.edu/abs/2010AGUFM.T44B..05F/abstract>
- Feuillet, N., Beauducel, F., Jacques, E., Tapponnier, P., Delouis, B., Bazin, S., Vallée, M., & King, G. C. P. (2011). The Mw = 6.3, November 21, 2004, les Saintes earthquake (Guadeloupe): Tectonic setting, slip model and static stress changes. *Journal of Geophysical Research: Solid Earth*, 116(10). <https://doi.org/10.1029/2011JB008310>
- Feuillet, N., Beauducel, F., & Tapponnier, P. (2011). Tectonic context of moderate to large historical earthquakes in the Lesser Antilles and mechanical coupling with volcanoes. *Journal of Geophysical Research: Solid Earth*, 116(10). <https://doi.org/10.1029/2011JB008443>
- Feuillet, N., Leclerc, F., Tapponnier, P., Beauducel, F., Boudon, G., le Friant, A., Deplus, C., Lebrun, J. F., Necessian, A., Saurel, J. M., & Clément, V. (2010). Active faulting induced by slip partitioning in montserrat and link with volcanic activity: New insights from the 2009 GWADASEIS marine cruise data. *Geophysical Research Letters*, 37(19), 1–6. <https://doi.org/10.1029/2010GL042556>
- Feuillet, N., Manighetti, I., & Tapponnier, P. (2001). Extension active perpendiculaire à la subduction dans l'arc des Petites Antilles (Guadeloupe, Antilles françaises). *Comptes Rendus de l'Académie Des Sciences - Series IIA - Earth and Planetary Science*, 333(9), 583–590. [https://doi.org/10.1016/S1251-8050\(01\)01543-9](https://doi.org/10.1016/S1251-8050(01)01543-9)
- Feuillet, N., Manighetti, I., Tapponnier, P., & Jacques, E. (2002). Arc parallel extension and localization of volcanic complexes in Guadeloupe, Lesser Antilles. *Journal of Geophysical Research: Solid Earth*, 107(B12), ETG 3-1-ETG 3-29. <https://doi.org/10.1029/2001jb000308>
- Feuillet, N., Tapponnier, P., Manighetti, I., Villemant, B., & King, G. C. P. (2004). Differential uplift and tilt of Pleistocene reef platforms and Quaternary slip rate on the Morne-Piton normal fault (Guadeloupe, French West Indies). *Journal of Geophysical Research: Solid Earth*, 109(B2). <https://doi.org/10.1029/2003jb002496>
- Garroq, C. (2021). Apport de l'imagerie sismique à la compréhension de la dynamique arrière-arc des Petites Antilles au Cénozoïque. *Ph.D. Thesis, Géosciences Montpellier*. <https://tel.archives-ouvertes.fr/tel-03342546>
- Garroq, C., Lallemand, S., Marcaillou, B., Lebrun, J. F., Padron, C., Klingelhoefer, F., Laigle, M., Münch, P., Gay, A., Schenini, L., Beslier, M. O., Cornée, J. J., Mercier de Lépinay, B., Quillévéré, F., BouDagher-Fadel, M., Agranier, A., Arcay, D., Audemard, F., Boucard, M., ... Yates, B. (2021). Genetic Relations Between the Aves Ridge and the Grenada Back-Arc Basin, East Caribbean Sea. *Journal of Geophysical Research: Solid Earth*, 126(2), e2020JB020466. <https://doi.org/10.1029/2020JB020466>
- Geoter. (2002). Révision du zonage sismique de la France - Etude Probabiliste - Synthèse de l'étude.
- Girardin, N., Feuillard, M., & Viode, J. P. (1991). Regional seismic network in the Lesser Antilles Arc: Shallow seismicity (1981-1988). *Bulletin Société Géologique Française*, 162(6), 1003–1015.
- Gómez-Capera, A. A., Stucchi, M., Arcila, M., Bufaliza, M., Choy, J., Minaya, E., Leyton, L., Pirchiner, M., Rendón, H., Rodriguez, L., Sarabia, A., Tavera, H., Yepes, H., De, O.,

- Calixto, S., & Paz, L. (2017). Updated earthquake catalog for South America: Time window pre-1964. *16th World Conference on Earthquake, 16WCEE 2017*.
- González, O. L., Clouard, V., & Zahradnik, J. (2017). Moment tensor solutions along the central Lesser Antilles using regional broadband stations. *Tectonophysics*, *717*, 214–225. <https://doi.org/10.1016/j.tecto.2017.06.024>
- Grindlay, N. R., Mann, P., Dolan, J. F., & Gestel, J. P. van. (2005). Neotectonics and subsidence of the northern Puerto Rico-Virgin Islands margin in response to the oblique subduction of high-standing ridges. *Special Paper of the Geological Society of America*, *385*, 31–60. <https://doi.org/10.1130/0-8137-2385-X.31>
- Gutscher, M. A., Westbrook, G. K., Marcaillou, B., Graindorge, D., Gailler, A., Pichot, T., & Maury, R. C. (2013). How wide is the seismogenic zone of the Lesser Antilles forearc? *Bulletin de La Societe Geologique de France*, *184*(1–2), 47–59. <https://doi.org/10.2113/gssgfbull.184.1-2.47>
- Harmon, N., Rychert, C. A., Goes, S., Maunder, B., Collier, J., Henstock, T., Lynch, L., & Rietbrock, A. (2021). Widespread Hydration of the Back Arc and the Link to Variable Hydration of the Incoming Plate in the Lesser Antilles From Rayleigh Wave Imaging. *Geochemistry, Geophysics, Geosystems*, *22*(7). <https://doi.org/10.1029/2021GC009707>
- Harmon, N., Rychert, C., Collier, J., Henstock, T., van Hunen, J., & Wilkinson, J. J. (2019). Mapping geologic features onto subducted slabs. *Geophysical Journal International*, *219*(2), 725–733. <https://doi.org/10.1093/gji/ggz290>
- Hayes, G. P., McNamara, D. E., Seidman, L., & Roger, J. (2014). Quantifying potential earthquake and tsunami hazard in the Lesser Antilles subduction zone of the Caribbean region. *Geophysical Journal International*, *196*(1), 510–521. <https://doi.org/10.1093/GJI/GGT385>
- Heuret, A., Lallemand, S., Funicello, F., Piromallo, C., & Faccenna, C. (2011). Physical characteristics of subduction interface type seismogenic zones revisited. *Geochemistry, Geophysics, Geosystems*, *12*(1), n/a-n/a. <https://doi.org/10.1029/2010GC003230>
- Hicks, S. P., Bie, L., Rychert, C. A., Harmon, N., Goes, S., Rietbrock, A., Wei, S. S., Collier, J. S., Henstock, T. J., Lynch, L., Prytulak, J., Macpherson, C. G., Schlaphorst, D., Wilkinson, J. J., Blundy, J. D., Cooper, G. F., Davy, R. G., & Kendall, J.-M. (2023). Slab to back-arc to arc: Fluid and melt pathways through the mantle wedge beneath the Lesser Antilles. *Science Advances*, *9*(5). <https://doi.org/10.1126/sciadv.add2143>
- Ito, Y., & Obara, K. (2006). Dynamic deformation of the accretionary prism excites very low frequency earthquakes. *Geophysical Research Letters*, *33*(2), L02311. <https://doi.org/10.1029/2005GL025270>
- James F. Lander, Whiteside Lowell S., & Patricia A. Lockridge. (2002). A brief history of tsunami in the Caribbean Sea. *Science of Tsunami Hazards*, *20*(2). https://www.researchgate.net/publication/38112210_A_brief_history_of_tsunami_in_the_Caribbean_Sea
- Jany, I., Scanlon, K. M., & Mauffret, A. (1990a). Geological interpretation of combined Seabeam, Gloria and seismic data from Anegada Passage (Virgin Islands, north Caribbean). *Marine Geophysical Researches 1990 12:3*, *12*(3), 173–196. <https://doi.org/10.1007/BF02266712>
- Jany, I., Scanlon, K. M., & Mauffret, A. (1990b). Geological interpretation of combined Seabeam, Gloria and seismic data from Anegada Passage (Virgin Islands, north Caribbean). *Marine Geophysical Researches 1990 12:3*, *12*(3), 173–196. <https://doi.org/10.1007/BF02266712>
- Kanamori, H. (1971). Seismological evidence for a lithospheric normal faulting — the Sanriku earthquake of 1933. *Physics of the Earth and Planetary Interiors*, *4*(4), 289–300. [https://doi.org/10.1016/0031-9201\(71\)90013-6](https://doi.org/10.1016/0031-9201(71)90013-6)

- Kopp, H., Weinzierl, W., Becel, A., Charvis, P., Evain, M., Flueh, E. R., Gailler, A., Galve, A., Hirn, A., Kandilarov, A., Klaeschen, D., Laigle, M., Papenberg, C., Planert, L., & Roux, E. (2011). Deep structure of the central Lesser Antilles Island Arc: Relevance for the formation of continental crust. *Earth and Planetary Science Letters*, *304*(1–2), 121–134. <https://doi.org/10.1016/j.epsl.2011.01.024>
- Laigle, M., Becel, A., de Voogd, B., Sachpazi, M., Bayrakci, G., Lebrun, J. F., & Evain, M. (2013). Along-arc segmentation and interaction of subducting ridges with the Lesser Antilles Subduction forearc crust revealed by MCS imaging. *Tectonophysics*, *603*, 32–54. <https://doi.org/10.1016/j.tecto.2013.05.028>
- Laigle, M., Hirn, A., Sapin, M., Bécél, A., Charvis, P., Flueh, E., Diaz, J., Lebrun, J. F., Gesret, A., Raffaele, R., Galvé, A., Evain, M., Ruiz, M., Kopp, H., Bayrakci, G., Weinzierl, W., Hello, Y., Lépine, J. C., Viodé, J. P., ... Nicolich, R. (2013). Seismic structure and activity of the north-central Lesser Antilles subduction zone from an integrated approach: Similarities with the Tohoku forearc. In *Tectonophysics* (Vol. 603, pp. 1–20). <https://doi.org/10.1016/j.tecto.2013.05.043>
- Laigle, M., Lebrun, J.-F., & Hirn, A. (2007). *SISMANTILLES 2 cruise, RV L'Atalante*. <https://doi.org/https://doi.org/10.17600/7010020>
- Laurencin, M., Graindorge, D., Klingelhoefer, F., Marcaillou, B., & Evain, M. (2018). Influence of increasing convergence obliquity and shallow slab geometry onto tectonic deformation and seismogenic behavior along the Northern Lesser Antilles zone. *Earth and Planetary Science Letters*, *492*, 59–72. <https://doi.org/10.1016/J.EPSL.2018.03.048>
- Laurencin, M., Marcaillou, B., Graindorge, D., Klingelhoefer, F., Lallemand, S., Laigle, M., & Lebrun, J. F. (2017). The polyphased tectonic evolution of the Anegada Passage in the northern Lesser Antilles subduction zone. *Tectonics*, *36*(5), 945–961. <https://doi.org/10.1002/2017TC004511>
- Laurencin, M., Marcaillou, B., Graindorge, D., Lebrun, J. F., Klingelhoefer, F., Boucard, M., Laigle, M., Lallemand, S., & Schenini, L. (2019). The Bunce Fault and Strain Partitioning in the Northern Lesser Antilles. *Geophysical Research Letters*, *46*(16), 9573–9582. <https://doi.org/10.1029/2019GL083490>
- Lay, T., Kanamori, H., Ammon, C. J., Koper, K. D., Hutko, A. R., Ye, L., Yue, H., and Rushing, T. M.: Depth-varying rupture properties of subduction zone megathrust faults, *J. Geophys. Res.-Sol. Ea.*, *117*, B04311, <https://doi.org/10.1029/2011JB009133>, 2012
- Lay, T. (2015). The surge of great earthquakes from 2004 to 2014. *Earth and Planetary Science Letters*, *409*, 133–146. <https://doi.org/10.1016/J.EPSL.2014.10.047>
- Le Roy, S., Lemoine, A., Nachbaur, A., Legendre, Y., Lambert, J., & Terrier, M. (2017). Détermination de la submersion marine liée aux tsunamis en Martinique. *BRGM/RP-66547-FR*.
- Lebrun, J.-F., & Lallemand, S. E. (2017). *GARANTI cruise. RV L'Atalante*.
- Leclerc, F. (2014). Déformation active permanente induite par le méga-chevauchement dans l'arc antillais : Apport des complexes récifaux quaternaires. *Sorbonne Paris Cité*.
- Leclerc, F., Feuillet, N., & Deplus, C. (2016). Interactions between active faulting, volcanism, and sedimentary processes at an island arc: Insights from Les Saintes channel, Lesser Antilles arc. *Geochemistry, Geophysics, Geosystems*, *17*(7), 2781–2802. <https://doi.org/10.1002/2016GC006337>
- Lindner, M., Rietbrock, A., Bie, L., Goes, S., Collier, J., Rychert, C., Harmon, N., Hicks, S. P., Henstock, T., & group, the V. working. (2023). Bayesian regional moment tensor from ocean bottom seismograms recorded in the Lesser Antilles: Implications for regional stress field. *Geophysical Journal International*, *233*(2), 1036–1054. <https://doi.org/https://doi.org/10.1093/gji/ggac494>

- Lynch, L. L. (2005). The programme for the assessment of seismic hazard in the English speaking eastern Caribbean territories: current status and the way forward. *Special Two-Day Conference on Earthquake Engineering*.
- Manaker, D. M., Calais, E., Freed, A. M., Ali, S. T., Przybylski, P., Mattioli, G., Jansma, P., Prépetit, C., & de Chabaliér, J. B. (2008). Interseismic Plate coupling and strain partitioning in the Northeastern Caribbean. *Geophysical Journal International*, 174(3), 889–903. <https://doi.org/10.1111/j.1365-246X.2008.03819.x>
- Mann, P., Schubert, C., & Burke, K. (1991). Review of Caribbean neotectonics. *The Caribbean Region*, 307–338. <https://doi.org/10.1130/DNAG-GNA-H.307>
- Mann, P., Taylor, F. W., Edwards, R. L., & Ku, T. L. (1995). Actively evolving microplate formation by oblique collision and sideways motion along strike-slip faults: An example from the northeastern Caribbean plate margin. *Tectonophysics*, 246(1–3), 1–69. [https://doi.org/10.1016/0040-1951\(94\)00268-E](https://doi.org/10.1016/0040-1951(94)00268-E)
- Marcaillou, B., Klingelhofer, F., Laurencin, M., Lebrun, J.-F., Laigle, M., Lallemand, S., Schenini, L., Gay, A., Boucard, M., Ezenwaka, K., & Graindorge, D. (2021). Pervasive detachment faults within the slow spreading oceanic crust at the poorly coupled Antilles subduction zone. *Communications Earth & Environment*, 2(1). <https://doi.org/10.1038/s43247-021-00269-6>
- Massin, F., Clouard, V., Vorobieva, I., Beauducel, F., Saurel, J. M., Satriano, C., Bouin, M. P., & Bertil, D. (2021). Automatic picking and probabilistic location for earthquake assessment in the lesser antilles subduction zone (1972-2012). In *Comptes Rendus - Geoscience* (Vol. 353, Issue S1). Academie des sciences. <https://doi.org/10.5802/crgeos.81>
- Mazzotti, S., Aubagnac, C., Bollinger, L., Coca Oscanoa, K., Delouis, B., do Paco, D., Doubre, C., Godano, M., Jomard, H., Larroque, C., Laurendeau, A., Masson, F., Sylvander, M., & Trilla, A. (2021). FMHex20: An earthquake focal mechanism database for seismotectonic analyses in metropolitan France and bordering regions. *BSGF - Earth Sciences Bulletin*, 192. <https://doi.org/10.1051/bsgf/2020049>
- McCann, W. R., Dewey, J. W., Murphy, A. J., & Harding, S. T. (1982). A large normal-fault earthquake in the overriding wedge of the Lesser Antilles subduction zone: the earthquake of 8 October 1974. *Bulletin of the Seismological Society of America*, 72(6), 2267–2283.
- McCann, W. R., Sykes, L. R., McCann, W. R., & Sykes, L. R. (1984). Subduction of aseismic ridges beneath the Caribbean Plate: Implications for the tectonics and seismic potential of the northeastern Caribbean. *JGR*, 89(B6), 4493–4519. <https://doi.org/10.1029/JB089IB06P04493>
- McGuire, R. K. (2004). Seismic hazard and risk analysis. *Earthquake Engineering Research Institute*, 221.
- McNutt, S. R., & Roman, D. C. (2015). Volcanic Seismicity. In *The Encyclopedia of Volcanoes* (pp. 1011–1034). Elsevier. <https://doi.org/10.1016/b978-0-12-385938-9.00059-6>
- Meng, L., Ampuero, J.-P., Stock, J., Duputel, Z., Luo, Y., & Tsai, V. C. (2012). Earthquake in a Maze: Compressional Rupture Branching During the 2012 Mw 8.6 Sumatra Earthquake. *Science*, 337(6095), 724–726. <https://doi.org/10.1126/science.1224030>
- Obana, K., & Kodaira, S. (2009). Low-frequency tremors associated with reverse faults in a shallow accretionary prism. *Earth and Planetary Science Letters*, 287(1–2), 168–174. <https://doi.org/10.1016/j.epsl.2009.08.005>
- Oral, E., & Satriano, C. (2021). Future magnitude 7.5 earthquake offshore Martinique: Spotlight on the main source features controlling ground motion prediction. *Geophysical Journal International*, 227(2), 1076–1093. <https://doi.org/10.1093/gji/ggab245>

- Padron, C., Klingelhoefer, F., Marcaillou, B., Lebrun, J. F., Lallemand, S., Garroq, C., Laigle, M., Roest, W. R., Beslier, M. O., Schenini, L., Graindorge, D., Gay, A., Audemard, F., Münch, P., Klingelhoefer, F., Marcaillou, B., Lebrun, J. F., Lallemand, S., Laigle, M., ... Yates, B. (2021). Deep Structure of the Grenada Basin From Wide-Angle Seismic, Bathymetric and Gravity Data. *Journal of Geophysical Research: Solid Earth*, *126*(2). <https://doi.org/10.1029/2020JB020472>
- Pagani, M., Garcia-Pelaez, J., Gee, R., Johnson, K., Poggi, V., Silva, V., Simionato, M., Styron, R., Viganò, D., Danciu, L., Monelli, D., & Weatherill, G. (2020). The 2018 version of the Global Earthquake Model: Hazard component. *Earthquake Spectra*, *36*(1_suppl), 226–251. <https://doi.org/10.1177/8755293020931866>
- Patriat, M., Pichot, T., Westbrook, G. K., UMBER, M., Deville, E., Bénard, F., Roest, W. R., & Loubrieu, B. (2011a). Evidence for Quaternary convergence across the North America–South America plate boundary zone, east of the Lesser Antilles. *Geology*, *39*(10), 979–982. <https://doi.org/10.1130/G32474.1>
- Patriat, M., Pichot, T., Westbrook, G. K., UMBER, M., Deville, E., Bénard, F., Roest, W. R., & Loubrieu, B. (2011b). Evidence for Quaternary convergence across the North America–South America plate boundary zone, east of the Lesser Antilles. *Geology*, *39*(10), 979–982. <https://doi.org/10.1130/G32474.1>
- Paulatto, M., Laigle, M., Galve, A., Charvis, P., Sapin, M., Bayrakci, G., Evain, M., & Kopp, H. (2017). Dehydration of subducting slow-spread oceanic lithosphere in the Lesser Antilles. *Nature Communications*, *8*. <https://doi.org/10.1038/ncomms15980>
- Peruzza, L., Azzaro, R., Gee, R., D’Amico, S., Langer, H., Lombardo, G., Pace, B., Pagani, M., Panzera, F., Ordaz, M., Suarez, M. L., & Tusa, G. (2017). When probabilistic seismic hazard climbs volcanoes: the Mt. Etna case, Italy – Part 2: Computational implementation and first results. *Natural Hazards and Earth System Sciences*, *17*(11), 1999–2015. <https://doi.org/10.5194/nhess-17-1999-2017>
- Peter, G., & Westbrook, G. K. (1976). Tectonics of Southwestern North Atlantic and Barbados Ridge Complex. *AAPG Bulletin*, *60*(7), 1078–1106. <https://doi.org/10.1306/C1EA3622-16C9-11D7-8645000102C1865D>
- Philibosian, B., Feuillet, N., Weil-Accardo, J., Jacques, E., Guihou, A., Mériaux, A. S., Anglade, A., Saurel, J. M., & Deroussi, S. (2022). 20th-century strain accumulation on the Lesser Antilles megathrust based on coral microatolls. *Earth and Planetary Science Letters*, *579*. <https://doi.org/10.1016/j.epsl.2021.117343>
- Philippon, M.; Roger, J.; Lebrun, J.F.; Thinon, I.; Foix, O.; Mazzotti, S.; Gutscher, M.A.; Montheil, L.; Cornée, J.J.; (*under review at Marine Geology*): “Forearc crustal faulting and associated tsunami hazard in the upper plate of subduction zones. Case study of the Morne Piton Fault system (Lesser Antilles, Guadeloupe Archipelago)”
- Pichot, T., Patriat, M., Westbrook, G. K., Nalpas, T., Gutscher, M. A., Roest, W. R., Deville, E., Moulin, M., Aslanian, D., & Rabineau, M. (2012). The Cenozoic tectonostratigraphic evolution of the Barracuda Ridge and Tiburon Rise, at the western end of the North America-South America plate boundary zone. *Marine Geology*, *303–306*, 154–171. <https://doi.org/10.1016/j.margeo.2012.02.001>
- Polonia, A., Bonatti, E., Camerlenghi, A., Lucchi, R. G., Panieri, G., & Gasperini, L. (2013). Mediterranean megaturbidite triggered by the AD 365 Crete earthquake and tsunamis. *Scientific Reports*, *3*. <https://doi.org/10.1038/SREP01285>
- Régnier, J., Michel, C., Bertrand, E., & Guéguen, P. (2013). Contribution of ambient vibration recordings (Free-field and buildings) for post-seismic analysis: the case of the Mw 7.3 Martinique (French Lesser Antilles) earthquake, November 29, 2007. *Soil Dynamics and Earthquake Engineering*, *50*, 162–167. <https://doi.org/https://doi.org/10.1016/j.soildyn.2013.03.007>

- Reid, H. F., & Taber, S. (1920). The Virgin Islands earthquakes of 1867-1868. *Bulletin of the Seismological Society of America*, 10(1), 9–30.
<https://doi.org/10.1785/BSSA0100010009>
- Robson, G. R. (1964). An earthquake catalogue for the Eastern Caribbean 1530-1960. *Bulletin of the Seismological Society of America*, 54(2), 785–832.
<https://doi.org/10.1785/BSSA0540020785>
- Robson, G. R., & Tomblin, J. F. (1951). Catalogue of the Active Volcanoes of the World: West Indies. *Michigan University*.
- Roest, W. R., & Collette, B. J. (1986). The Fifteen Twenty Fracture Zone and the North American-South American plate boundary. *Journal of the Geological Society*, 143(5), 833–843. <https://doi.org/10.1144/GSJGS.143.5.0833>
- Ruff, L., & Kanamori, H. (1983). Seismic coupling and uncoupling at subduction zones. *Tectonophysics*, 99(2–4), 99–117. [https://doi.org/10.1016/0040-1951\(83\)90097-5](https://doi.org/10.1016/0040-1951(83)90097-5)
- Ruiz, M., Galve, A., Monfret, T., Sapin, M., Charvis, P., Laigle, M., Evain, M., Hirn, A., Flueh, E., Gallart, J., Diaz, J., & Lebrun, J. F. (2013). Seismic activity offshore Martinique and Dominica islands (Central Lesser Antilles subduction zone) from temporary onshore and offshore seismic networks. *Tectonophysics*, 603, 68–78.
<https://doi.org/10.1016/j.tecto.2011.08.006>
- Russo, R. M., Okal, E. A., & Rowley, K. C. (1992). Historical seismicity of the southeastern Caribbean and tectonic implications. *Pure and Applied Geophysics PAGEOPH*, 139(1), 87–120. <https://doi.org/10.1007/BF00876827>
- Saurel, J.-M., Bouin, M.-P., Satriano, C., Lemarchand, A., OVSG Team, & OVSM Team. (2022). 2014-2019 Antilles IPGP merged seismic catalog. In *IPGP Research Collection*, VI. <https://doi.org/https://doi.org/10.18715/IPGP.2022.13ylhaal>
- Schlaphorst, D., Kendall, J. M., Baptie, B., Latchman, J. L., & Tait, S. (2017). Gaps, tears and seismic anisotropy around the subducting slabs of the Antilles. *Tectonophysics*, 698, 65–78. <https://doi.org/10.1016/J.TECTO.2017.01.002>
- Schlaphorst, D., Kendall, J. M., Collier, J. S., Verdon, J. P., Blundy, J., Baptie, B., Latchman, J. L., Massin, F., & Bouin, M. P. (2016). Water, oceanic fracture zones and the lubrication of subducting plate boundaries—insights from seismicity. *Geophysical Journal International*, 204(3), 1405–1420. <https://doi.org/10.1093/GJI/GGV509>
- Sedan, O., & Terrier, M. (2001). Travaux de reconnaissance pour l'étude de paléosismicité de la faille du May (Guadeloupe). *BRGM/RP-51420-FR*.
- Seibert, C., Feuillet, N., Ratzov, G., Beck, C., Morena, P., Johannes, L., Ducassou, E., Cattaneo, A., Goldfinger, C., Moreno, E., Bieber, A., & Caseis Cruise Party. (2022). Late Quaternary sedimentary record of large earthquakes in the Lesser Antilles : implications for the megathrust behavior. *Volcanism, Seismicity and Tectonics of the Greater and Lesser Antilles, Scientific Meetings, OVSM-IPGP-PREST*.
- Shepherd, J. B., & Lynch, L. L. (2003). Seismic hazard assessment and microzonation of Trinidad and Tobago. *Final Report, National Emergency Management Agency of Trinidad and Tobago. Seismic Research Unit, University of West Indies, St. Augustine, Trinidad*.
- Shepherd, J. B., Tomblin, J. F., & Woo, D. A. (1971). Volcano-seismic crisis in Montserrat, West Indies, 1966–67. *Bulletin Volcanologique*, 35(1), 143–162.
<https://doi.org/10.1007/BF02596813/METRICS>
- Speed, R. C., & Larue, D. K. (1982). Barbados: Architecture and implications for accretion. *Journal of Geophysical Research*, 87(B5), 3633.
<https://doi.org/10.1029/JB087iB05p03633>
- Stiros, S. C. (2001). The AD 365 Crete earthquake and possible seismic clustering during the fourth to sixth centuries AD in the Eastern Mediterranean: a review of historical and

- archaeological data. *Journal of Structural Geology*, 23(2–3), 545–562.
[https://doi.org/10.1016/S0191-8141\(00\)00118-8](https://doi.org/10.1016/S0191-8141(00)00118-8)
- Styron, R., García-Pelaez, J., & Pagani, M. (2020). CCAF-DB: The Caribbean and Central American active fault database. *Natural Hazards and Earth System Sciences*, 20(3), 831–857. <https://doi.org/10.5194/NHESS-20-831-2020>
- Symithe, S., Calais, E., De Chabaliér, J. B., Robertson, R., & Higgins, M. (2015). Current block motions and strain accumulation on active faults in the Caribbean. *Journal of Geophysical Research: Solid Earth*, 120(5), 3748–3774.
<https://doi.org/10.1002/2014JB011779>
- Ten Brink, U., & Lin, J. (2004). Stress interaction between subduction earthquakes and forearc strike-slip faults: Modeling and application to the northern Caribbean plate boundary. *Journal of Geophysical Research: Solid Earth*, 109(12), 1–15.
<https://doi.org/10.1029/2004JB003031>
- Ten Brink, U. S., Bakun, W. H., & Flores, C. H. (2011). Historical perspective on seismic hazard to Hispaniola and the northeast Caribbean region. *Journal of Geophysical Research: Solid Earth*, 116(B12), 12318. <https://doi.org/10.1029/2011JB008497>
- Terrier, M. (1996). Microzonage des communes de Fort-de-France - Schoelcher - le Lamentin : Failles actives. *BRGM R38988*, 52p., 25 Fig., 3 Tabl., 3 Ann., 1 Pl.
- Torrini, R., & Speed, R. C. (1989). Tectonic wedging in the forearc basin: Accretionary prism transition, Lesser Antilles forearc. *Journal of Geophysical Research: Solid Earth*, 94(B8), 10549–10584. <https://doi.org/10.1029/JB094IB08P10549>
- Tsang, L. L. H., Meltzner, A. J., Hill, E. M., Freymueller, J. T., & Sieh, K. (2015). A paleogeodetic record of variable interseismic rates and megathrust coupling at Simeulue Island, Sumatra. *Geophysical Research Letters*, 42(24), 10585–10594.
<https://doi.org/10.1002/2015GL066366>
- Uchida, N., Kirby, S. H., Okada, T., Hino, R., & Hasegawa, A. (2010). Supraslab earthquake clusters above the subduction plate boundary offshore Sanriku, northeastern Japan: Seismogenesis in a graveyard of detached seamounts? *Journal of Geophysical Research: Solid Earth*, 115(9). <https://doi.org/10.1029/2009JB006797>
- van Benthem, S., Govers, R., Spakman, W., & Wortel, R. (2013). Tectonic evolution and mantle structure of the Caribbean. *Journal of Geophysical Research: Solid Earth*, 118(6), 3019–3036. <https://doi.org/10.1002/JGRB.50235>
- van Rijsingen, E. M., Calais, E., Jolivet, R., de Chabaliér, J. B., Jara, J., Symithe, S., Robertson, R., & Ryan, G. A. (2021). Inferring Interseismic Coupling Along the Lesser Antilles Arc: A Bayesian Approach. *Journal of Geophysical Research: Solid Earth*, 126(2). <https://doi.org/10.1029/2020JB020677>
- van Rijsingen, E. M., Calais, E., Jolivet, R., de Chabaliér, J. B., Robertson, R., Ryan, G. A., & Symithe, S. (2022). Ongoing tectonic subsidence in the Lesser Antilles subduction zone. *Geophysical Journal International*, 231(1), 319–326.
<https://doi.org/10.1093/GJI/GGAC192>
- Vanneste, L. E., & Larter, R. D. (2002). Sediment subduction, subduction erosion, and strain regime in the northern South Sandwich forearc. *Journal of Geophysical Research: Solid Earth*, 107(B7), EPM 5-1-EPM 5-24. <https://doi.org/10.1029/2001JB000396>
- Vermeersch, F., Lambert, J., Fabris, H., & Legendre, D. (2002). Mise en œuvre du projet « SisDom ». Base de données de la sismicité historique des Antilles françaises et de la mer Caraïbe. Vermeersch F., Lambert J., avec la collaboration de Fabris H., Legendre D. (2002) –Mise en œuvre du projet « SisDom ». Base de données de la sismicité historique des Antilles françaises et de la mer Caraïbe. *BRGM/RP-51543-FR*, 0–48.

- Vernant, P., Reilinger, R., & McClusky, S. (2014). Geodetic evidence for low coupling on the Hellenic subduction plate interface. *Earth and Planetary Science Letters*, 385, 122–129. <https://doi.org/10.1016/J.EPSL.2013.10.018>
- Villafuerte, C., Cruz-Atienza, V. M., Tago, J., Solano-Rojas, D., Franco, S., Garza-Girón, R., Dominguez, L. A., & Kostoglodov, V. (2021). Slow slip events and megathrust coupling changes reveal the earthquake potential before the 2020 Mw 7.4 Huatulco, Mexico, event. *Authorea*.
- Weichert, D. H. (1980). Estimation of the earthquake recurrence parameters for unequal observation periods for different magnitudes. *Bulletin of the Seismological Society of America*, 70(4), 1337–1346. <https://doi.org/10.1785/BSSA0700041337>
- Weil-Accardo, J., Feuillet, N., Jacques, E., Deschamps, P., Beauducel, F., Cabioch, G., Tapponnier, P., Saurel, J. M., & Galetzka, J. (2016). Two hundred thirty years of relative sea level changes due to climate and megathrust tectonics recorded in coral microatolls of Martinique (French West Indies). *Journal of Geophysical Research: Solid Earth*, 121(4), 2873–2903. <https://doi.org/10.1002/2015JB012406>
- Wells, D. L., & Coppersmith, K. J. (1994). New Empirical Relationships among Magnitude, Rupture Length, Rupture Width, Rupture Area, and Surface Displacement. In *Bulletin of the Seismological Society of America* (Vol. 84, Issue 4).
- Westbrook, G. K., Mascle, A., & Biju-Duval, B. (1984). Geophysics and the structure of the Lesser Antilles Forearc. *Biju-Duval, B., Moore, J.V., et al. (Eds), Initial Reports of the Deep Sea Drilling Project. 78A-78B*, 23–38.
- Westbrook, G. K., Smith, M. J., Peacock, J. H., & Poulter, M. J. (1982). Extensive underthrusting of undeformed sediment beneath the accretionary complex of the Lesser Antilles subduction zone. *Nature*, 300(5893), 625–628. <https://doi.org/10.1038/300625A0>
- Willmore, P. L. (1952). The Earthquake Series in St. Kitts – Nevis, 1950–51: With Notes on Soufrière Activity in the Lesser Antilles. *Nature*, 169(4306), 770–772. <https://doi.org/10.1038/169770a0>
- Ye, L., Lay, T., Kanamori, H., & Rivera, L. (2016). Rupture characteristics of major and great (Mw ≥ 7.0) megathrust earthquakes from 1990 to 2015: 2. Depth dependence. *Journal of Geophysical Research: Solid Earth*, 121(2), 845–863. <https://doi.org/10.1002/2015JB012427>
- Yokoyama, I. (2009). The largest magnitudes of earthquakes associated with some historical volcanic eruptions and their volcanological significance. *Annals of Geophysics*, 44(5–6). <https://doi.org/10.4401/ag-3553>
- Zimmerman, M. T., Shen-Tu, B., Shabestari, K., & Mahdyiar, M. (2022). A Comprehensive Hazard Assessment of the Caribbean Region. *Bulletin of the Seismological Society of America*, 112(2), 1120–1148. <https://doi.org/10.1785/0120210157>

Annexes

Crustal area sources - first part

Zone ID	Structural region	Significant earthquake from catalogs and advices (M>5 or IE>7)	Deformation regime	Mmax cat ISCU (Mw) - CDSA (M) / Mmax structure / Mmax proxy (Mw)	Short description of source area boundaries (map view)
AW-1	Accretionary prism	<ul style="list-style-type: none"> 1728, 1890 and 1922, EI=7 * 1910, Mw=6.5 ** 	Reverse	<ul style="list-style-type: none"> Mmax cat 5.7 - 5.2 Mmax structure - Mmax proxy - 	<ul style="list-style-type: none"> East: subduction trench West: backstop North: Tiburon ridge, that stoppes sediments progression to the north from Orinoco river South: progressive disappearance of the prism
AW-2	Accretionary prism	<ul style="list-style-type: none"> 1900 with EI=8 * 	Reverse	<ul style="list-style-type: none"> Mmax cat 4.9 - 4.2 Mmax structure - Mmax proxy - 	<ul style="list-style-type: none"> East: subduction trench West: backstop North: Barracuda ridge. North to it, the obliquity is responsible for the change of deformation regime at the trench from sediment accretion to the south of the ridge and erosion to the north of it South: Tiburon ridge that stoppes sediments progression in this area
AW-3	Accretionary prism	-	Strike-slip	<ul style="list-style-type: none"> Mmax.cat 4.6 - 4.2 Mmax.struct - Mmax proxy - 	<ul style="list-style-type: none"> North East: subduction trench South West: 10 km south west of the Bunce fault, that marks the backstop West: transition to the Puerto-Rico subduction system South: Barracuda ridge, limit with sediment accretion (south) to erosion (north) trench regime
FAA	Forearc bassin and active volcanic arc	<ul style="list-style-type: none"> 1834, 1886 and 1905 with EI=8 * 1865 with EI=8.5 * 1946, Mw=5.7 	Normal	<ul style="list-style-type: none"> Mmax.cat 5.7 - 4.5 Mmax.struct - Mmax proxy - 	<ul style="list-style-type: none"> East: backstop West: the end of the volcanic arc North: GNSS velocity gradient between Sainte-Lucia and Saint-Vincent-and-Genardines South: El-Pilar strike-slip fault system and its high earthquake density
FA-1	Forearc bassin	<ul style="list-style-type: none"> 1839 with EI=8 * 1702 with EI=8.5 * 2014, Mw=5.2 	Normal	<ul style="list-style-type: none"> Mmax.cat 5.2 - 5.3 Mmax.struct 7.0-7.3 Mmax.proxy - 	<ul style="list-style-type: none"> East: backstop West: beginning of the active volcanic arc North: Marie-Galante fault system South: GNSS velocity gradient between Sainte-Lucia and Saint-Vincent-and-Genardines and change in earthquake density between FAA and FA-1
FA-2a	Marie-Galante rift	<ul style="list-style-type: none"> 1851 with EI=7 * 1897 with EI=8 * 1950, Mw=5.7 *** 	Normal	<ul style="list-style-type: none"> Mmax.cat 5.7 - 4.8 Mmax.struct 7.0-7.3 Mmax.proxy - 	<ul style="list-style-type: none"> East: end of the Marie-Galante system West: end of the Marie-Galante system North: change in GNSS vector directions and the end of the Marie-Galante system, north of Gosier and Roche-de-May faults South: end of the Marie-Galante system, south of the Morne-Piton fault
A-1	Active volcanic arc	<ul style="list-style-type: none"> 1870 and 1906 EI=7.5 * 2004, M=6.3 	Normal	<ul style="list-style-type: none"> Mmax.cat 6.3 Mmax.struct 7.0-7.3 Mmax.proxy - 	<ul style="list-style-type: none"> East: forearc bassin of the FA-1 source area West: end of the volcanic arc North: Marie-Galante fault system South: GNSS velocity gradient between Sainte-Lucia and Saint-Vincent-and-Genardines
A-2	Active volcanic arc	<ul style="list-style-type: none"> 1690 EI=IX (Feuillet et al. 2011 and references therein) 1833 and 1848, EI=7.5 * 1935, Mw=6.2 1985, Mw=6.3 	Normal and sinistral strike-slip	<ul style="list-style-type: none"> Mmax.cat 6.3 Mmax.struct 7.0-7.3 Mmax.proxy - 	<ul style="list-style-type: none"> North-East: Kallinago Trough West: Anegada passage South: end of the volcanic arc South-east: UL diffuse limit and its decrease in earthquake density
DP-1	Outer-rise	<ul style="list-style-type: none"> 2016, M=5.6 (USGS) 	Normal and strike-slip	<ul style="list-style-type: none"> Mmax.cat 4.5 Mmax.struct - Mmax.proxy 8.0-8.6 (Meng et al., 2012) 	<ul style="list-style-type: none"> East: 200 km from the trench West: trench South: end of the subduction system North: change in crust properties
DP-2	Outer-rise	<ul style="list-style-type: none"> 2003, M=6.7 (USGS) 	Normal and strike-slip	<ul style="list-style-type: none"> Mmax.cat 6.0 Mmax.struct - Mmax.proxy 8.0-8.6 (Meng et al., 2012) 	<ul style="list-style-type: none"> East: 200 km from the trench West: trench North: end of the subduction system South: change in crust properties
		* Historical seismicity, with macro-seismic data currently being processed.		** Doubt about the source location, which differs according to the references.	*** No information in literature.

Annex table 1: Crustal area sources and corresponding characteristics resume part 1.

Crustal area sources - second part

Zone ID	Structural region	Significant earthquake from catalogs and advices (M>5 or IE>7)	Deformation regime	Mmax cat ISCU (Mw) - CDSA (MI) / Mmax structure / Mmax proxy (Mw)	Short description of source area boundaries (map view)
FA-2b	Forearc bassin	• 1914, Mw=7.0 **	Normal	• Mmax.cat 4.9 • Mmax.struc - • Mmax.proxy -	• East: backstop • West: beginning of the Marie-Galante system • North: east extension of the FA-2a north limit • South: east extension of the FA-2a south limit
FA-3	V-shaped bassin and inactive volcanic arc	• 1843, El=9.5 * • 1690, 1842, 1735 and 1895, El=7.5 * • 1967, Mw=6.4 • 1974, El=8, Mw=6.5 to 7.5 **	Normal	• Mmax.cat 6.4 • Mmax.struc 7.0-7.3 • Mmax.proxy -	• East: backstop • West: active volcanic arc • North: FA-4 source area and its decrease in earthquake density, where faults are almost inactives • South: FA-2 source area and its decrease in earthquake density
FA-4	Anegada faults and bassins	• 1835, El=7.5 * • 1925, Mmax=6.2 **	Normal	• Mmax.cat 6.2 • Mmax.struc 7.0-7.5 • Mmax.proxy -	• South-East: FA-3 source area and its increase in earthquake density • West: end of the Anegada Passage fault system west extension • North: backstop marks by the Bunce fault and the north of the Sombrero inactive bassin • South-west: active volcanic arc (A-2) and strike slip to normal Anegada Passage section (AP)
AP	South Anegada Passage	• 1867, M=7.2 (Reid and Taber, 1920)	Strike slip to normal	• Mmax.cat 3.9 • Mmax.struc 7.0-7.5 • Mmax.proxy -	• East: active volcanic arc • West: end of Anegada passage fault and bassin system • North: Puerto-Rico crustal fault system • South: Muertos fault system
BA	Backarc region	-	-	• Mmax.cat 5.6	• Model limit: catalog does not include all the seismicity specific to the system
MF	Eastern end of the Muertos fault	-	Reverse	• Mmax.cat 4.7	• Model limit: catalog does not include all the seismicity specific to the system
NB	Eastern end of the Puerto-Rico subduction	-	Reverse	• Mmax.cat 5.9	• Model limit: catalog does not include all the seismicity specific to the system
SB	Eastern end of the El Pilar fault system	-	Strike-slip	• Mmax.cat 6.9	• Model limit: catalog does not include all the seismicity specific to the system
AW-4	Eastern end accretionary prism of the Puerto-Rico subduction	-	Reverse	• Mmax.cat 4.9	• Model limit: catalog does not include all the seismicity specific to the system
AWD	Accretionary wedge progressive death	-	Reverse	• Mmax.cat 6.1	• Model limit: catalog does not include all the seismicity specific to the system
	* Historical seismicity, with macro-seismic data currently being processed.		** Doubt about the source location, which differs according to the references.		*** No information in literature.

Annex table 2: Crustal area sources and corresponding characteristics resume part 2.

Interface

Zone ID	Structural region	Significant earthquake from catalogs and advices (M>5 or IE>7)	Deformation regime	Mmax cat ISCU (Mw) - CDSA (MI) / Mmax structure / Mmax proxy (Mw)	Short description of source area boundaries (map view)
DI-1	Moderate slip earthquake domain, high high-frequency content, supposed to be coupled 35-65 km	<ul style="list-style-type: none"> • 1946, Ms 6-7 (Russo & Okal, 1992) • 1999, Mw=5.8 • 2017, Mw=5.8 	Reverse	<ul style="list-style-type: none"> • Mmax.cat 5.8 • Mmax.struct >9 • Mmax.proxy 7-8 	<ul style="list-style-type: none"> • East: limit between moderate slip to large slip domains • West: end of seismogenic zone domain, limit of the deepest reverse focal mechanism • North: Tiburon ridge, marks the diffuse limit between the north and south American plates, and the change in subduction obliquity with an increase of the slab lateral curvature • South: end on known slab interface
UI-1	Large slip earthquake domain, moderate high-frequency content, supposed to be uncoupled 0-35 km	<ul style="list-style-type: none"> • 1839, M=7.5-8 (Bernard & Lambert, 1988) ** • 1919, Mw=6.06 *** • 2015, Mw=6.5 *** 	Reverse	<ul style="list-style-type: none"> • Mmax.cat 6.5 • Mmax.struct >9 • Mmax.proxy 8.5-9 	<ul style="list-style-type: none"> • East: subduction trench • West: limit between moderate slip to large slip domains • North: Tiburon ridge, marks the diffuse limit between the north and south American plates, and the change in subduction obliquity with an increase of the slab lateral curvature • South: end of known slab interface
DI-2	Moderate slip earthquake domain, high high-frequency content, supposed to be coupled 35-65 km	<ul style="list-style-type: none"> • 1969, Mw=6 *** • 1982, Mw=6 *** 	Reverse	<ul style="list-style-type: none"> • Mmax.cat 6 • Mmax.struct >9 • Mmax.proxy 7-8 	<ul style="list-style-type: none"> • West: Puerto-Rico subduction • South-west: end of seismogenic zone domain, limit of the deepest reverse focal mechanism • North-east: limit between moderate slip to large slip domains • South: Tiburon ridge, marks the diffuse limit between the north and south American plates, and the change in subduction obliquity with an increase of the slab lateral curvature
UI-2	Large slip earthquake domain, moderate high-frequency content, supposed to be uncoupled 0-35 km	<ul style="list-style-type: none"> • 1843, M=8-8.5 (Bernard & Lambert, 1988) ** • 1906, M=6.3 ** • 2016, Mw=6 *** 	Reverse	<ul style="list-style-type: none"> • Mmax.cat 6.3 • Mmax.struct >9 • Mmax.proxy 8.5-9 	<ul style="list-style-type: none"> • West: Puerto-Rico subduction • South-west: limit between moderate slip to large slip domains • North-east: subduction trench • South: Tiburon ridge, marks the diffuse limit between the north and south American plates, and the change in subduction obliquity with an increase of the slab lateral curvature
DI-3	Puerto-Rico subduction	-	Reverse	<ul style="list-style-type: none"> • Mmax.cat 4.6 	<ul style="list-style-type: none"> • Model limit: catalog does not include all the seismicity specific to the system
UI-3	Puerto-Rico subduction	-	Reverse	<ul style="list-style-type: none"> • Mmax.cat 6.1 	<ul style="list-style-type: none"> • Model limit: catalog does not include all the seismicity specific to the system
		* Historical seismicity, with macro-seismic data currently being processed.	** Doubt about the source location, which differs according to the references.	*** No information in literature.	

Annex table 3: Interface area sources and corresponding characteristics resume.

Intraslab

Zone ID	Structural region	Significant earthquake from catalogs and advices (M>5 or IE>7)	Deformation regime	Mmax cat ISCU (Mw) - CDSA (MI) / Mmax structure / Mmax proxy (Mw)	Short description of source area boundaries (map view)
SD	Slab detachment area	-	-	<ul style="list-style-type: none"> • Mmax.cat 4.9 • Mmax.struct - • Mmax.proxy - 	<ul style="list-style-type: none"> • East: presence of slab • West: end of known slab • South: end of known slab
SI-2	Slab intermediate depth area with constant high dipping	<ul style="list-style-type: none"> • 1953, Mw=7.3 (Russo et al. 1992) • 1976, Mw=5.2 *** 	Reverse to strike-slip	<ul style="list-style-type: none"> • Mmax.cat 5.2 • Mmax.struct - • Mmax.proxy 8.0-8.3 (Tarazona et al. 2023, and references therein) 	<ul style="list-style-type: none"> • East: change in the slab bending • West: presence of slab detachment • North: change in seismicity density • South: change in seismicity density
SI-3	Slab intermediate depth area with constant high dipping	<ul style="list-style-type: none"> • 1914, Mw=7 ** • 2007, Mw=7.4 	Normal to strike-slip	<ul style="list-style-type: none"> • Mmax.cat 7.4 • Mmax.struct - • Mmax.proxy 8.0-8.3 (Tarazona et al. 2023, and references therein) 	<ul style="list-style-type: none"> • East: change in slab bending • West: presence of slab detachment • North-West: diffuse limit with change in stress deformation • South: change in seismicity density
SI-4	Slab intermediate depth area with constant high dipping	<ul style="list-style-type: none"> • 1987, Mw=5 *** 	-	<ul style="list-style-type: none"> • Mmax.cat 5 • Mmax.struct - • Mmax.proxy 8.0-8.3 (Tarazona et al. 2023, and references therein) 	<ul style="list-style-type: none"> • South-East: diffuse limit with change in stress deformation • West: Puerto-Rico subduction • North: change in slab bending • South: presence of slab detachment
SB-2	Slab bending area	<ul style="list-style-type: none"> • 1984, Mw=5.7 *** 	-	<ul style="list-style-type: none"> • Mmax.cat 5.7 • Mmax.struct - • Mmax.proxy 8.0-8.3 (Tarazona et al. 2023, and references therein) 	<ul style="list-style-type: none"> • East: change in the slab bending • West: change in the slab bending • North: change in seismicity density • South: change in seismicity density
SB-3	Slab bending area	<ul style="list-style-type: none"> • 1969, Mw=5.9 *** • 1914, Mw=7 ** 	Normal-strike-slip to reverse-strike-slip (from north to south)	<ul style="list-style-type: none"> • Mmax.cat 5.9 • Mmax.struct - • Mmax.proxy 8.0-8.3 (Tarazona et al. 2023, and references therein) 	<ul style="list-style-type: none"> • South-East: diffuse limit with change in stress deformation • West: Puerto-Rico subduction • North: subduction trench • South: change in slab bending
SB-4	Slab bending area	<ul style="list-style-type: none"> • 1988, Mw=5.4 *** 	-	<ul style="list-style-type: none"> • Mmax.cat 5.4 • Mmax.struct - • Mmax.proxy 8.0-8.3 (Tarazona et al. 2023, and references therein) 	<ul style="list-style-type: none"> • South-East: diffuse limit with change in stress deformation • West: Puerto-Rico subduction • North: change in slab bending • South: change in slab bending
		* Historical seismicity, with macro-seismic data currently being processed.	** Doubt about the source location, which differs according to the references.	*** No information in literature.	

Annex table 4: Intraslab area sources and corresponding characteristics resume part 1.

Intraslab

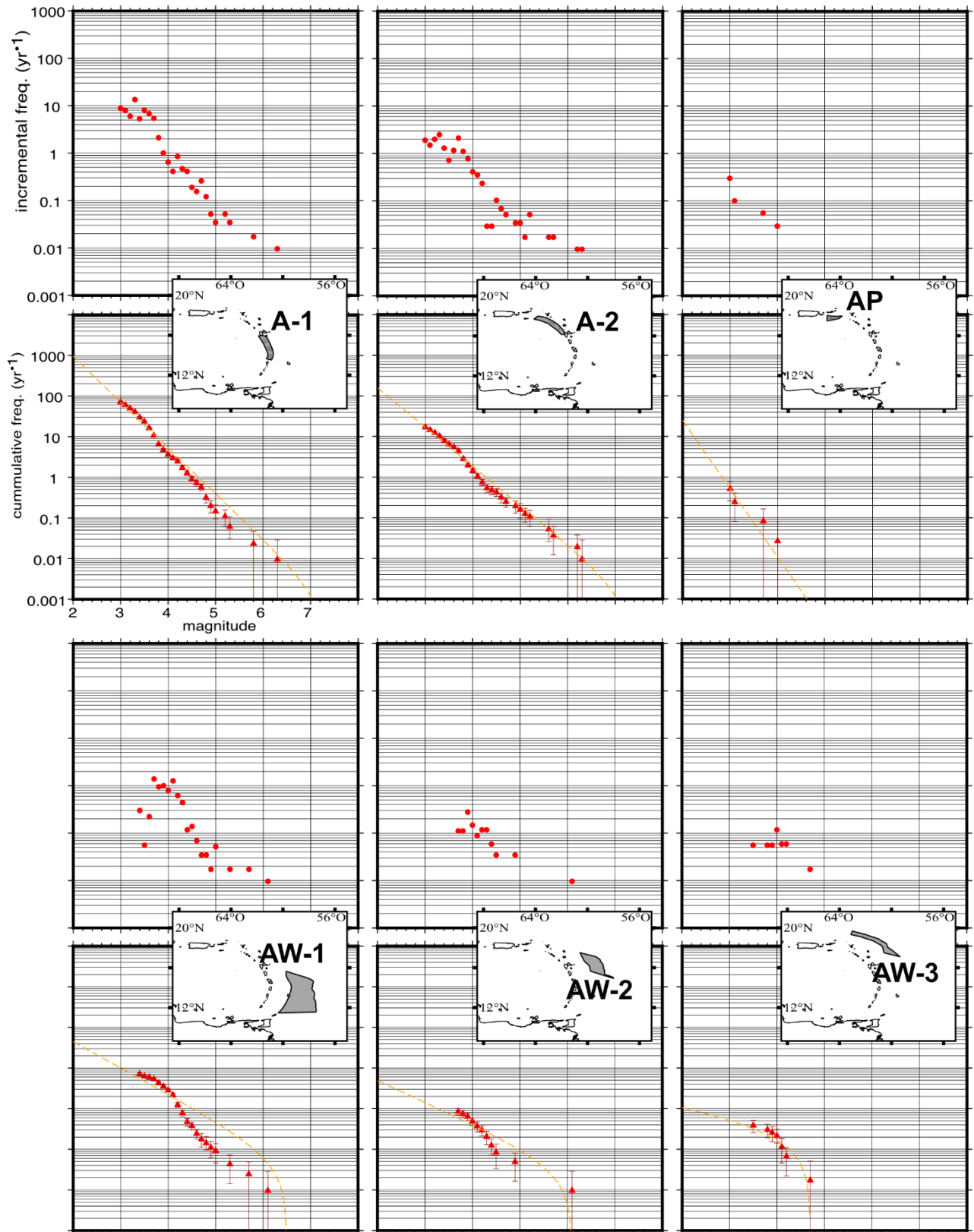
Zone ID	Structural region	Significant earthquake from catalogs and advices (M>5 or IE>7)	Deformation regime	Mmax cat ISCU (Mw) - CDSA (Ml) / Mmax structure / Mmax proxy (Mw)	Short description of source area boundaries (map view)
SS-1	Slab near surface area with constant low dipping	• 1986, Mw=5.2 ***	-	• Mmax.cat 5.2 • Mmax.struct - • Mmax.proxy 8.0-8.3 (Tarazona et al. 2023, and references therein)	• East: subduction trench • West: change in the slab bending and corresponding stress deformation • North: change in seismicity density • South: end of known slab
SS-2	Slab near surface area with constant low dipping	• 1997, Mw=6.1 • 1969, Mw=7.2 ** (Dorel, 1981) • 2014, Mw6.5 **	Normal to strike-slip	• Mmax.cat 6.5 • Mmax.struct - • Mmax.proxy 8.0-8.3 (Tarazona et al. 2023, and references therein)	• East: subduction trench • West: change in the slab bending and corresponding stress deformation • North: diffuse limit with change in stress deformation • South: change in seismicity density
SS-3	Slab near surface area with constant low dipping	• 1986, Mw=5.5 ***	-	• Mmax.cat 5.5 • Mmax.struct - • Mmax.proxy 8.0-8.3 (Tarazona et al. 2023, and references therein)	• South-East: diffuse limit with change in stress deformation • West: Puerto-Rico subduction • North: subduction trench • South: change in slab bending
SI-1	Slab intermediate depth area with constant high dipping	-	-	• Mmax.cat 6.5	• Model limit: catalog does not include all the seismicity specific to the system
SB-1	Slab bending area	-	Normal to strike-slip	• Mmax.cat 6	• Model limit: catalog does not include all the seismicity specific to the system
SI-5	Slab intermediate depth area with constant high dipping	-	-	• Mmax.cat 6.1	• Model limit: catalog does not include all the seismicity specific to the system
SB-5	Slab bending area	-	Reverse to strike-slip	• Mmax.cat 5.2	• Model limit: catalog does not include all the seismicity specific to the system
SS-4	Slab near surface area with constant low dipping	-	Reverse to strike-slip	• Mmax.cat 5.9	• Model limit: catalog does not include all the seismicity specific to the system
	* Historical seismicity, with macro-seismic data currently being processed.		** Doubt about the source location, which differs according to the references.		*** No information in literature.

Annex table 5: Intraslab area sources and corresponding characteristics resume part 2.

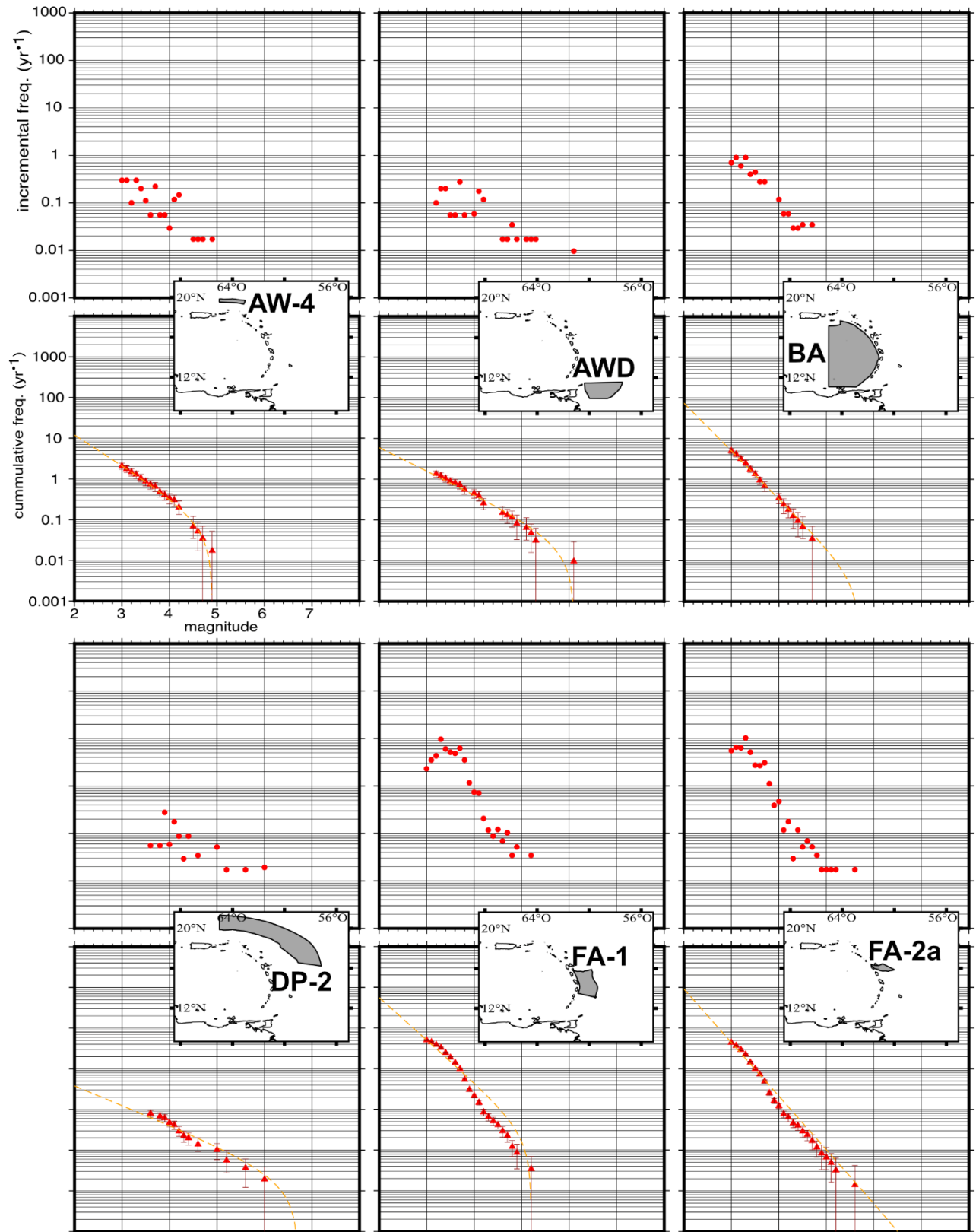
Mantle Wedge

Zone ID	Structural region	Significant earthquake from catalogs and advices (M>5 or IE>7)	Deformation regime	Mmax cat ISCU (Mw) - CDSA (Ml) / Mmax structure / Mmax proxy (Mw)	Short description of source area boundaries (map view)
PRM	Puerto Rico Mantle Wedge Subduction Zone	-	-	• Mmax.cat 5.2	• Model limit: catalog does not include all the seismicity specific to the system
NMS	North Lesser Antilles Mantle Wedge	-	-	• Mmax.cat 4.7 • Mmax.struct - • Mmax.proxy 4.5 (Davey & Ristau, 2011)	• North: Puerto Rico subduction system • South: Increase in seismic activity • East: Subducting slab and crust Moho physical limit • West: Loss of seismic activity
MS	Central Lesser Antilles Mantle Wedge	• 1974, Ms=7.1-7.6 (McCann et al., 1982) **	Normal to strike-slip	• Mmax.cat 6.3 • Mmax.struct - • Mmax.proxy 4.5 (Davey & Ristau, 2011)	• North: Decrease in seismic activity • South: Decrease in seismic activity • East: Subducting slab and crust Moho physical limit • West: Loss of seismic activity
SMS	South Lesser Antilles Mantle Wedge	-	-	• Mmax.cat 5.9	• Model limit: catalog does not include all the seismicity specific to the system
	* Historical seismicity, with macro-seismic data currently being processed.		** Doubt about the source location, which differs according to the references.		*** No information in literature.

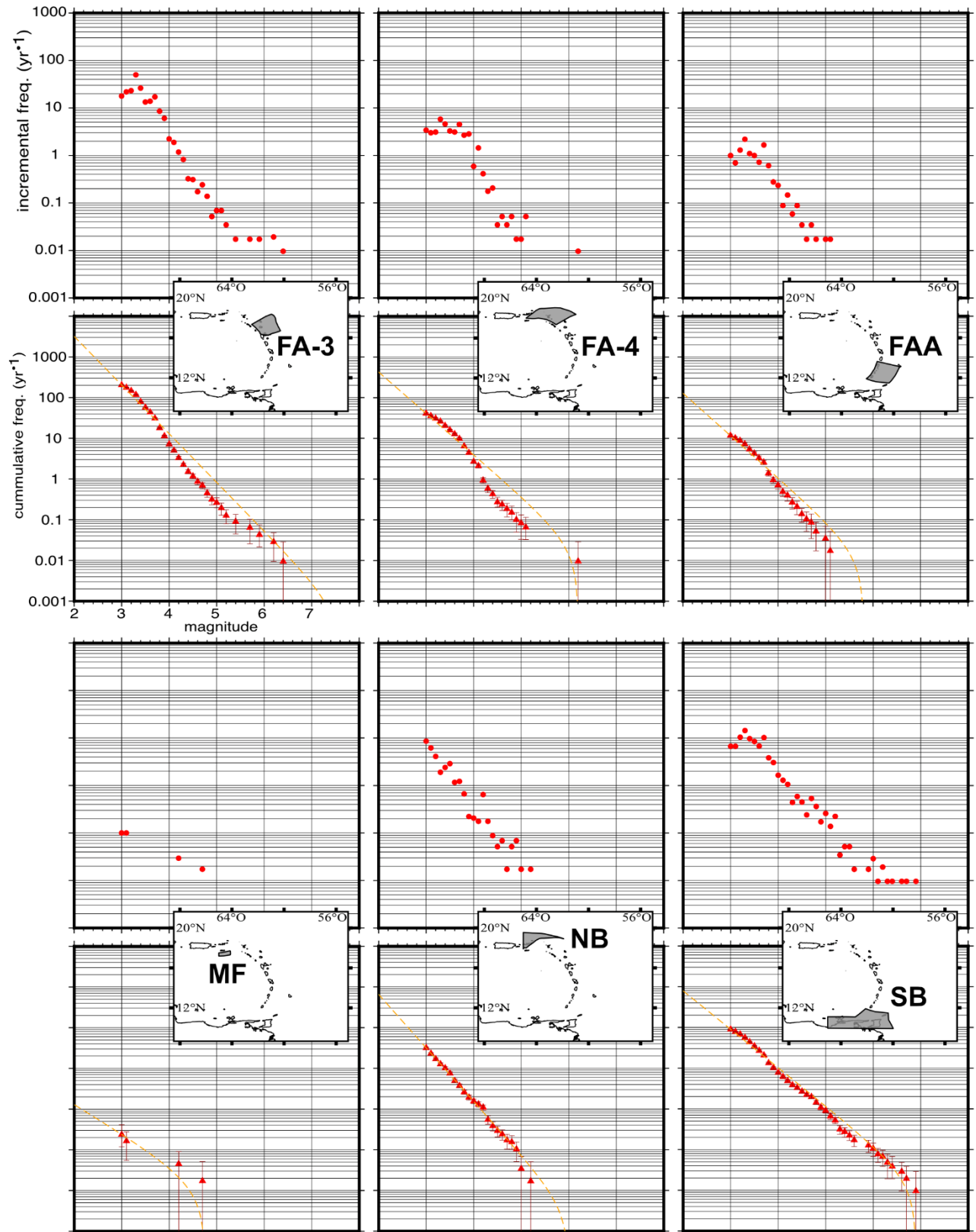
Annex table 6: Mantle wedge area sources and corresponding characteristics resume.



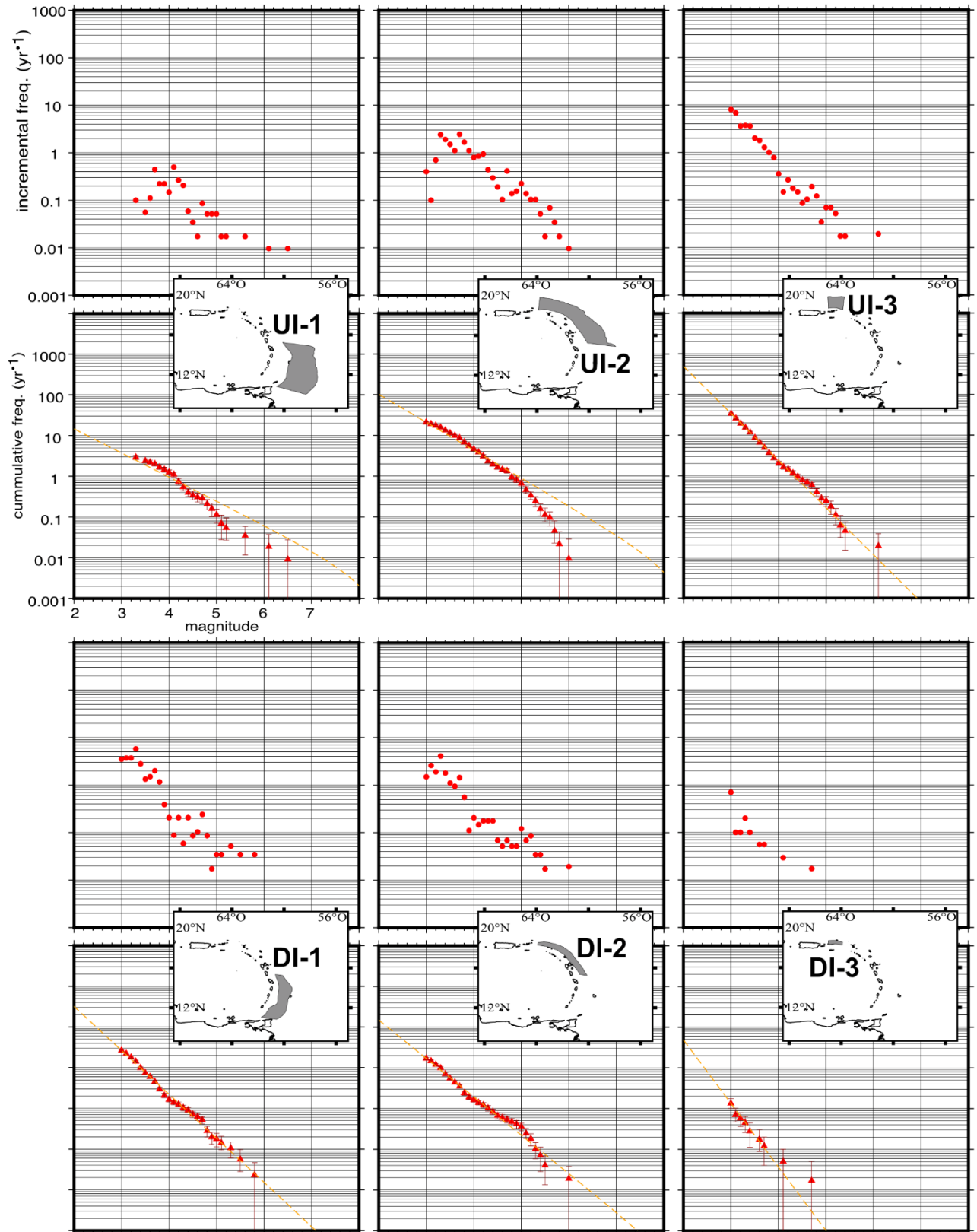
Annex 1: MDF and GR distributions for each seismogenic zone (inset).



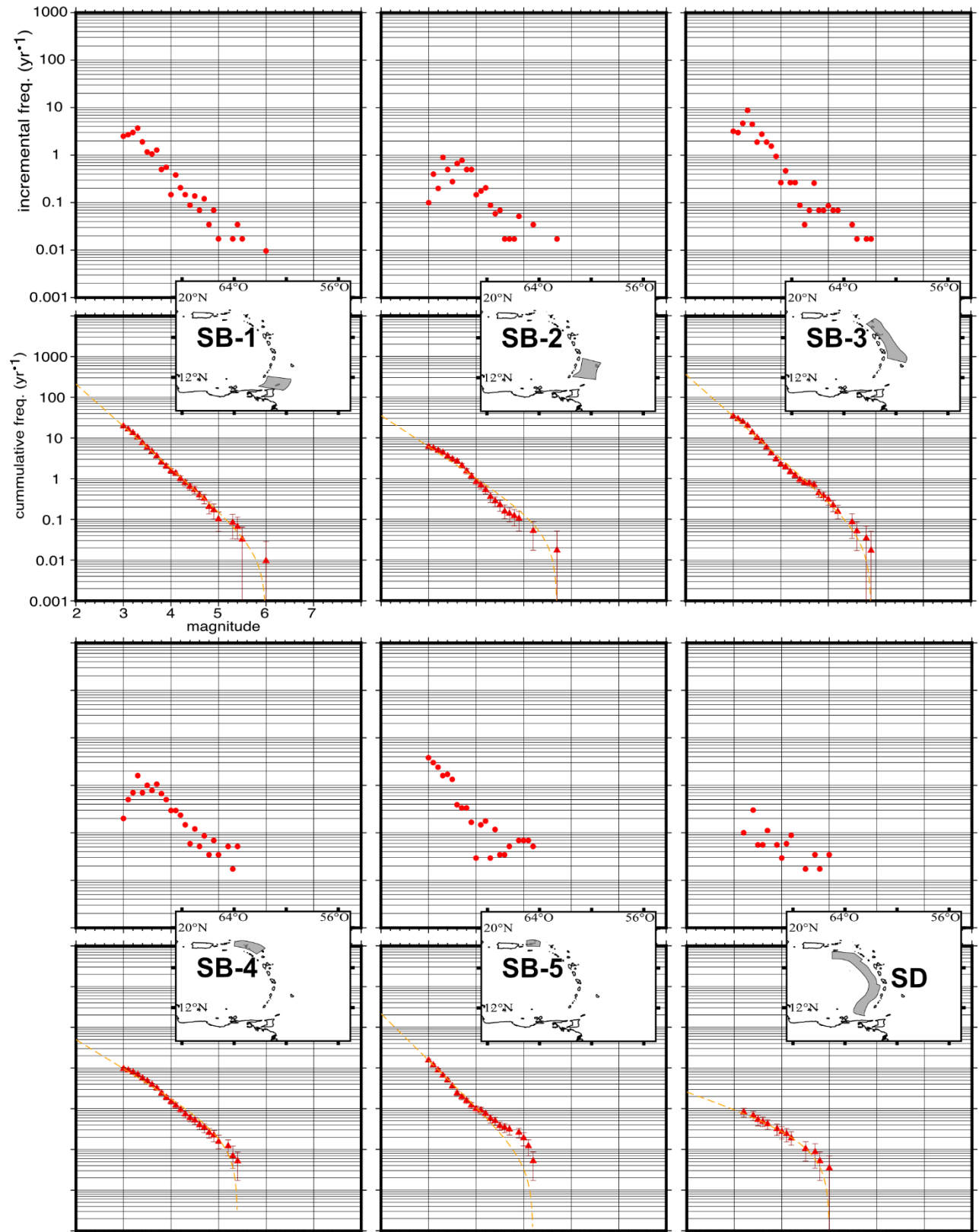
Annex 2: MDF and GR distributions for each seismogenic zone (inset).



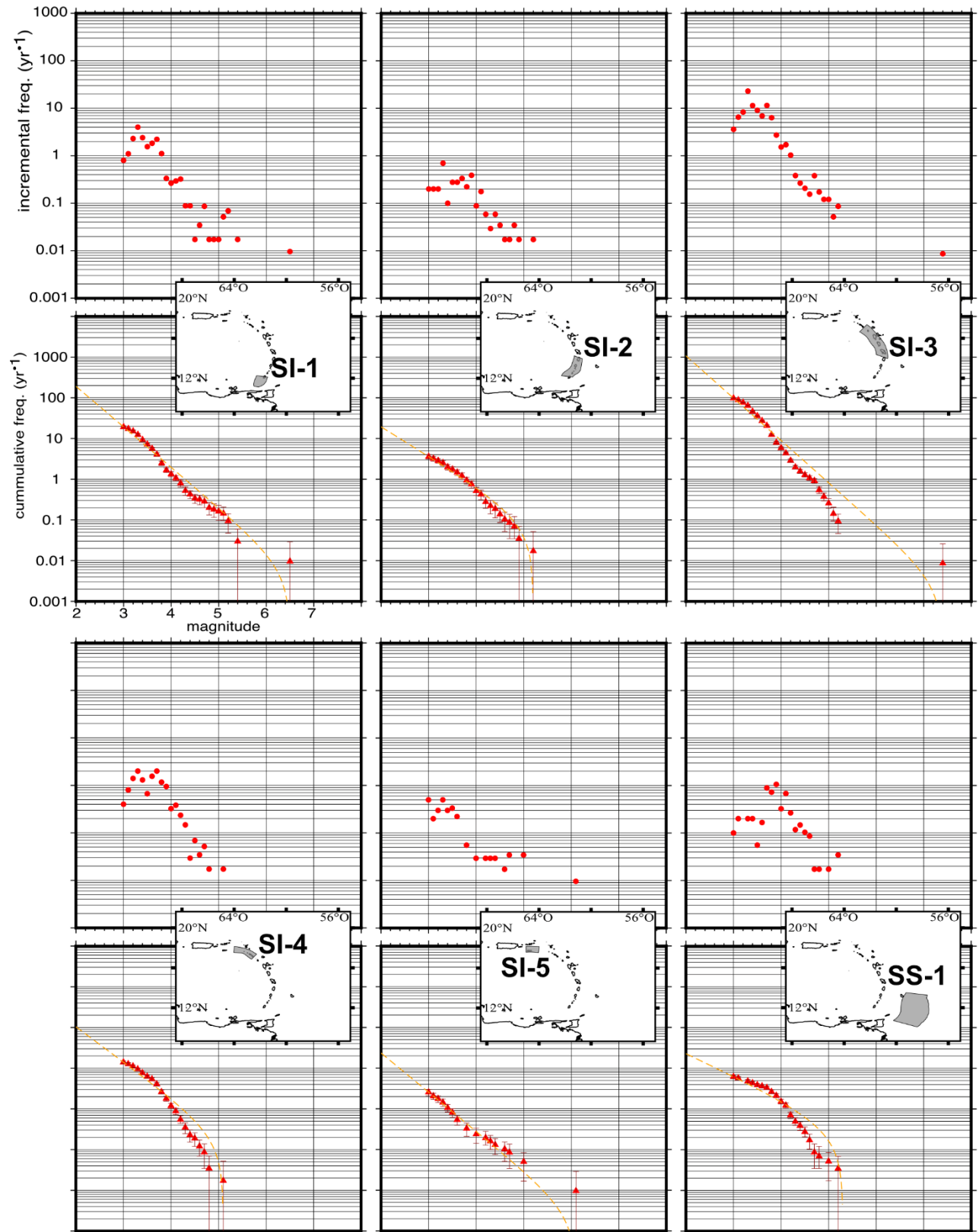
Annex 3: MDF and GR distributions for each seismogenic zone (inset).



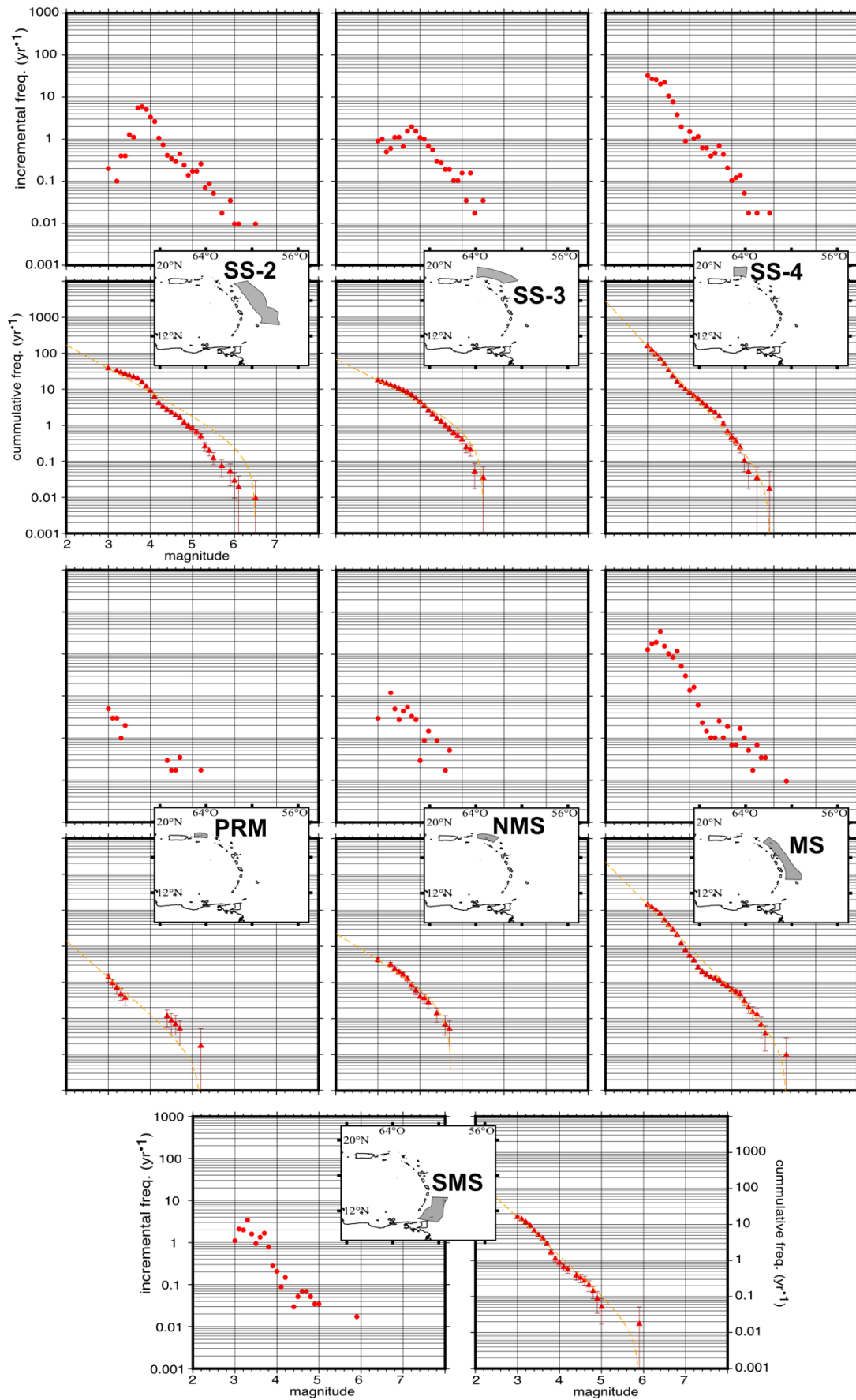
Annex 4: MDF and GR distributions for each seismogenic zone (inset).



Annex 5: MDF and GR distributions for each seismogenic zone (inset).



Annex 6: MDF and GR distributions for each seismogenic zone (inset).



Annex 7: MDF and GR distributions for each seismogenic zone (inset).